The quiet 2013 Hurricane season in the North Atlantic: Causes and role of subtropical dry air intrusions into the Main Developing Region

Die ruhige nordatlantische Hurrikan Saison 2013: Gründe und Auswirkungen des Einmischens von trockenen, subtropischen Luftmassen in die tropische Hauptentstehungszone

Master's Thesis in Meteorology
by

Pila Bossmann

November 2015

Karlsruher Institut für Technologie

INSTITUTE OF METEOROLOGY AND CLIMATE RESEARCH - TROPOSPHERE RESEARCH
KARLSRUHE INSTITUTE OF TECHNOLOGY (KIT)

Adviser:	Prof. Dr. Andreas Fink
Second Adviser:	Prof. Dr. Peter Knippertz

Zusammenfassung

Obwohl die meisten saisonalen Vorhersagen eine überdurschnittlich hohe Sturmaktivität prognostizierten, war die nordatlantische Hurrikan Saison 2013 eine der schwächsten seit 1983, bei Betrachtung der geringen Anzahl an Hurrikans. Zutreffend vorhergesagt, sorgten hohe Meeresoberflächentemperaturen in dem Hauptentstehungsgebiet der Hurrikans, einem Bereich zwischen westafrikanischer Küste und der Karibik, für ausreichend latente Wärme, um die Zyklogenese von tropischen Stürmen fördern. Unter anderem traf die Vorhersage jedoch nicht auf die verstärkte vertikale Windscherung zu. Zusätzlich gab es ungewöhnlich trockene Luftmassen im Bereich des Hauptentstehungsgebiets, die vermehrt tropische Zyklogenese verhinderten.

In dieser Arbeit werden die Gründe für diese "Vorhersage Pleite" diskutiert. Dabei liegt der Fokus hauptsächlich auf der Herkunft der trockenen Luftmassen. Es werden Analysen klimatologischer Art von atmosphärischen Parametern, die wichtig für tropische Zyklogenese sind dargestellt. Zusätzlich wird eine Trajektorien-Analyse an Fallstudien sich nicht-entwickelnder, wellenartigen atmosphärischne Störungen, sogennanten "African easterly waves", veranschaulicht.

Das Zentrum des Hauptentstehungsgebiets war aufgrund von großflächiger Absinkbewegungen in der oberen Troposphäre ungewöhnlich trocken. Diese Absinkbewegungen führten letztendlich zu Einmischungen trockener, subtropischer Luft in das Hauptentstehungsgebiet. Prozesse wie diese schwächten oder verhinderten sogar starke tropische Konvektion in Verbindung mit einzelnen African easterly waves. Zuätzlich wurde die Konvektion einzelner Wellen von trockener Luft, die aus der Sahara advehiert wurde, unterdrückt. Verstärkte vertikale Windscherung, die aufgrund von vermehrten tropischen Trögen in der oberen Tropospäre auftrat, war der Hauptgrund, der tropische Zyklogenese vermehrt in der Karibik verhinderte.

Daraus lässt sich folgern, dass vor allem die Kombination aus subtropischem Absinken trockener Luft und Einmischung in das Hauptentstehungsgebiet, zusammen mit verstärkter vertikaler Windscherung in der Karibik, die tropische Zyklogenese entscheidend negativ beeinflussten.

Abstract

Despite various predictions calling for above normal activity, the Atlantic hurricane season 2013 has been the quietest season since 1983 in terms of hurricane numbers. Correctly predicted, high sea surface temperatures in the main developing region of the North Atlantic provided enough latent heat for tropical genesis. But alongside other factors, the seasonal forecasts fell short in predicting high vertical wind shear. Additionally, anomalously dry air masses were present in the main developing region, increasing the inhibiting factors of tropical cyclogenesis.

In this work, reasons for the forecast bust are discussed, especially focusing on the origin of dry air masses. A climatological analysis of tropical cyclogenesis related atmospheric parameters is presented. A case specific trajectory analysis of different non-developing wave-like tropical disturbances, called African easterly waves, is presented as well.

The central main developing region is found to have been anomalously dry as a result of large-scale upper level convergence that led to subsiding dry air intrusions from the subtropics into the main developing region. This process weakened or even inhibited tropical deep convection initiated by African easterly waves. Additionally, the convection of individual easterly waves was negatively affected by dry air masses from the Saharan air layer. Increased vertical wind shear, as a result of tropical upper tropospheric troughs, was identified of being the main impeding factor of tropical genesis in the Caribbean Sea.

This leads to the assumption that a combination of frequent subtropical dry air intrusions into the central main developing region and higher values of vertical wind shear in the western main developing region negatively affected tropical cyclogenesis in a crucial manner.

Contents

1. Introduction

The National Oceanic and Atmospheric Administration (NOAA), as well as several other international institutes, issue a probabilistic seasonal hurricane forecast based on predictions for various large-scale climate factors like the Sea Surface Temperature (SST) or the El Niño-Southern Oscillation (ENSO) and on climate models. Uncertainties concerning the effects of ENSO on the atmospheric and oceanic circulations and model prediction errors of atmospheric parameters highly complicate the seasonal forecasts. Also weather patterns that are not predictable on a seasonal scale have a certain impact on the seasonal hurricane forecast (NOAA, 2013).

With the official ending of the Atlantic hurricane season 2013 on 30 November 2013, all seasonal forecasts overestimated the hurricane activity. The Atlantic hurricane season 2013 was predicted to be highly active with an occurrence of seven to eleven hurricanes, three to six of them strengthening to major hurricanes. Hurricanes are strong Tropical Cyclones (TC) that are categorized from 1 to 5 by their one-minute maximum sustained wind speed on the Saffir-Simpson hurricane wind scale (Saffir, 1973; Simpson and Saffir, 1974). A storm of category 3 or higher is classified as major hurricane (cf. Table A.1. Despite favorable environmental conditions, only two category 1 hurricanes developed during this unusually quiet season.

The forecast bust of 2013 questioned the reliability of seasonal forecasts. These are a crucial source of information to assure that there is enough time to establish protection for people and infrastructure in the affected regions both in Central and North America. The goal of this study is to find reasons and explanations for the unpredicted low hurricane activity in 2013 over the tropical North Atlantic.

Typical precursors for TCs are convective disturbances that have been initiated over the mountain region in East Africa and propagate primarily into the Main Developing Region (MDR) of the North Atlantic ocean. These disturbances are called African Easterly Waves (AEWs). Their further life cycle is influenced by a variety of factors such as high SSTs, low vertical wind shear and dry air. Especially the last factor plays a major role for the development or non-development of AEWs into TCs (Schwendike and Jones, 2010). The MDR is defined as a region where most TCs develop. It ranges from 9-21.5°N from the West African coast to the Caribbean Sea (Goldenberg et al., 2001). Favorable environmental conditions for tropical cyclogenesis are frequently met in this region during the Atlantic hurricane season.

To gain a comprehensive overview of the hurricane season, a climatological analysis is performed, investigating inhibiting factors for the entire MDR and aiming at the identification of correlations between the parameters. Anomalies corresponding to a 31-year mean from 1983-2013 are analyzed and partially compared to the season of 1994, which showed even less activity than the season of 2013, and to the season of 2005, the strongest seasons on record.

A crucial factor that led to the poorly predicted season of 2013 is to be found in the frequent occurrence of anomalously dry air masses over the tropical North Atlantic (Blake, 2014). On the one hand, TC activity is impacted negatively by dry air masses, originating from the Saharan Air Layer (SAL) (Dunion and Velden, 2004). On the other hand, subtropical dry air intrusions after Rossby Wave Breaking (RWB) in the subtropics (Allen et al., 2009) have the same potential to strongly prevent convection in mid-levels, which in turn is an essential process for hurricanes to develop from initial tropical disturbances. Therefore, this work also addresses the question concerning the origin of these unusually dry air masses leading to the quiet season of 2013 in greater detail. In case studies, backward trajectories for investigating the present air masses at the starting points are calculated for several non-developing AEWs.

A short theoretical background to TC genesis, atmospheric waves, the Saharan Air Layer (SAL), RWB and forecast methods is given in Chapter 2, followed by a specification of applied methods and used data in Chapter 3. In Chapter 4, two different forecasts of the Atlantic hurricane season are discussed and a climatological analysis, including anomalies of the fundamental TC parameters (e.g. SST, vertical wind shear or low-level relative vorticity) of the hurricane season 2013 is presented. Afterwards a detailed case specific analysis of four AEWs is discussed in Chapter 5. At the end, the results of the climatological analysis and the case studies are discussed and summarized in Chapter 6.

2. Theoretical Background

2.1 Tropical Cyclone Genesis

An independent weather system with organized convection is called tropical disturbance and can strengthen to a TC, which is a rapid rotating storm system. Tropical disturbances give name to non-frontal, wandering systems developing in the tropics or subtropics. They have diameters between 200-600 km and can sustain convection up to 24 hours or more (Landsea, 2011). By the definition of Frank (1987), TC genesis is the modification of a tropical disturbance to a tropical depression, which is a TC that has maximal sustained wind speeds of at least 17 ms^{-1} (U.S. 1 minute average standard) and a closed circulation (Landsea, 2011). For a tropical disturbance to transit into a tropical depression, favorable environmental conditions are essential. SSTs above 26.5°C, a deep layer of conditional instability from the surface to the mid-levels, high mid-level humidity to prevent cooling effects from evaporating downdrafts, low 850-200 hPa vertical wind shear and increased low-level absolute vorticity are mandatory conditions for TC genesis, but do not guarantee a formation (Briegel and Frank, 1997). These favorable conditions are widely met during the Atlantic hurricane season between June and November in the MDR, illustrated in Figure 2.1 by the red frame. It includes the tropical Atlantic Ocean and the Caribbean See.

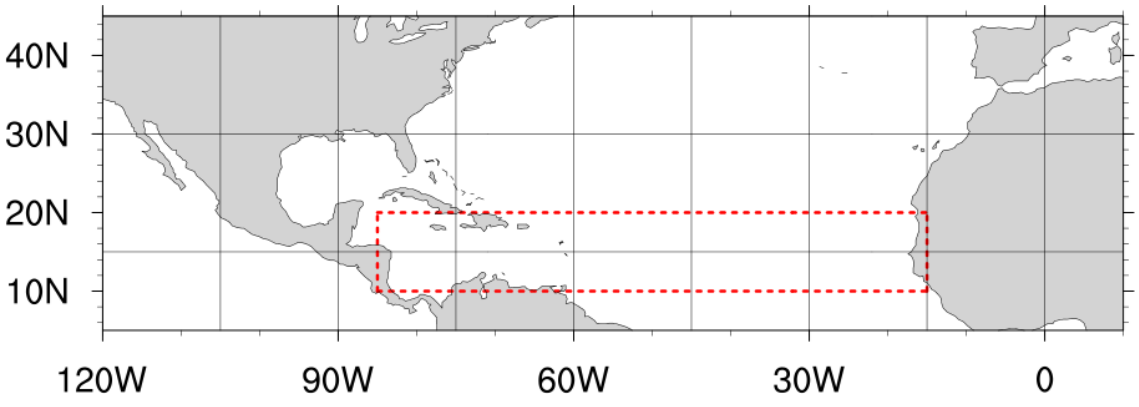

Figure 2.1: Main Developing Region in the tropical North Atlantic

There are several phenomena on the synoptic scale influencing the generation of TCs by modifying the surrounding mean flow. Some will be only briefly mentioned, whereas the important ones for this study are described in more detail subsequently. Wave-like disturbances can enhance both, low-level relative vorticity and organized deep convection, and also affect the environmental wind

field. Additionally, they have a significant impact on TC genesis (Ritchie and Holland, 1999). The Madden-Julian-Oscillation (MJO), an 40-50 days ongoing oscillation traveling eastward from the Indian Ocean (Madden and Julian, 1994), or equatorial Rossby waves can affect TC genesis on a larger scale by modifying the mean flow in which smaller waves are embedded. Especially waves that form over North Africa and propagate westward onto the Atlantic are accountable for about half the TCs developing in the Atlantic basin (Frank and Clark, 1980). The so-called African Easterly Waves are further explained in Chapter 2.1.1.

Another phenomenon that affects the Atlantic hurricane season is El Niño, which is part of the El Niño/Southern Oscillation ENSO. A strong El Niño event can affect the Atlantic hurricane activity negatively (Gray, 1984). Higher SSTs in the tropical eastern and central Pacific are associated with a strong El Niño event, which leads to enhanced deep cumulus convection in this area. This is linked to anomalously strong upper tropospheric westerlies over the Caribbean Sea and western tropical Atlantic. As a consequence, increased vertical wind shear occurs in this region. The number of hurricane days (maximum sustained wind speeds of more than 34 ms^{-1}) were correlated to El Niño events between 1900 and 1983. It was found that the highest numbers of hurricane days in a season took place in non-El Niño years. The opposite phenomenon is called La Niña and is characterized by cold SSTs in the central eastern Pacific and leads to reduced vertical wind shear in the Caribbean, which can enhance tropical cyclogenesis (Gray, 1984).

2.1.1 African Easterly Waves

Well before 1950, from Africa westward traveling disturbances already have been presented as precursors of Tropical Cyclones (TCs) (e.g. Piersig, 1936; Regula, 1936). Carlson (1969), for example, identified those disturbances as African Easterly Waves (AEWs), that form eastward of the Greenwhich meridian. The structure and origin of AEWs has been further analyzed by Burpee (1972), investigating data from eight African stations between 5-15°N for a period of 5 years (1960-1964). He confirmed Carlsons (1969) results of AEWs having a wavelength of 2000-4000 km and a period of 3-5 days. Furthermore, he found that AEWs occur between June and October and have their maximum values of relative vorticity near the 700 hPa level, where the African Easterly Jet (AEJ) occurs close to 10°N. The AEJ is a result from the temperature gradient between the hot Sahara in the north and the cooler tropics in the south. Barotropic-baroclinic instabilities of the AEJ provide AEWs with energy (Burpee, 1972). AEWs mostly have their origin north or south of the AEJ (Burpee, 1974). Propagating westward, the large majority of AEWs does not develop into TCs. However, about half of the seasonal TCs have their origin in AEWs (Frank, 1970). AEWs occur north and south of the AEJ. It is found that although the northern AEWs outnumber the southern AEWs by approximately 20%, the southern AEWs are more likely to develop into major hurricanes, because AEWs that form north of the AEJ are shallower and drier (Chen et al., 2008). Their maximum occurs underneath the jet level, close to 850 hPa. In Figure 2.2a the formation location of TCs that originated from AEW (red dots) and non-AEW (blue dots) is illustrated. The associated southern AEW (blue triangles) and

northern AEWs (red triangles) are shown in Figure 2.2(b), and Figure 2.2c respectively during the hurricane seasons of 1979-2006. The origin of the southern and northern AEWs are marked as blue and red open triangles respectively, as well as their trajectories before they strengthened to TCs (dashed lines). Superimposed on all pictures is the 925 hPa streamlines of July-September and the 600 hPa easterly jet core (black solid line).

2.1.2 Saharan Air Layer

The Saharan Air Layer (SAL) is an increased layer of Saharan air loaded with mineral dust, that occurs over the North Atlantic ocean in the MDR between the Sahara desert and the North American continent. It appears during the North African summer months and is supposed to affect the Atlantic hurricane activity negatively (Dunion and Velden, 2004). The increased layer consists of a very dry, well-mixed layer that can exceed 500 hPa. This layer is undercut by a layer of cool, moister low-level marine air and has its base near 850 hPa. Often associated with AEWs it can inhibit convection by enhancing the trade wind inversion. This is a result of the absorption of solar radiation by the mineral dust at its base. Low-level temperature inversions stabilize the lower troposphere and inhibit the vertical ascent of convective air masses. Another characteristic of the SAL is the enhanced lower vertical wind shear that is induced when the SAL's southern boundary is associated with the AEJ near 700 hPa. High vertical wind shear can lead to disruption of convection and affect tropical cyclogenesis negatively. The dry air masses in the lower- to mid-levels can intrude into the circulation of a convective system and lead to convective driven downdrafts that act against the ascending motion and therefore against further development of convective systems (Dunion and Velden, 2004). Despite the former mentioned, Braun (2010) hypothesizes that the SAL is not necessarily an inhibiting phenomenon, as mid-to-upper-level dryness is often a result of subsiding air, rather than a result of the SAL. He states, SAL's dryness concentrates in lower to mid-level up to 700 hPa and is characterized by moister air above 700 hPa. Another controversial aspect is that tropical storms often form at the southern boundary of the SAL where the AEJ can both enhance and inhibit further development Braun (2010).

2.1.3 Rossby Wave Breaking

Planetary- or Rossby Wave Breaking (RWB) is associated with tropopause folds where stratospheric air can irreversibly intrude into the troposphere (McIntyre and Palmer, 1983). Often the location of the tropopause is defined as a PV surface. There is no standard PV value, but from observations Haynes et al. (1995) defined the so-called dynamical tropopause as the 2 PVU surface (Potential Vorticity Unit, 1 PVU = $10^{-6} m^2 s^{-1} K\ kg^{-1}$). RWB is defined as a southward-directed reversed Potential Vorticity (PV) gradient of a certain strength (Baldwin and Holton, 1988). It occurs on the Northern and Southern Hemisphere between the mid-latitudes and subtropics. PV is dislocated from the Rossby wave and propagates poleward or equatorward (Postel and Hitchman, 1999). RWB is primarily strongly asymmetric and can be categorized into four categories, although symmetrical RWB can be observed as well. In Figure 2.3 the categories are illustrated. Rossby waves can break cyclonally and anticyclonically in both directions, poleward and equa-

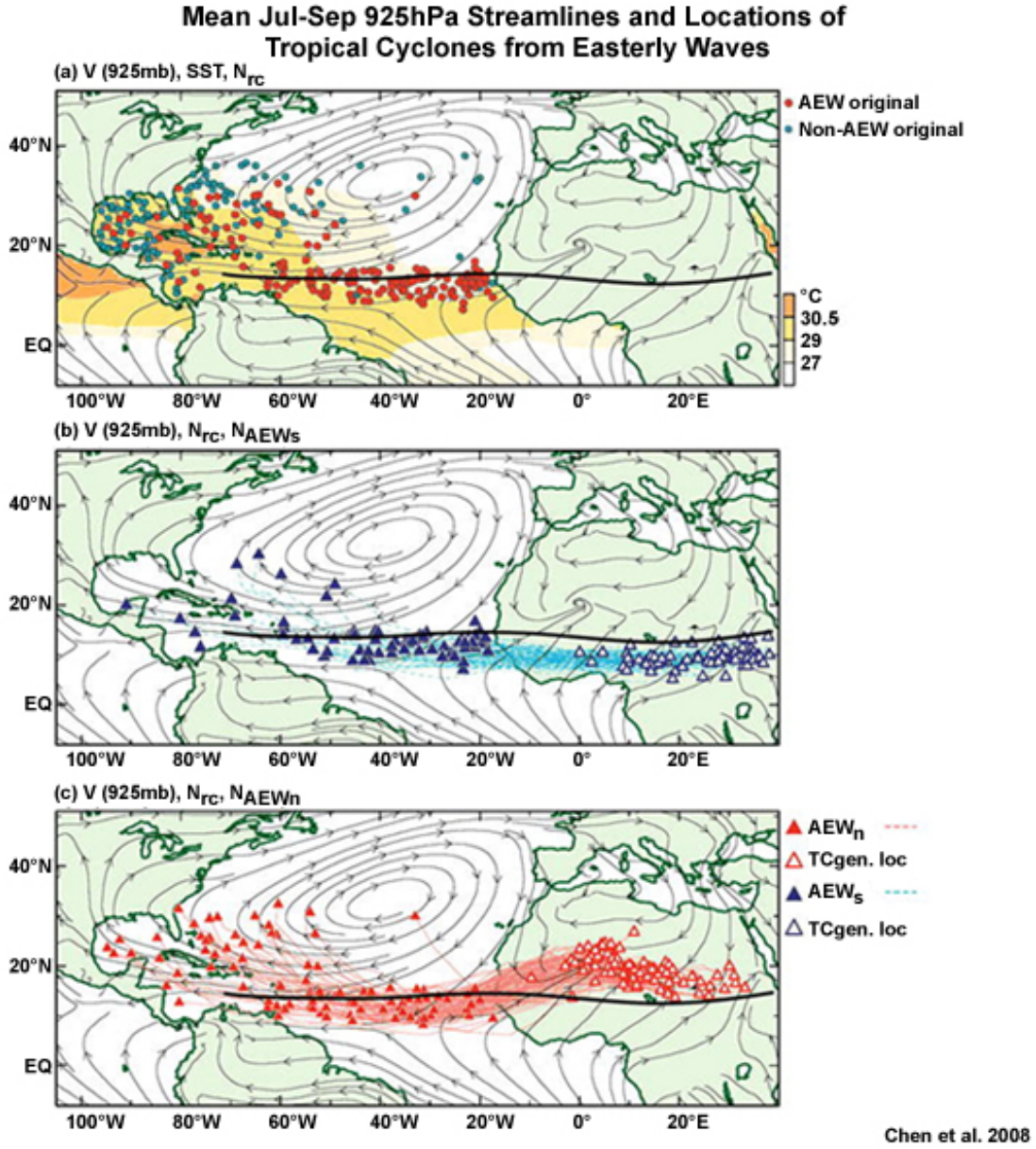

Figure 2.2: Mean 925 hPa streamlines of July-September superimposed with formation locations of TCs that originated from (a) AEW- (red dots) and non-AEW related processes (light blue dots), (b) southern AEWs (blue triangles) and (c) northern AEWs (red triangles) during the hurricane seasons of 1979-2006. Genesis locations of southern and northern AEWs are marked by blue and red open triangles respectively. Superimposed are their trajectories (dashed lines) before transforming into TCs. The 600 hPa easterly jet core (with isotach less than 7 ms^{-1}) is depicted with a thick solid line in all panels (Chen et al. (2008)).

torward. Rossby waves breaking cyclonically are specified as P1 when they break poleward and LC2, when they break equatorward. Anticyclonical breaking is specified as P2, when the direction is poleward and LC1, when they break equatorward (Gabriel and Peters, 2008).

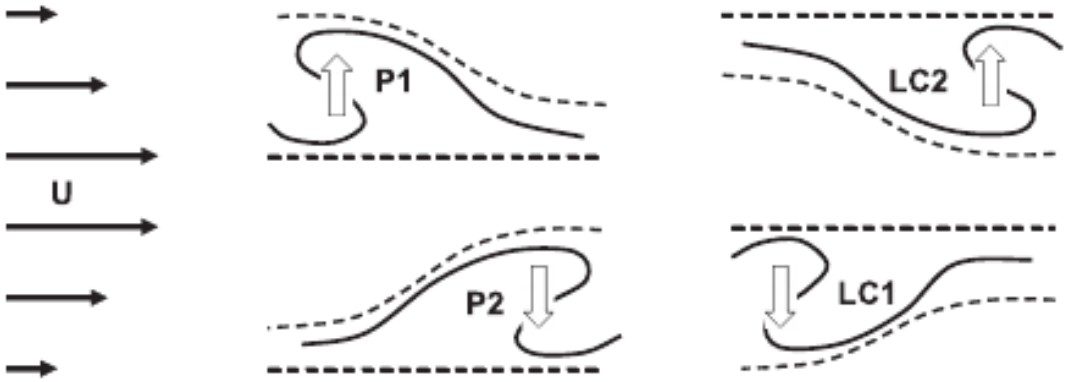

Figure 2.3: Idealized pictures of asymmetric RWB events in a horizontal plane indicated by potential vorticity (black lines): cyclonically sheared waves breaking predominantly in poleward (P1) or equatorward (LC2) direction, and anticyclonically sheared waves breaking predominantly in poleward (P2) or equatorward (LC1) direction; black arrows: westerly jet with horizontal shear; dashed lines: geopotential of a basic flow; and white arrows: meridional eddy fluxes down the gradient of the westerly jet (Gabriel and Peters, 2008).

With the folding tropopause, dry air from the stratosphere can intrude into the troposphere and form a layer of dry upper level air. Descending dry air from such tropopause folds is linked to both inhibition and enhancement of convection in the tropics. Convection is initiated and supported downstream of the PV outbreak where a high moisture gradient can be found (Allen et al., 2009; Funatsu and Waugh, 2008). Inhibition takes place within the dry air masses directly (Allen et al., 2009).

2.2 Current State of Research - Developing/Non-Developing African Easterly Waves

In the following, different factors that favor or penalize the intensification of AEWs to TC are presented (sorted by researches).

2.2.1 Hopsch et al., 2010

In this work, Hopsch et al. (2010) (HTHA10) used a 40 year Re-Analysis (ERA-40) dataset of the ECMWF and satellite brightness temperatures between July-September 1979-2001 to create a climatology of AEW structures originating over West Africa.
Identifying all AEWs that occurred in that time-span, HTHA10 found that the ratio of developers and non-developers differ strongly between July and August/September. In July, only one

in 16 AEWs developed, whereas in August and September one in four and one in five, respectively, AEWs developed. Besides fundamental parameters like warm SSTs and low vertical wind shear that favor development, different evolution of AEW structures were the main reason for development/non-development. HTHA10 hypothesized a scheme for developing/non-developing characteristics of AEWs. Both, developing and non-developing AEWs have a similar evolution before they arrive the coast of West Africa. Two days before reaching the coast, the AEWs have a distinctive cold-core structure and show convective activity over the Highlands of Guinea. Although the evolution is similar, non-developing AEWs show weaker amplitudes, weaker low-level circulations and less convection. Developing AEWs are characterized by a strong AEW trough, containing more intense Mesoscale Convective Systems (MCS), increased convective activity between the Guinean Highlands and the West African coast and intensified low-level vorticity. When developing AEWs reach the coast, their structure transformed to warm-core, whereas non-developing AEWs maintained a cold-core structure. Ongoing convection over the ocean in the developing AEWs leads to TC genesis, while the convection in non-developing AEWs decays. Another important factor of development is the dry air mass ahead of the AEW between the mid- to upper troposhpere. The analysis showed that non-developing AEWs had a stronger dry signal downstream. This is also the main factor why some of the most intense AEWs did not develop during the investigated period. Those AEWs were characterized by even stronger convection at the West African coast and higher vorticity in low-levels than developing AEWs, resulting in theoretically ideal conditions for development. However, HTHA10 hypothesized that a too intense dry air signal in mid- to upper-levels inhibited TC genesis and led to weakening of the convection over the ocean.

2.2.2 Arnault and Roux, 2011

Arnault and Roux (2011) investigated five seasons (July-September of 2004-2008) of TC genesis that took place in the eastern tropical Atlantic (east of 30°W) near the Cape Verde Islands. TCs with origin near the Cape Verde Islands were often more violent and long-lived, because they had more time to strengthen over warm ocean waters before decaying over land. Beside fundamental environmental conditions for TC development (e.g. low vertical wind shear and water temperatures above 26°C over a depth of 60m), it is vital for TC genesis that both, an intense AEW trough and a low-level cyclonic circulation, occurring near the West African coast in between the north-easterly trade winds and south-westerly monsoon flow, are present at the same time. Additionally, deep convection near the circulation center can support development and lead to a pressure decrease in the lower- to mid-levels. The anticyclonic flow corresponding with the upstream AEW ridge to the east, however, can negatively affect TC genesis, if it is intensified by mid-level anticyclonic Sarahan air. By stretching the evolving cyclonic structure north-westward, the associated deep convection, the vorticity perturbations and the mass field get disturbed to a point where further development is inhibited. A schematic view of the represented developing/non-developing conditions of AEW near the Cape Verde Island is shown in Figure 2.4.

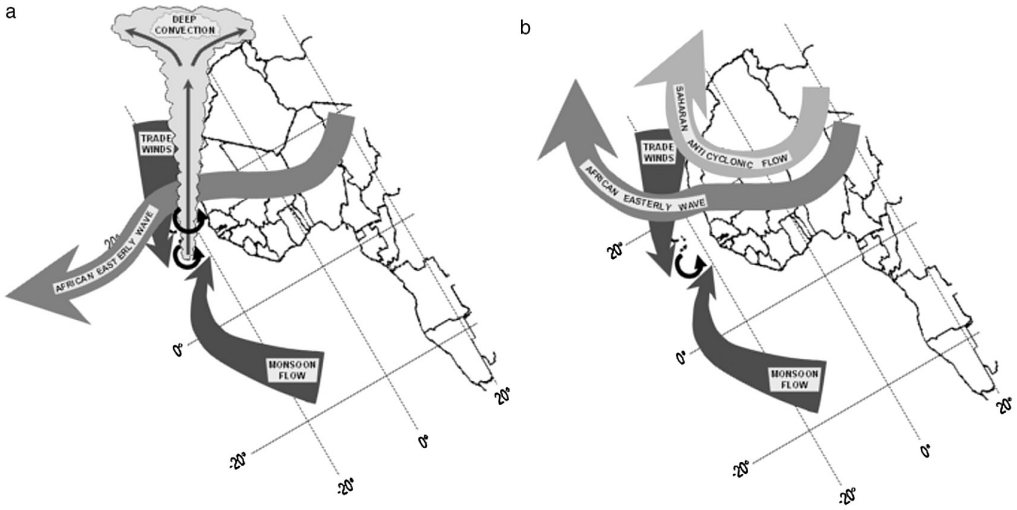

Figure 2.4: (a) successful and (b) failed Cape Verde tropical cyclogenesis, Arnault and Roux (2011)

2.2.3 Ross and Krishnamurti, 2007 and 2009

In contrast to many other studies, Ross and Krishnamurti (2007) focused on the structure of AEWs occurring near the 850 hPa level during June-October 2001. They found that two "wave regimes" exist northward and southward of the AEJ at low-levels. These regimes are somehow correlated to the vorticity maximum at 700 hPa south of the jet. However, they focused on the interaction of the northern and southern wave regime. Merging of the cyclonic vorticity centers of the wave regimes over the eastern Atlantic can lead to intensified wave patterns and eventually to development of the wave. In contrast, the convergence of the tracks of the vorticity centers only, can maintain the vorticity centers of both waves out of phase so that they propagate separately over the ocean. The last case, however, appeared more often than the rare case of two vorticity centers merging over the eastern Atlantic.

In a following study, Zipser et al. (2009) investigated the development of AEW regarding barotropic energy conversions during the NAMMA field program (NASA-African Monsoon Multidisciplinary Analysis). During the campaign they found that two of the AEWs showed positive barotropic energy conversion in combination with positive diabatic heating. This process occurred in waves that had a northeast-southwest tilt to the trough axis and at the same time maximum winds at the west side of the axis. The investigated non-developing wave had similar diabatic heating, but negative barotropic energy conversion, a northwest-southeast tilt and maximum winds at the east side of the trough axis.

2.2.4 Schwendike and Jones, 2010

Schwendike and Jones (2010) (SJ) focused on the question about how the synoptic scale interacts with the convective scale by comparing the different evolution of MCSs in one AEW during its movement over the West African continent and later over the eastern Atlantic in September 2006.

Using Consortium of Small-scale Modeling (COSMO) model runs, SJ found that the quickly increasing convection of the MCS over land developed ahead of the AEW trough. The tilted structure and strong downdrafts, due to mid-level dryness, resulted in distinct cold pools that propagated westward and supported the development of the MCS. As the MCS decayed, new convective bursts developed as the AEW moved over the eastern Atlantic. The environment was more favorable over the ocean, which led to ongoing convective bursts. But another MCS could only form as the AEW crossed the path of a secondary heat low, that separated earlier from the main heat low above the Sahara. The low level positive vorticity anomaly of the heat low supported the mid-level AEW relative vorticity and initiated stronger convection and increased cyclonic circulation that ultimately led to the development of hurricane Helene.
A, from the main Saharan heat low separated, secondary heat low that moves southwest onto the eastern Atlantic, can trigger convection in AEW troughs, when the AEW moves over the low-level cyclonic circulation of the heat low. This process can eventually lead to further development of an AEW.

2.3 Tropical Cyclone Seasonal Forecasts

In the following a definition of Atlantic hurricane season activity and the scheme used by the Colorado State University (CSU) for the seasonal forecast will be presented.

2.3.1 Definition of Atlantic Hurricane Season Activity

Every year seasonal predictions for the upcoming Atlantic hurricane season are released by several national meteorological services. National Oceanic and Atmospheric Administration (NOAA) Climate Prediction Center (CPC) issue their first outlook for the season at the end of May.
NOAA's yearly Atlantic hurricane season outlook is of the probabilistic kind and officially produced by hurricane scientists from the National Hurricane Center (NHC) and the Hurricane Research Divison (HRD). NOAA's given activity range has a likelihood of 70%, implying that 7 out of 10 seasons with similar conditions fall within the given activity range.

NOAA and the Colorado State University categorize the seasons according to their deviation from the mean activity level of the years 1981-2010. The 30-year average consists of 12.1 named storms (max. 1-minute surface wind of 39-73 mph (~63-118 km/h)), whereof 6.4 develop into hurricanes (max. 1-minute surface wind of at least 74 mph (119 km/h)) and 2.7 become major hurricanes. (max. 1-minute surface wind of exceeds 111 mph (~179 km/h)).

$$ACE = 10^{-4} \sum v_{max}^2. \tag{2.1}$$

ACE is defined as the sum of the maximum sustained wind speeds (in knots) taken at 6-hourly intervals for all tropical storms ($v_{max} \geq$ 35 kts (65 km/h)) and is an index for the overall activity during a season (Bell et al., 2000). ACE aggregates to an 30-year average of 92.5.

NOAA uses the combination of the number of named storms, hurricanes and major hurricanes and the ACE index to rate the seasonal forecast into above normal, near normal and below normal.
An above normal season distinguishes by an ACE index of 120% or more of the average, at least 13 named storms, whereof 7 become hurricanes and 3 develop into major hurricanes.
A near normal season distinguishes by an ACE index of 71.4-120% of the average and the average number of storms.
A below normal season distinguishes by an ACE index of less than 71.4% of the average, or a maximum of 9 named storms, whereas 4 or less become hurricanes and only one or none develops into a major hurricane (NOAA, 2015).

2.3.2 Theory behind the Extended Range Forecast of Atlantic Seasonal Hurricane Activity by Klotzbach and Gray

Being part of the Tropical Meteorology Project from the Colorado State University, Dr. Phil Klotzbach and Prof. William Gray feature the CSU's yearly seasonal hurricane forecasts. They provide seasonal Atlantic hurricane forecasts with extended range in April as well as updates in early June at the beginning of the Atlantic hurricane season and in early August, which marks the beginning of the main hurricane season. Their forecasts are based on statistical prediction schemes that have been developed since the early 1980s using the data of past years as a basis of a reliable hindcast model. Statistical models using data of past years are based on the assumption that a future atmosphere behaves as the atmosphere has been behaving in the past. The main focus is on the Net Tropical Cyclone (NTC) Activity in contrary to NOAA's outlook that focuses on the ACE parameter.

$$NTC = (\%NS + \%NSD + \%H + \%HD + \%MH + \%MHD)/6 \tag{2.2}$$

Season's percentage mean of Named Storms (NS), Named Storm Days (NSD), Hurricanes (H), Hurricane Days (HD), Major Hurricanes (MH) and Major Hurricane Days (MHD) are averaged to the NTC and give one single parameter for the activity of a hurricane season based on all parameters (Gray et al., 1994).

3. Data and Methods

In the following, the workflows and methods applied in this work are explained. The C3Workflows were embedded in the project C3-INAD (Towards an INfrastructure for general Access to climate Data) that took place from October 2010 until September 2013 and were used to calculate the integrated precipitable water content, potential vorticity and troughs. A general method for tracking analysis was employed to track AEWs (Thorncroft and Hodges, 2001) and the Lagrarian Analysis Tool version 2.0 was used to calculate backward trajectories of air masses (Sprenger and Wernli, 2015). For the workflows and the tracking program ERA-Interim data was used. The ERA-Interim dataset (Dee et al., 2011) comes from a global atmospheric reanalysis from 1979 by the European Centre for Medium-Range Weather Forecasts (ECMWF). The horizontal grid spacing is $\approx$ 80 km (T255 spectral) on 60 vertical levels from the ground up to 0.1 hPa.

3.1 Qflux

For climatological analysis of the humidity balance it is important to know whether storms occurring in the tropics, subtropics or midlatitudes have the ability to produce heavy precipitation as a result of high water vapor content in the atmosphere. The diagnostic workflow "Qflux" calculates the integrated humidity flux in kg m^{-1}s^{-1}, the integrated humidity flux convergence in mm day^{-1} and the integrated precipitable water in kg m^{-2} to investigate air masses regarding their humidity balance.

$$\vec{Q} = \frac{1}{g} \sum_{p_b}^{p_t} q \cdot \vec{v} \cdot \Delta p. \tag{3.1}$$

For calculation of the integrated humidity flux vector (3.1) the two-dimensional windfield $\vec{v}$, the temperature and the specific humidity q on discrete pressure levels is used. The summation of the horizontal humidity flux over selected pressure levels (bottom-level p_b to top-level p_t) results in the vertical integrated humidity flux. The convergence of the integrated humidity flux represents sources and sinks of the humidity flux. Positive values (here convergence) often result in precipitation. It is calculated in spherical coordinates between discrete grid points.

To use this workflow it is necessary to provide the parameters (temperature, two-dimensional wind field and specific humidity) on discrete pressure levels. It is possible to select the pressure levels for integration, the time period and the region that shall be investigated. An output file is created with the data of the integrated humidity flux, its divergence and the precipitable water for

the selected pressure level, time period and region. GrADS is used to plot the time-average of the integrated humidity flux and its divergence. An example can be found in Figure 3.1.

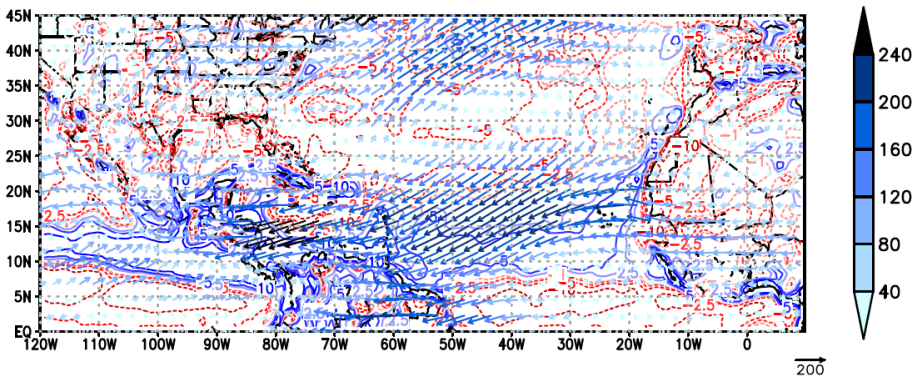

Figure 3.1: Time-averaged -integrated humidity flux in kg $m^{-1}s^{-1}$ (contour) and -integrated humidity flux convergence in mm day^{-1} (vectors) averaged over 600-850 hPa (August - October 2013)

3.2 Trough Identification

Troughs are usually correlated with cyclogenesis and precipitation. The workflow "Trough Identification" is a tool for through identification in different heights. An algorithm to detect troughs, their troughaxis and troughaxispoints is used, based on the analysis of a east-west gradient of geopotential height on a discrete pressure level (e.g. 300 hPa) after Knippertz (2004).

$$TP(P) = \overline{Z_1 + Z_3} - \overline{Z_2} \tag{3.2}$$

After taking the average over three gridpoint boxes (Z_1 (3x5); Z_2 (3x4); Z_3 (3x5)) at a discrete pressure level, the Trough-Parameter (TP) at the center P of Z_2 is calculated (see Fig. 3.2). The trough parameter represents the zonal geopotential height gradient. Given that a threshold of 25 gpm is exceeded, P is identified as TroughPoint (TP). A trough point that is located along a longitudinal range of troughpoints and has a maximum value, is designated as a Trough Axis Point (TAP). If several TAP are longitudinal not further away than 2 grid points (5°), the TAPs are denoted as Trough Axis (TA). For using the workflow, a file with the parameter geopotential height or geopotential on a discrete pressure level is needed. It is then possible to choose the period and region that shall be analyzed. The data is cut to the chosen time period, region and pressure level with Climate Data Operators (CDOs) and used in the workflow. The output file contains the TP, TAP and TA for every timestep, the mean TP and TAP, the total and relative distribution of troughpoints and TAPs. Exemplarily, plots of the relative distribution of troughpoints (Fig. 3.3) and TAPs (Fig. 3.4) are illustrated with GrADS.

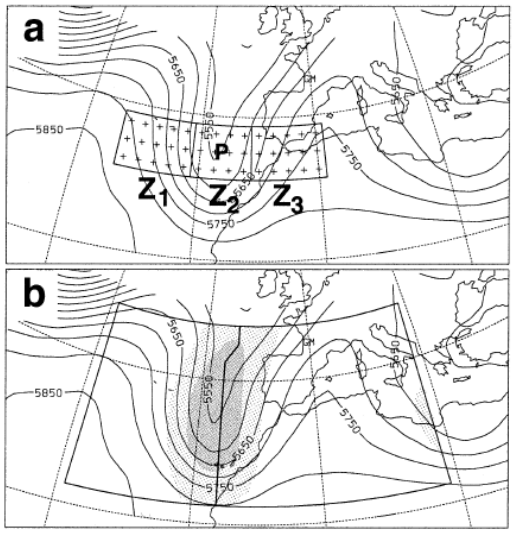

Figure 3.2: Illustration of the trough axis definition. (a) gridpoint boxes, (b) horizontal distribution of TP for underlaid real example (19 December 1992 12 UTC; light shading: TP >25 gpm, dark shading: TP >100 gpm) (Knippertz, 2004)

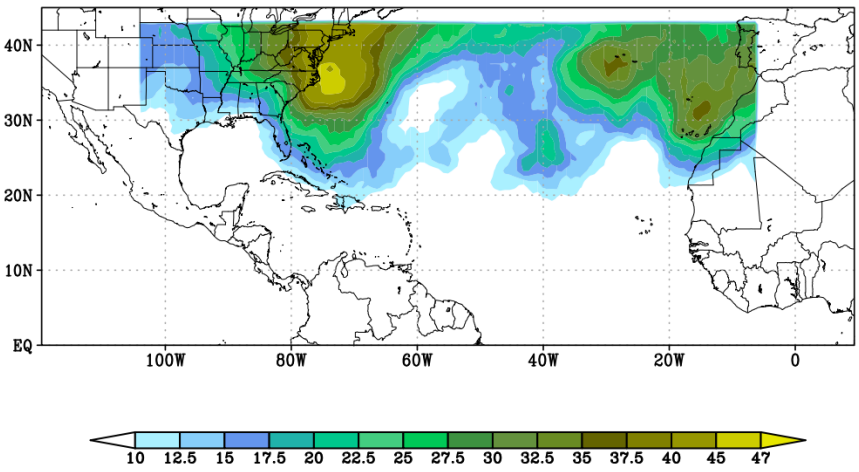

Figure 3.3: Relative frequency of troughpoints in the August-October 2013 period in % at 300 hPa.

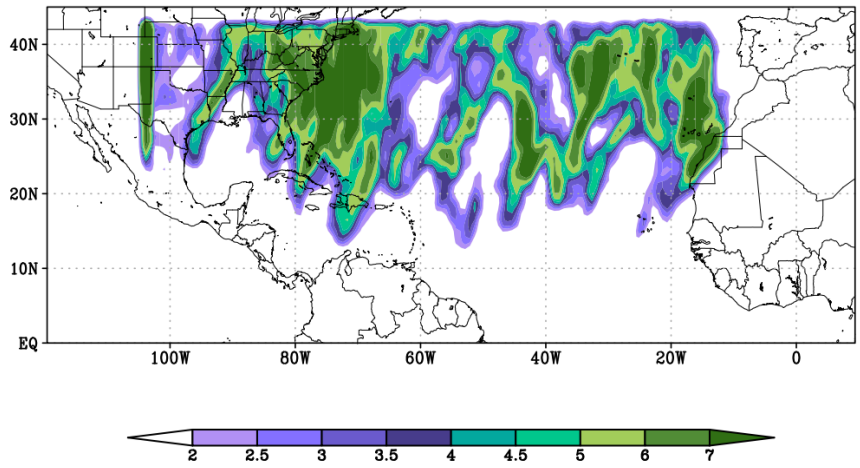

Figure 3.4: Relative frequency of troughaxispoints in the August-October 2013 period in % at 300 hPa.

3.3 Potential Vorticity

Troughs that expand from the mid-latitudes to the subtropics or even to the tropics can cause heavy precipitation and are correlated with numerous dynamical processes in the lower latitudes. In chapter 3.2, a workflow for trough identification is presented. For identifying troughs in the subtropics or tropics, however, this workflow is not suitable due to the small geopotential gradient occurring in lower latitudes. The workflow "Potential Vorticity" therefore uses the Potential Vorticity (PV) that shows a stronger gradient in the lower latitudes. The applied algorithm after Fröhlich and Knippertz (2008), can analyze both, the PV on a discrete pressure level (e.g. 500 hPa, 400 hPa) and the PV averaged over several pressure levels (Vertical Averaged PV (VAPV);e.g. 100-400 hPa). A file containing the PV or for calculation of PV necessary parameters of relative vorticity, temperature and the three dimensional wind field. The time period, region and pressure levels can be chosen at the beginning. To detect a PV-trough, a threshold of the PV value has to be exceeded. A threshold of +2.0 PVU is used (after definition of the tropical tropopause). The procedure identifies connected areas of PV $\geq$ 1.5 PVU between the equator and 25°N. Those areas are called PV-trough if they also fulfill the following criteria: 1. the southermost point of this area must be located 17.5°N or lower and 2. the area has to cover more than $15^{2\circ}$. Identifying PV-troughs from vertical averages is useful to analyze e.g. the humidity flux as it is correlated to the vertical expansion of a PV-trough. The workflow calculates time series of PV-troughs, their depth and their tilt that are stored on three-dimensional fields. In addition climatological properties e.g. the frequency of PV-troughs or length of their appearance are calculated. Examples are visualized with GrADS. Figure 3.5 shows the relative frequency of the PV-troughs, the time-averaged PV within the troughs is illustrated in Figure 3.6. The time-averaged -length of their appearance , -tilt and the -depth of the troughs are shown in Figure 3.7(a),(b) and (c), respectively.

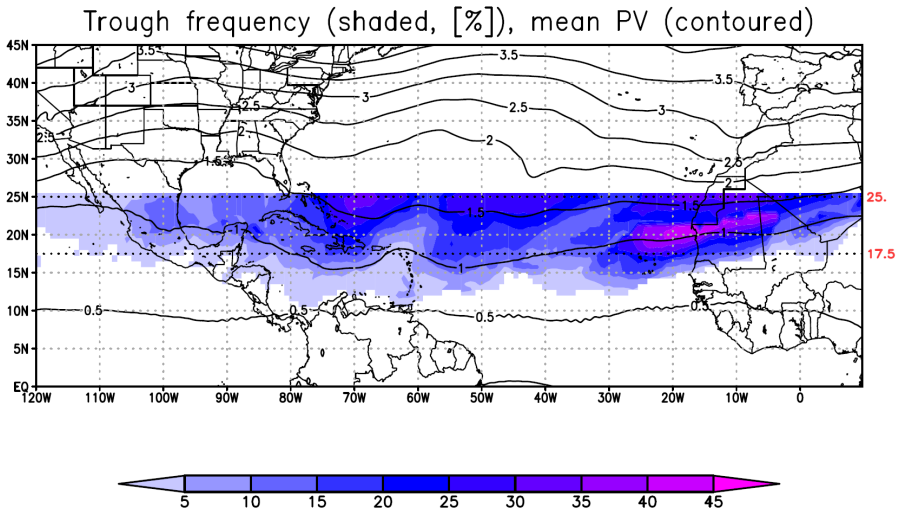

Figure 3.5: Relative Frequency of PV-troughs in % between 100-400 hPa and 25°N <= 17.5°N (August - October 2013).

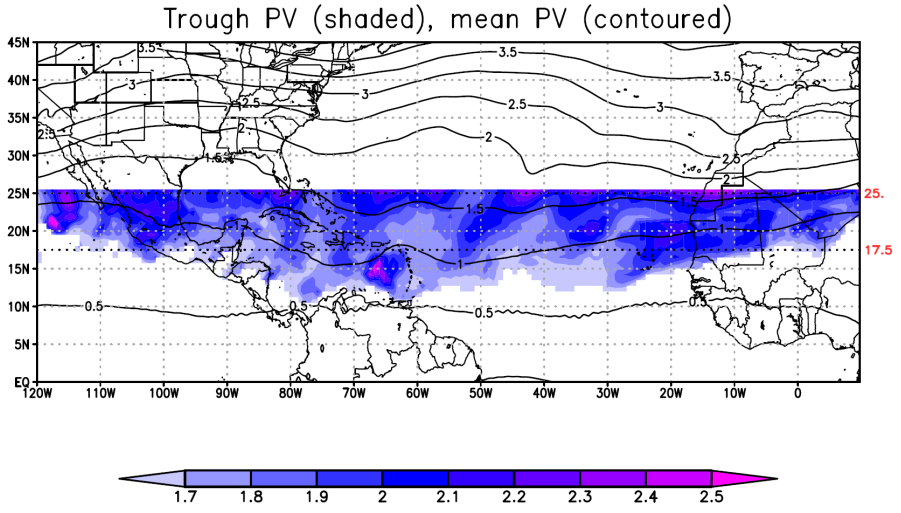

Figure 3.6: Mean PV of PV-troughs in PVU between 100-400 hPa and 25°N <= 17.5°N (August - October 2013).

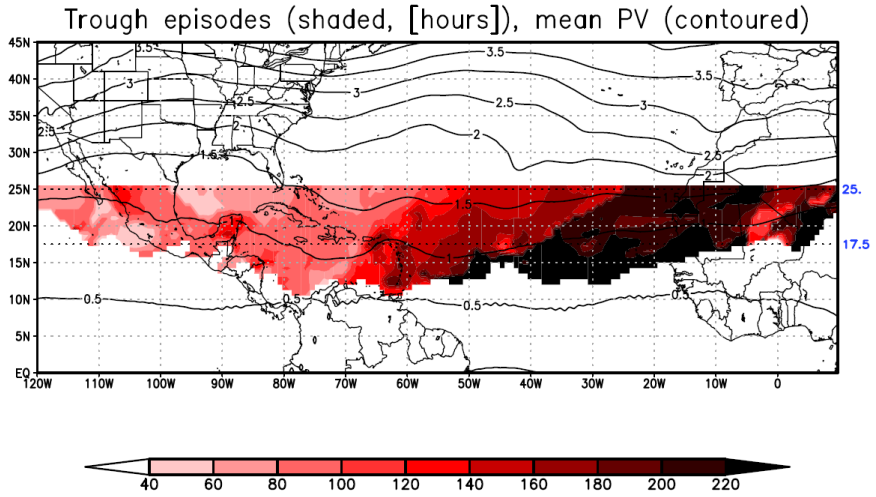

(a)

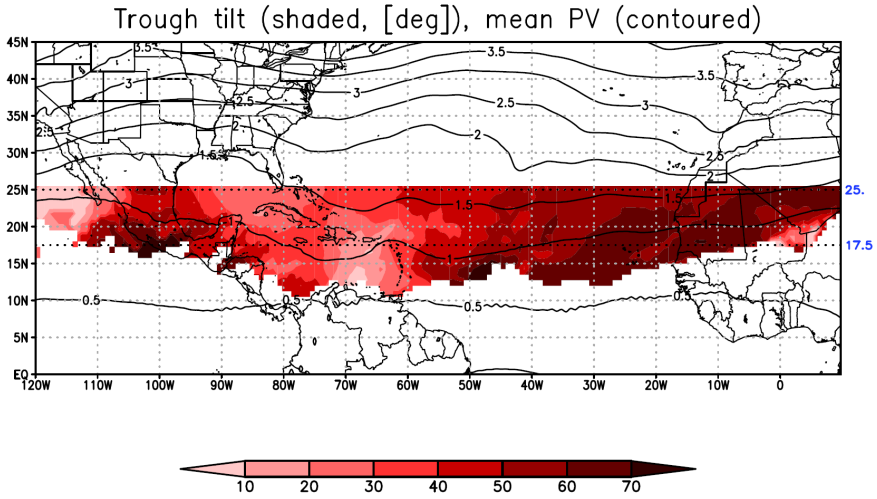

(b)

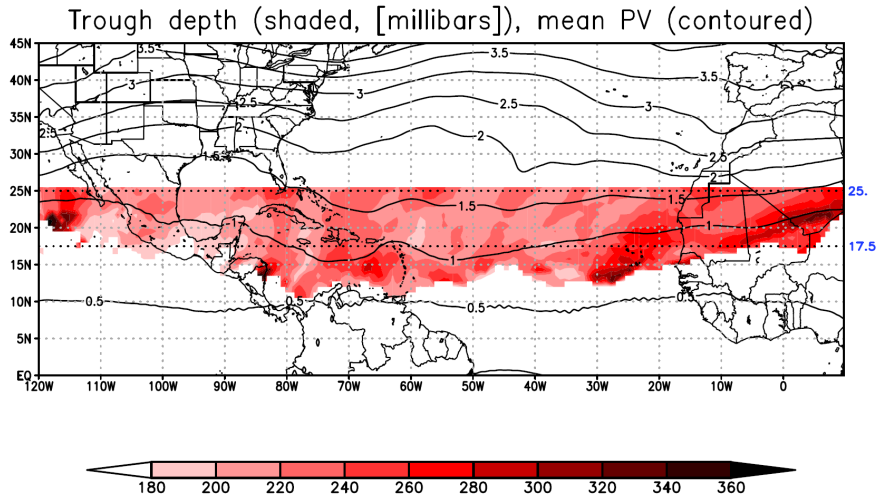

(c)

Figure 3.7: a) Mean lenght of appearance of PV-troughs in hours b) Mean tilt of PV-troughs in ° towards the meridian, positive clockwise c) Mean vertical depth of PV-troughs in mb - all between 100-400 hPa and 25°N <= 17.5°N (August - October 2013).

3.4 Methods for the Climatological Analysis

For the climataological analysis the anomalies of various atmospheric parameters were calculated by subtracting the arithmetic mean of a one, three or six months of the 31-year period from 1983-2013 from the corresponding arithmetic mean of the considered year.

$$ano_{p,t} = \overline{p_t} - \overline{p_T} \tag{3.3}$$

$$\overline{a_i} = \frac{1}{n}\sum_{i=1}^{n} a_i \tag{3.4}$$

Whereas in (3.3) p represents the atmospheric parameter on a lat-lon grid, t is the chosen period of time of one year and T the same period of time of 31 years. $ano_{p,t}$ stands for the anomalies of p in the time period t. The definition of the arithmetic mean can be found in (3.4).

$$\sigma = \sqrt{\frac{1}{n}\sum_{i=1}^{n}(p_i - \overline{p})^2} \tag{3.5}$$

To measure the significane of the anomalies, the anomalies were normalized with the climatological standard deviation σ of the 31-year time period (3.5). $\overline{p}$ is the arithmetic mean of one, three or six months of the years 1983-2013 on a lat-lon grid, p_i is the parameter on the lat-lon grid for one single timesteps and n denotes the number of timesteps used.

The normalized anomalies were measured in σ. The higher the σ values were, the more significant was the anomaly. Anomalies with low σ values were less significant, because the values have been more common in the 31-year time period.

3.5 Tracking Analysis Method

An automatic tracking method was developed (Hodges et al., 1994) to investigate atmospheric phenomena objectively and in a larger extent for a better statistical examination and comparison. In this work, ERA-Interim datasets were used to track positive relative vorticity centers, which are hereafter defined as AEW tracks. All AEWs in the June-November period, which were tracked for the 700 hPa level as AEW, tend to have their maximum relative vorticity values near the AEJ level. In case that the positive relative vorticity maxima exceeded a threshold of $+0.5{\cdot}10^{-5}\mathrm{s}^{-1}$ and had closed vorticity contours, an AEW was detected. The AEWs were tracked by minimizing a cost function, which is defined according to local speed and direction changes, to find coherent motion subjects. Using a threshold, stronger waves have been selected automatically. Waves that existed less than two days or traveled less than 10° ($\approx$ 1000 km) have been filtered as well (Thorncroft and Hodges, 2001).

3.6 Lagrangian Analysis Tool 2.0

For the case studies in Chapter 5, the tracked AEWs were investigated and some were chosen for further examination with the Lagrangian Analysis Tool Lagranto developed by Sprenger and Wernli (2015). With this tool it is possible to calculate forward and backward trajectories from a distinct starting point employing gridded wind fields, that originate from reanalysis or numerical model simulations. Lagranto basically solves the following trajectory equation numerically

$$\frac{D\vec{x}}{Dt} = \vec{u}(\vec{x}). \tag{3.6}$$

HERE, $\vec{u}$ is the three dimensional wind vector and $\vec{x}$ the location.
It can be used for different research areas e.g. cloud microphysics, orographic flows or the qunatitative analysis of moisture sources and transport, as the output files contain, besides the location in a lat/lon grid and pressure values, values of temperature, relative humidity and specific humidty.
In this work, Lagranto was applied to calculate five day backward trajectories from a starting point that was chosen as the start of a tracked AEW. The pressure course and the moisture content were investigated to find the origin of the air masses present at the starting point.

4. Forecasts of the Atlantic Hurricane Season and Climatological Study

In this Chapter, a climatological study of the hurricane season 2013 is presented. Starting with the forecasts for the season from the National Oceanic and Atmospheric Administration (NOAA) and the Colorado State University (CSU), the analysis of different hurricane related parameters will be discussed afterwards.

4.1 North Atlantic Hurricane Season 2013

Tropical Storm Risk (TSR, University College London) issued their first forecast in early December 2012, predicting an above normal season. An update followed in early April 2013, correcting the forecast minimally but still calling for an above normal season. Other services, including the CSU, released their first outlooks between the beginning of April and the end of May 2013. All released outlooks predicted an above-normal hurricane season (HRD, 2013) as well. During the ongoing hurricane season 2013, some of the services updated their outlook, though still predicting an above-normal season.

30 November 2013 marked the end of the second most quiet Atlantic hurricane season regarding the number of hurricanes on record since 1950. In contrary to the majority of seasonal forecasts, the season terminated as a below normal season.

4.1.1 NOAA's Outlook

In the following, the forecast for the hurricane season 2013 by NOAA will be presented. NOAA's annual forecasts are based on a combination of predicted large-scale climate factors that can affect the hurricane season and climate models. The tropical multidecadal signal consisting of the Atlantic Multidecadal Oscillation (AMO) that changes modes every few decades and influences the Atlantic SSTs, and the West African monsoon system, affecting precipitation in West Africa and atmospheric features (e.g. vertical wind shear and the strength of the Easterlies). Hence, AMO is one important large-scale climate factor. Other important factors are the anomaly of SSTs in the MDR in particular and the El Niño Southern Oscillation (ENSO) affecting the SSTs on the

tropical eastern Pacificr and thereby also the tropics and subtropics to a certain extend.

Climate models from various institutes (amongst others, the NOAA Climate Forecast System (CFS), the European Centre for Medium Range Weather Forecasting (ECMWF) and the EUROpean Seasonal to Inter-annual Prediction ensemble (EUROSIP)) predict the SSTs anomalies in the MDR and the ENSO index for the oncoming hurricane season directly (NOAA, 2013).

The tropical multidecadal signal has been showing high activity since 1995, favoring hurricane genesis with higher SSTs, weaker vertical wind shear and a wetter West African monsoon. Additionally, positive SSTs anomalies and a neutral ENSO index pointed to an above normal hurricane season.
In combination with the different model forecasts, NOAA expected a likelihood of 70% for an above normal season with the range of parameters found in Table 4.1. The other 30% consisting of 25% likelihood for a near normal season and only 5% likelihood for a below normal season (NOAA, 2013).

Table 4.1: List of predicted TCs for the hurricane season 2013 by NOAA

Parameter	**1981-2010 Mean**	**May 23rd 2013**	**August 8th 2013**
Named Storms	12.1	13-20	13-19
Hurricanes	6.4	7-11	6-9
Major Hurricanes	2.7	3-6	3-5
ACE	92.5	120%-205%	120%-190%

4.1.2 Extended Range Forecast of Atlantic Seasonal Hurricane Activity by Philip J. Klotzbach and William M. Gray (CSU)

In this section the forecast of the CSU will be presented. The four predictors used for the extended range forecast of the seasonal Atlantic hurricane activity (cf. Chapter 2.3.2) by Klotzbach et al. (2013) are shown in Figure 4.1.
(1) April-May SSTs in the region 15-55°N 15-35°W,
(2) April-May 200 hPa horizontal wind component u in the region 0-15°S 150°E-120°W,
(3) ECMWF May 1st SST forecast for September Nino 3 system in 5°S-5°N 90-150°W and
(4) May SLP (20-40°N, 30-50°W).
(1) and (2) and (3) have been favorable for hurricane development. Positive SST anomalies were found during April-May in the eastern Atlantic ocean, resulting in weaker vertical wind shear due to weaker upper tropospheric westerlies and weaker trade winds near 850 hPa and lower sea level pressure based on a weaker subtropical high. Ultimately, positive SST anomalies during springtime are associated with positive SST anomalies during the main hurricane season from August to October (ASO). Positive anomalies of 200 hPa level zonal winds near the south central

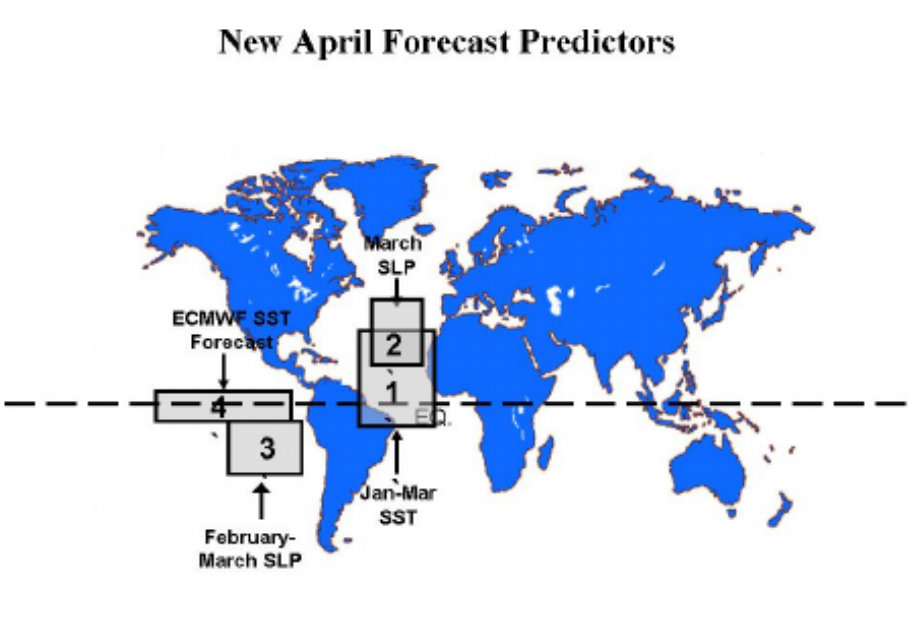

Figure 4.1: Location of four predictors used in the April extended range forecast of the CSU (Klotzbach et al., 2013)

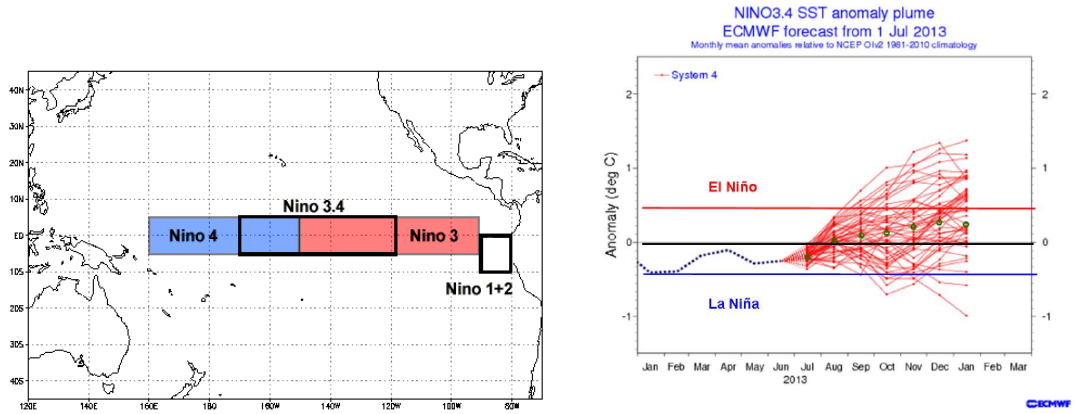

Figure 4.2: Left panel: Location of the Nino regions in the Pacific ocean (http://www1.ncdc.noaa.gov/pub/data/cmb/teleconnections/nino-regions.gif). Right panel: ECMWF ensemble model forecast for the Nino 3.4 region (Klotzbach and Gray, 2013c).

Pacific ocean indicate a predominant La Niña event, inhibiting a transition to an El Niño event. Positive anomalies are also correlated to higher SSTs, low sea level pressure and weaker wind shear. Negative SST anomalies in the eastern-central Pacific are associated with a La Niña event and correlated to weaker vertical wind shear specifically in the Caribbean Sea and eastern central Pacific (Klotzbach and Gray, 2013b) The ensemble forecast from the ECMWF for the Nino 3.4 region (Figure 4.2(a)) shows the range of possible outcome scenarios for the ongoing ENSO oscillation in Figure 4.2(b). The average of the ensemble members is ~0.2°C and stays within the neutral El Niño range, which means that no enhanced vertical wind shear is supposed to occur in the Caribbean (Gray, 1984).

Table 4.3: List of TCs during the hurricane season 2013

Highest Category	Name	Date	Maximal winds [kt]/ lowest SLP [mb]	ACE
TS	Andrea	June 5-7	55 kt / 992 mb	1.5
TS	Barry	June 17-20	40 kt / 1003 mb	0.6
TS	Chantal	July 7-10	55 kt / 1003 mb	2.1
TS	Dorian	July 23- August 3	50 kt / 1002 mb	2.6
TS	Erin	August 15-18	40 kt / 1006 mb	1.1
TS	Fernand	August 25-26	50 kt / 1001 mb	0.7
TS	Gabrielle	September 4-13	50 kt / 1003 mb	1.9
TD	Eight	September 6-7	30 kt / 1008 mb	-
H-1	Humberto	September 8-19	80 kt / 979 mb	8.8
H-1	Ingrid	September 12-17	75 kt / 983 mb	4.8
TS	Jerry	September 29 - October 3	45 kt / 1005 mb	1.7
TS	Karen	October 3-6	55 kt / 998 mb	2.4
TS	Lorenzo	October 21-24	45 kt / 1000 mb	1.7
TS	Melissa	November 18-21	55 kt / 980 mb	0.5
SS	Unnamed	December 5-7	45 kt / 997 mb	-

The condition of the predictors led to an above normal hurricane season activity, giving a similar range of TC parameters as NOAA's outlook. In the August update, the values of the TC parameters were slightly reduced, but still indicated an above normal season (Table 4.2).

Table 4.2: List of predicted TCs for the hurricane season 2013 by the CSU

Parameter	1981-2010 Median	April 10th 2013	June 3rd 2013	August 2nd 2013
Named Storms	12.0	18	18	18
Named Storm days	60.1	95	95	84.25
Hurricanes	6.5	9	9	8
Hurricane Days	21.3	40	40	35
Major Hurricanes	2.0	4	4	3
Major Hurricane Days	3.9	9	9	7
ACE	92.5	165	165	142
Net Tropical Cyclone Activity [%]	103	175	175	150

4.2 Climatological Analysis of the Atlantic Hurricane Season June-November 2013

The analysis of the Atlantic hurricane season 2013 will be discussed in this section. Tropical Storm (TS) Andrea marked the start of the hurricane season 2013 at 5 June. During the season a total of 13 named storms, one Tropical Depression (TD) and one Subtropical Storm (SS) developed. The exact dates, maximal sustained winds, lowest sea level pressure and ACE value can be

found in Table 4.3 and the storm tracks are illustrated in Figure 4.3.

The number of named storms just hit the range of predicted named storms in NOAA's outlook (Chapter 4.1.1). Only two named storms could reach hurricane status and did not exceed the intensity of category 1 (max. sustained wind speeds of 119-153 km/h). The low number of hurricanes, the absence of major hurricanes and an ACE index of only 36 marked the forecast bust of this hurricane season. Overall, the hurricane seasons activity was below normal and one of the weakest seasons ever recorded since 1950.

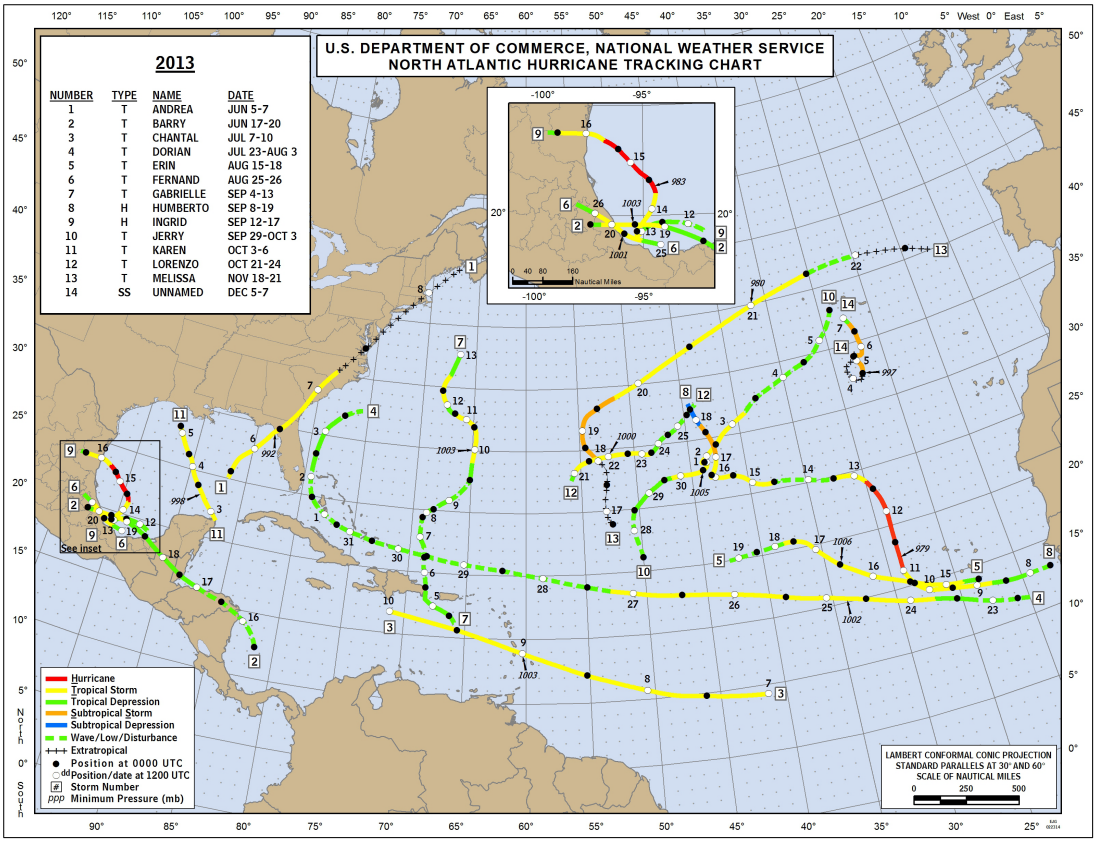

Figure 4.3: Tracks and intensity of the Tropical Cyclones during the hurricane season 2013, (http://www.nhc.noaa.gov/data/tracks/tracks-at-2013.png).

4.2.1 Parameter Anomalies regarding the 31-year Average between 1983-2013

In the following, a climatological study of the Atlantic hurricane season is presented to review the predicted environmental conditions in the MDR. Klotzbach and Gray (2013b) indicated that the predictors for the season in 2013 were similar to predictors of other above normal activity seasons including the strongest Atlantic hurricane season 2005. Hence, the parameter anomalies of the season 2005 are depicted for comparison. As the season 2013, however, turned out to be one of the quietest seasons ever, the anomalies of the even more quiet season of 1994 are illustrated for comparison as well. To give a better overview about the seasons, Figure 4.4 shows the storm

tracks of the season 1994 and 2005 respectively. The tracks of the hurricane season 2013 are shown in Figure 4.3.

The anomalies were calculated for the six-month period of the whole season June to November, as well as for the August-September (ASO) period. To analyze the ASO period in greater detail, the anomalies of the months August, September and October were examined individually.

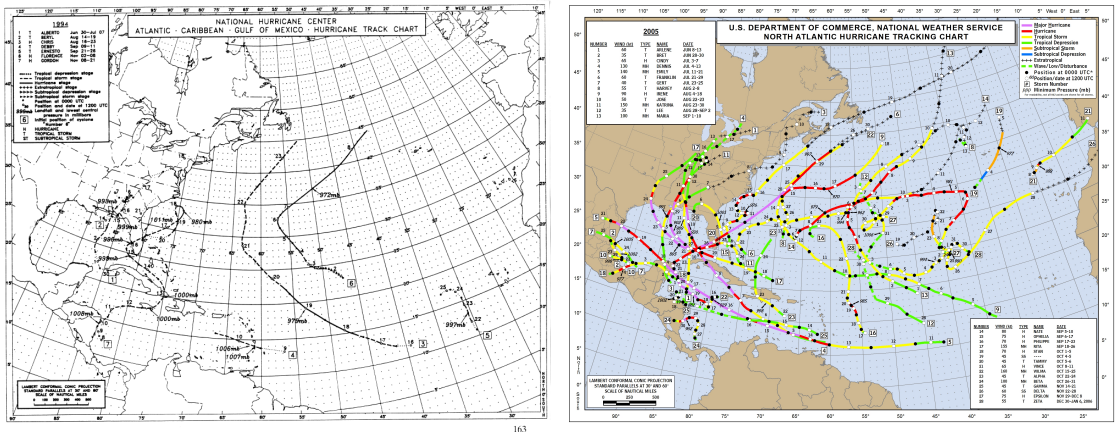

(a) **1994** (b) **2005**

Figure 4.4: Tracks and intensity of the Tropical Cyclones during the season 1994 (a) and 2005 (b), http://www.nhc.noaa.gov/archive/storm_wallets/atlantic/atl1994/tracks94.gif, http://www.nhc.noaa.gov/data/tracks/tracks-at-2005.png.

4.2.2 Sea Surface Temperature and Vertical Wind Shear

In this section, the SST anomalies, the average vertical wind shear as well as the vertical wind shear anomalies are discussed.

The Entire Hurricane Season June to November

The SSTs for the Hurricane Season 2013 from June until November were between 0.2-0.4 K colder than the 31 year average in the eastern MDR (except close to the West African Coast) and slightly higher than average west of 45°W (Figure 4.5(a), shaded contour). The significance ranges between $\pm 1\ \sigma$ (Figure A.4(a)) and gives no indicator for exceptional anomalies for the six-month time period. The overall higher SSTs, that were determined in early spring in 2013 (cf. Chapter 4.1.2), did not continue to increase as rapidly as predicted. Especially the eastern MDR stayed cooler as expected, which is a possible reason for the reduced TC activity in the season of 2013.

Looking at the six-month SST anomalies of the seasons 1994 and 2005, the differences to the anomalies of the season 2013 are significant. In 1994, the entire MDR region showed negative SST anomalies of -0.2 K up to values around -0.6 K (Figure 4.5(b)). Especially in the central

MDR (15-20°N 30-60°W), the significance of the negative SST anomalies ranged between 2-3 σ (Figure A.4(b)). The positive SST anomalies in the season of 2005 (Figure 4.5(c)) are even more significant with values of 3 σ around 18°N 60°W (Figure A.4(c)). The negative SST anomalies in 1994 extremely reduced the latent heat and were one reason why this season was extremely quiet. In contrast, the strong positive anomalies in 2005 enhanced tropical cyclogenesis.

Given that the vertical wind shear anomalies do not act as direct indicator of enhanced or oppressed hurricane development, the average vertical wind shear is discussed first. In 2013, the values ranged between 8-16 m s^{-1} in the MDR (Figure 4.5(a), contour lines). Only wind shear below 8 m s^{-1} (dotted region) is considered to be favorable for TC genesis. Hence, the vertical wind shear was too strong on average to favor the genesis of TCs. The vertical shear anomalies were overall positive in the MDR (Figure A.4(a)). Near the Caribbean Sea, the anomalous vertical wind shear values exceeded +2 m s^{-1}. Especially the high wind shear in the Caribbean Sea was poorly predicted. According to the forecast of neutral El Niño conditions, the vertical wind shear should have been reduced in this region. The prediction of the El Niño index, however, was correct. Only the reducing effect on the vertical wind shear was not forecasted. The high values of vertical wind shear acted strongly inhibiting in the Caribbean.

The averaged vertical wind shear pattern in 1994 (Figure 4.5(b)) resembles the averaged pattern of the season 2013, but was nearly 2 m s^{-1} weaker than the values in 2013. Especially the eastern MDR showed weaker vertical wind shear than the season in 2013. This is also visible looking at the shear anomalies of the season 1994, where the eastern MDR shows negative values up to -2 m s^{-1} (Figure A.4(b)). The vertical wind shear did overall not affect this season negatively. The averaged wind shear in season 2005 (Figure 4.5(c)) had broader regions with shear values below 8 m s^{-1}. Especially in the Caribbean Sea, the values were significantly lower than in the seasons 1994 and 2013. This can also be seen in negative shear anomalies of up to -6 m s^{-1} in the western MDR with a significance between -0.5-1.5 σ (Figure A.4(c)). The low vertical wind shear therefore was another enhancing environmental condition for this season.

Main Hurricane Season from August to October

The SST anomalies were more significant (Figure A.5) in the ASO period for all investigated seasons, than they were for the entire season. This leads to the assumption that the months June, July and November acted compensatory for the six-month average in all seasons.

For the ASO period in 2013 (Figure 4.6(a)), stronger positive SST anomalies were present in the western and central MDR up to 35°W, with a slightly increased significance (Figure A.5(a), shaded contour). Looking at only the three-month period, the SSTs were not an inhibiting parameter anymore.

Both, the main season of 1994 and of 2005 (Figure 4.6(b) and (c)) showed higher negative and

positive SST anomaly values respectively, with an increased significance in the central MDR for the ASO period of 1994 (Figure A.5(b)) and near 60°W for the ASO period of 2005 (Figure A.5(c)). That supports the assumption that the SST anomalies have been an important factor for the outcome of the hurricane activity in 1994 and 2005.

The averaged vertical wind shear was nearly decreased by 50% in the ASO period of 2013 compared to the entire season in Figure 4.5(a) with a broader region of favorable shear in the eastern MDR and Gulf of Mexico. The maximum of averaged shear shifted from the central and eastern MDR in June-November 2013 to the western MDR near the Caribbean Sea in the main season of 2013 (Figure 4.6(a)), creating more favorable conditions for TC genesis in the eastern MDR and therefore for Cape Verde hurricanes to develop. Nine from 14 named storms developed during the ASO period, whereof eight developed in regions with an average vertical shear below 8 m s^{-1}.

In the main season of 2005, the averaged shear became more favorable as well (Figure 4.6(c)). Only the main season of 1994 did not differ much compared to the averaged shear of corresponding entire season (Figure 4.6(b)). The values of the shear anomaly did not show any greater differences compared to the particular six-month time period.

Monthly Discussion of the Main Hurricane Season

In August 2013, distinctive negative SST anomalies could be found in the eastern MDR and the Caribbean Sea. Only a smaller region between 50-70° was slightly higher than average. These anomalies, however, were not significant for this month in comparison with the 31-year average. In the North Atlantic both, significant negative anomalies (-2 σ) in the eastern part and significant positive anomalies (+2-3 σ) in the western and central North Atlantic could be found (Figure A.6). One tropical storm developed in the Gulf of Mexico where positive SSTs were present and one storm developed in the eastern MDR despite the negative SST anomalies (Figure A.1(a)). Overall, the season in 2013 has been quiet until then. The average vertical wind shear was below 8 m s^{-1} in a narrow band of about 5° extension from the West African Coast to the Coast of South America (Figure A.1(a), contour lines), but still anomalously higher than average. In the Caribbean positive shear anomalies, however, were significantly high for this month (Figure A.6), whereas the anomalies in the whole MDR were only slightly positive. The SST and the vertical wind shear had a negative influence on tropical genesis in this month (Figure A.1(a)).

In September 2013 (Figure A.2), similar patterns of SST anomalies (shaded contour) compared to August 2013 could be found. The SST anomalies were more distinct in September though, amplifying the anomalies by values between 0.2-0.6 K throughout the MDR. Especially in September 2013, the anomalies became positive in a wider range of the MDR with a maximum near the northern coast of South America. The averaged vertical wind shear (contour lines) was widely favorable for TC genesis in the MDR in September 2013 (Figure A.2), only over the Caribbean

more significant positive shear anomalies with values up to +1.5 σ occurred (Figure A.8). However, hurricane Ingrid developed in the Gulf of Mexico in September despite an averaged high vertical wind shear. During the development of Ingrid, lower vertical wind shear was present in the Gulf of Mexico. The other three named storms, including the second hurricane Humberto, developed east of 70°W (Figure 4.3), where the SSTs and vertical wind shear were enhancing on average.

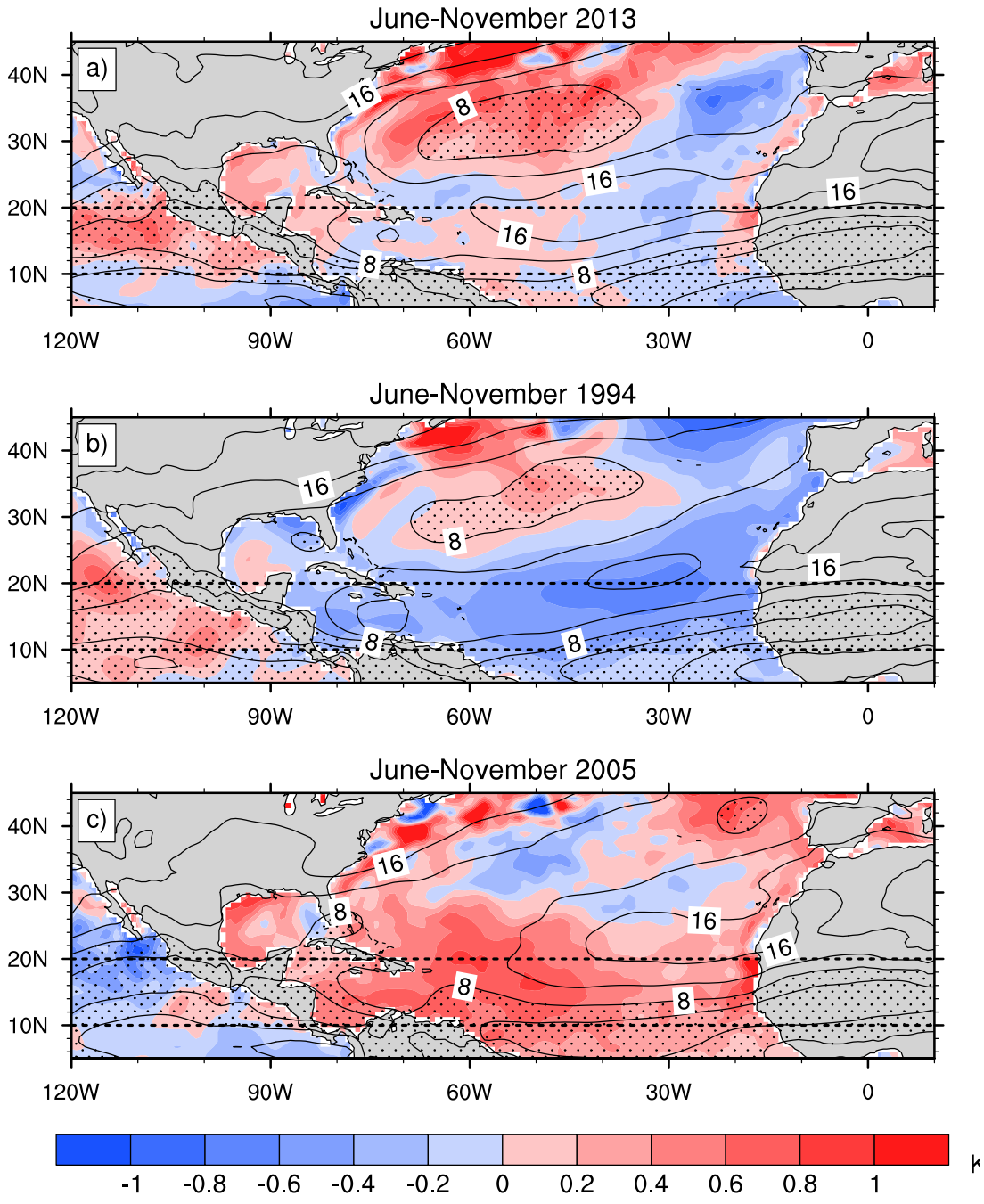

Figure 4.5: SST anomaly in K (shaded contour) and average vertical wind shear in m s^{-1} (contour lines) from June to November. Dotted regions indicate averaged wind shear below 8 m s^{-1}.

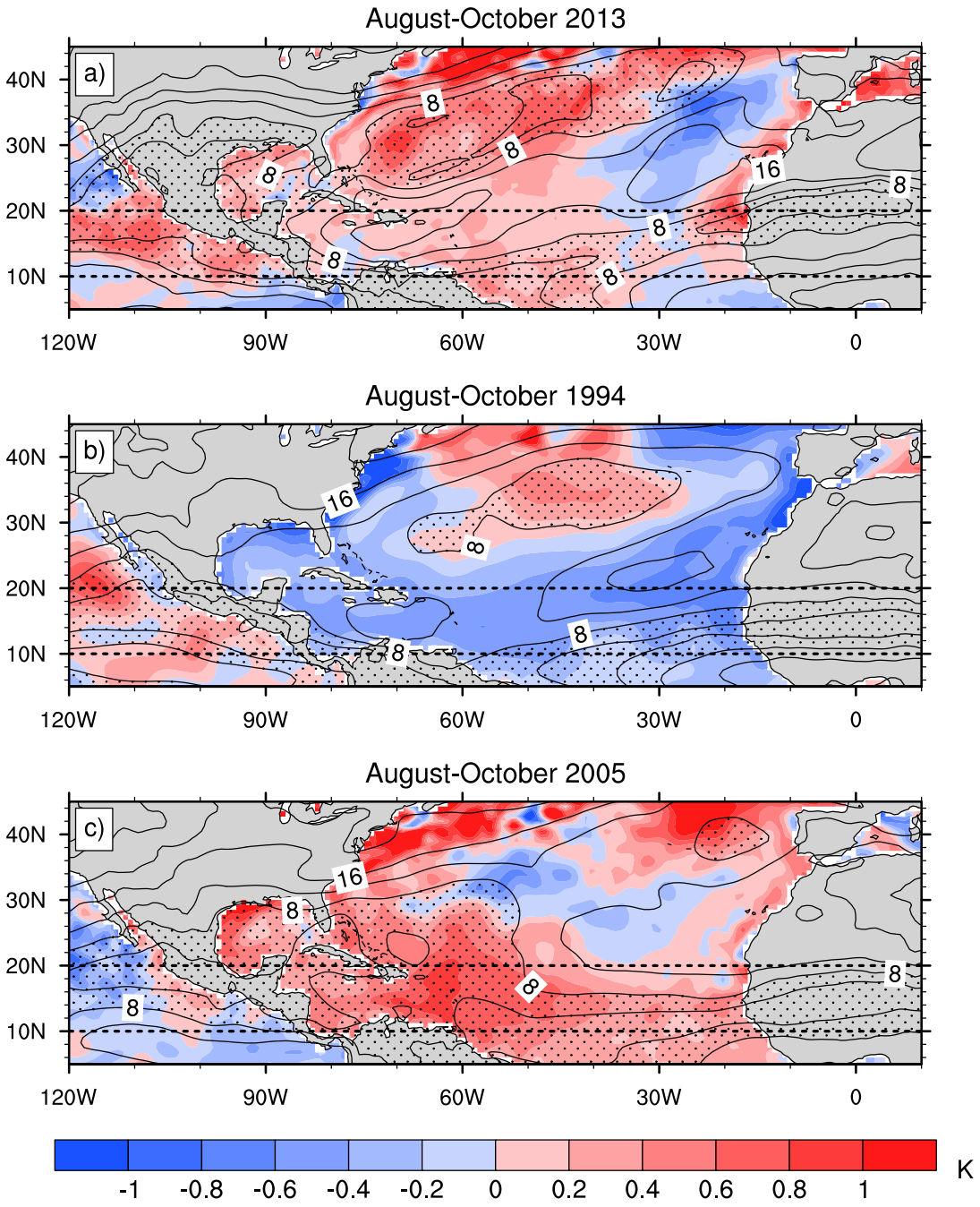

Figure 4.6: SST anomaly in K (shaded contour) and average vertical wind shear in m s^{-1} (contour lines) from August to October. Dotted regions indicate averaged wind shear below 8 m s^{-1}.

In October 2013, the positive SST anomalies continued to increase in the central tropical Atlantic (Figure A.3), which was significant for this month (Figure A.7). The averaged vertical shear naturally increased again in October 2013(Figure A.3), but was significantly low (up to -1 σ) in the central tropical Atlantic (Figure A.9). Combined with unusual high values of SST, tropical storm Lorenzo could form in this area on 21 October 2013 5° north of the MDR.

Summarizing the effect the SSTs and vertical wind shear had on tropical cyclogenesis, it was found that the SST anomalies were positive in the entire MDR for the six-month hurricane season in 2013. Sole exception was a smaller region in the eastern MDR. In the ASO period of 2013 the SST anomalies were overall positive for the months September and October for the MDR and therefore not a reason for the quiet outcome. In contrast, in the season of 1994 the strongly negative SST anomalies throughout the entire MDR were an inhibiting factor for tropical cyclogenesis. In 2005, the strongly positive SSTs were anomalously high and affected the Atlantic hurricane activity positively.
The increased vertical wind shear in the Caribbean during the entire season of 2013 inhibited TC genesis in this region. In the season of 1994, the vertical wind shear did not play a strong role in suppressing the hurricane activity. In 2005, the reduced values of vertical wind shear in the western MDR affected tropical cyclogenesis positive.

4.2.3 Troughpoints and Sea Level Pressure

'Troughpoint' is a parameter calculated by the C3Workflow 'Troughident' and defines the position and quantity of troughs (cf. Chapter 3.2). The troughpoints were calculated for the 300 hPa level and in the following, the troughpoint anomalies and the sea level pressure anomalies are presented. It is to note that troughs are much more variable than the SST, which only change slowly. Hence, the averaged and anomaly values are smaller. The same applies for the sea level pressure, although this quantity does not vary as much as propagating troughs. Standardized anomalies did not show any significance due to the large variance of these parameters for being part of weather patterns.

The Entire Hurricane Season June to November

For the period June to November, the troughpoint anomalies were not very significant for all three years (Figure 4.7). However, some structures could be found even for the six-month period of the complete hurricane seasons. The faint structure of a wave pattern can be seen in the season 2013 (Figure 4.7(a), shaded contour), where positive and negative troughpoint anomalies alternate. Positive anomalies were present, spreading from the east coast of North America down to the Caribbean, as well as near 40°W in the subtropical Atlantic and near the West coast of Africa. This means that in these regions troughs were present more frequently than in the other regions. Negative anomalies mark the regions where, by trend, more ridges were present during that period. In 2013, negative anomalies could be found in the Gulf of Mexico, near 60°W and most distinctively near 30°W in the subtropical Atlantic. In the regions with predominantal high pressure impact, upper level convergence lead to sinking motions. Subtropical air masses can be easily advected into tropical regions as a result of the anticyclonic flow and influence tropical convection.

A similar wave pattern could also be found in 1994, but with higher wavelengths (Figure 4.7(b)),

shaded contour). Also in 1994, a distinct negative anomaly marks the eastern part of the tropical and subtropical Atlantic, promoting anticyclonic flow of subtropical air masses into the tropics. Whereas in 2005 (Figure 4.7(c)), positive anomalies were strongly present in the central MDR and subtropical Atlantic, as well as in the eastern subtropical Atlantic.

The sea level pressure anomalies were negative in the entire MDR for the hurricane season 2013 (Figure 4.7(a), contour lines). In the subtropical region however, the anomalies were positive (dotted regions). This indicates that primarily higher pressure was present in that region. The positive anomalies had their maximum near the east coast of North America, which is only about 5° east of the distinct positive troughpoint anomaly and supposes that the negative sea level pressure anomalies and positive trough anomalies in the 300 hPa level are not necessarily correlated. The negative sea level pressure anomalies in the MDR favored tropical cyclogenesis.

In 1994, the sea level anomalies were to the greatest possible extent positive over the entire tropical and subtropical Atlantic (Figure 4.7(b), contour lines, dotted regions). Negative anomalies could only be found over the west African coast and the North American continent. This might be another possible reason for the quiet outcome of this season. Just the opposite could be observed in 2005, when there were even stronger negative sea level pressure anomalies present in the entire MDR and subtropical region. Their maximum could be found in the subtropical Atlantic just above the MDR near 55°W (Figure 4.7(c)). Although the anomalies were quite distinct, especially in 1994 and 2005, the values showed no greater significance as the anomalies fall into the range of variance of the 31-season period (not shown). Hence, these two seasons are not further investigated in the troughpoint and sea level pressure analysis.

Main Hurricane Season from August to October

During the ASO period, the troughpoint anomalies were more distinct but still not more significant. There were two conspicuous maxima of negative troughpoint anomalies over the subtropical Atlantic in the main season 2013 (Figure A.10, shaded contour). This strengthens the assumption that, in the three-month period, a comparatively little number of troughs was present in the subtropical region, as well as near the Gulf of Mexico. Near the east coast of North America, primarily troughs that stretch into tropical regions existed, as the anomaly was strongly positive.

A strong negative sea level pressure anomaly was present in the eastern MDR and the northwestern African coast in the main season 2013 (Figure A.10, contour lines). The positive anomalies were concentrated on the subtropical region and North America. This tightens the assumption that primarily high pressure systems have been present in the subtropical region, which enhanced upper level convergence.

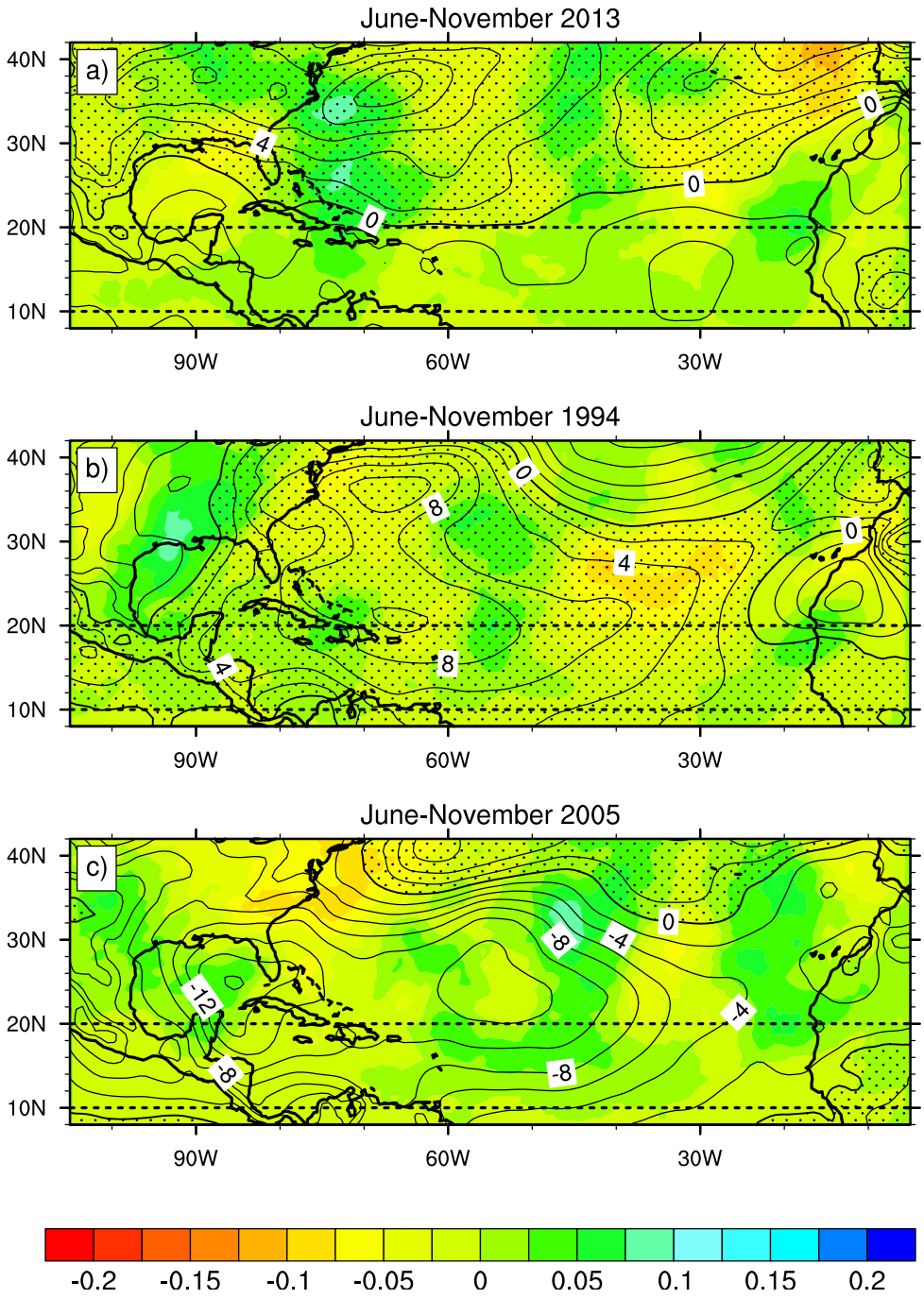

Figure 4.7: Troughpoint anomaly at 300 hPa (shaded contour) and surface pressure anomaly in 10^{-1} hPa (contour lines) from June to November. Dotted regions indicate a positive sea level pressure anomaly.

Monthly Discussion of the Main Hurricane Season

In the monthly breakdown, it can be seen that in September (Figure 4.8) and October 2013 (Figure A.12), the negative troughpoint anomalies were most distinctive in the subtropical region (shaded contour). During this two-month period, by trend, more high pressure systems existed just north of the eastern and central MDR. In August (Figure A.11) and September 2013 (Figure 4.8), the same wave pattern could still be found, whereas in October 2013 (Figure A.12) it was less distinctive. The negative anomaly was present near the east coast of North America with different amplitudes during the entire ASO period.

In August 2013 (Figure A.11), negative sea level pressure anomalies were present in the MDR with lower values up to -1.2 hPa and values around -2 hPa over the north-western African coast. In September 2013 (Figure 4.8), strongly negative sea level pressure anomalies could be found near the east coast of North America with values beyond -2 hPa and lighter negative anomalies over the MDR with values up to -1 hPa. In October 2013 (Figure A.12), mainly positive sea level pressure anomalies were present. Especially in September, but also in August, the sea level pressure acted enhancing for tropical cyclogenesis. The negative troughpoint anomaly however, was one inhibiting factor for tropical cyclogenesis as primarily ridges were present over the subtropical Atlantic and could advect dry air from the subtropics into the MDR.

Upper level troughs that extend into the tropics are called Tropical Upper Troposphgeric Troughs (TUTT) (Sadler, 1967). With their cyclonal air current they initiate a westerly flow at their southern edge in the upper troposphere. The trade winds in the lower levels, however, are easterly flows. Hence, a TUTT intensifies vertical wind shear in the troposphere at its southern edge. In the season of 2013, vertical wind shear was increased by the existing TUTT stretching from the east coast of North America to the Caribbean Sea (Figure 4.7(a) and Figure A.10), which can be confirmed by the increased vertical wind shear in the Caribbean during the ASO period (Figure 4.6(a)). This anomalous wave pattern has been found in the quiet season of 1994 as well. Blunden and Arndt (2014) found that the Atlantic hurricane season of 2013 and 1994 have been the only seasons in which this wave pattern occurred to this extent. In 1994, a strong El Niño was present, whereas in 2013 this was not the case. Additionally, no correlations could be found to other hurricane related parameters (Blunden and Arndt, 2014).

4.2.4 Specific Humidity and Relative Vorticity

In the following section, the specific humidity anomalies in 700 hPa, as well as the relative vorticity anomalies in 850 hPa will be discussed. For the examination of humidity, the specific humidity was chosen as it is not dependent on temperature and pressure. Especially the mid-level humidity is important for tropical genesis. Hence, the 700 hPa level was investigated. The relative vorticity anomalies did not show any significant abnormality. Furthermore, the relative vorticity is strongly coupled to pressure systems. In the tropics, the primarily occurring pressure systems are tropical

disturbances that eventually can develop into tropical cyclones. Averaging the relative vorticity over a long period of time and finally calculating the anomalies only indicate where these systems occurred more often in the investigated time period according to the average. For this reason, the relative vorticity anomalies are only displayed once for the Entire Hurricane Season from June to November. Relative vorticity is not an environmental condition, but rather a pressure system related parameter that is nevertheless important for tropical cyclogenesis.

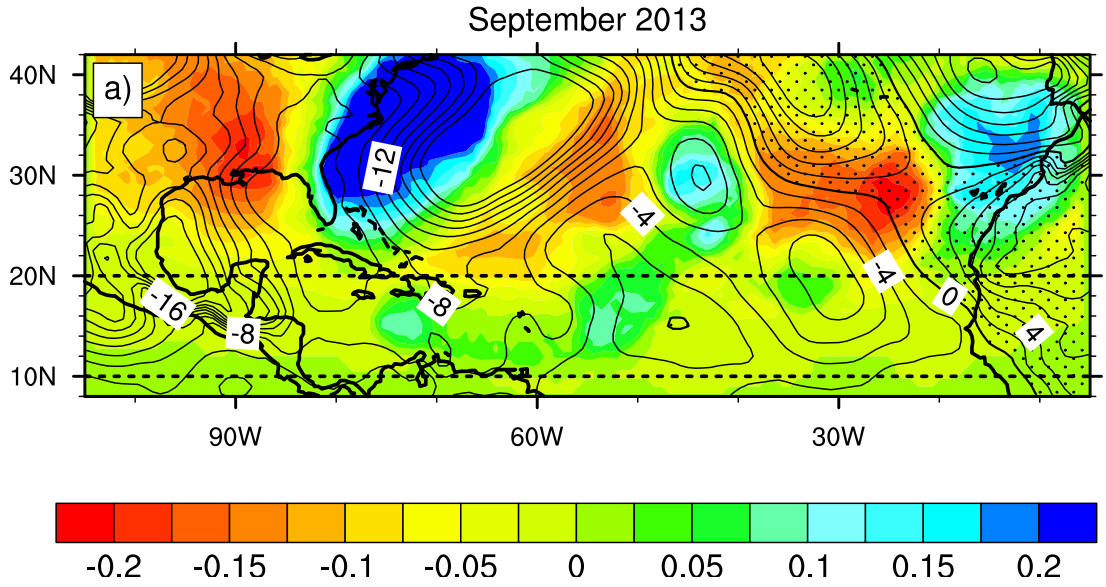

Figure 4.8: Troughpoint anomaly at 300 hPa (shaded contour) and surface pressure anomaly in 10^{-1} hPa (contour lines) from August to October 2013. Dotted regions indicate a positive sea level pressure anomaly.

The Entire Hurricane Season June to November

The specific humidity has been slightly lower than average in the central MDR during the hurricane season 2013 (Figure 4.9(a), shaded contour). In the eastern MDR and in the Gulf of Mexico the specific humidity anomaly was positive. The dry air masses that existed in the central MDR on average affected the tropical cyclogenesis strongly negative, whereas the moister air enhanced tropical genesis. The dry air is supposed to be the main reason for the quiet season 2013 (Klotzbach and Gray, 2013a). Looking back at the storm tracks in Figure 4.3, it is obvious that most of the storms formed in the moister air masses in the eastern MDR and near the Gulf of Mexico. Dry air masses were also present between the subtropics and mid-latitudes east of 40°W, whereas the subtropical region just above the MDR was primarily moister averaged over the Entire Hurricane Season.

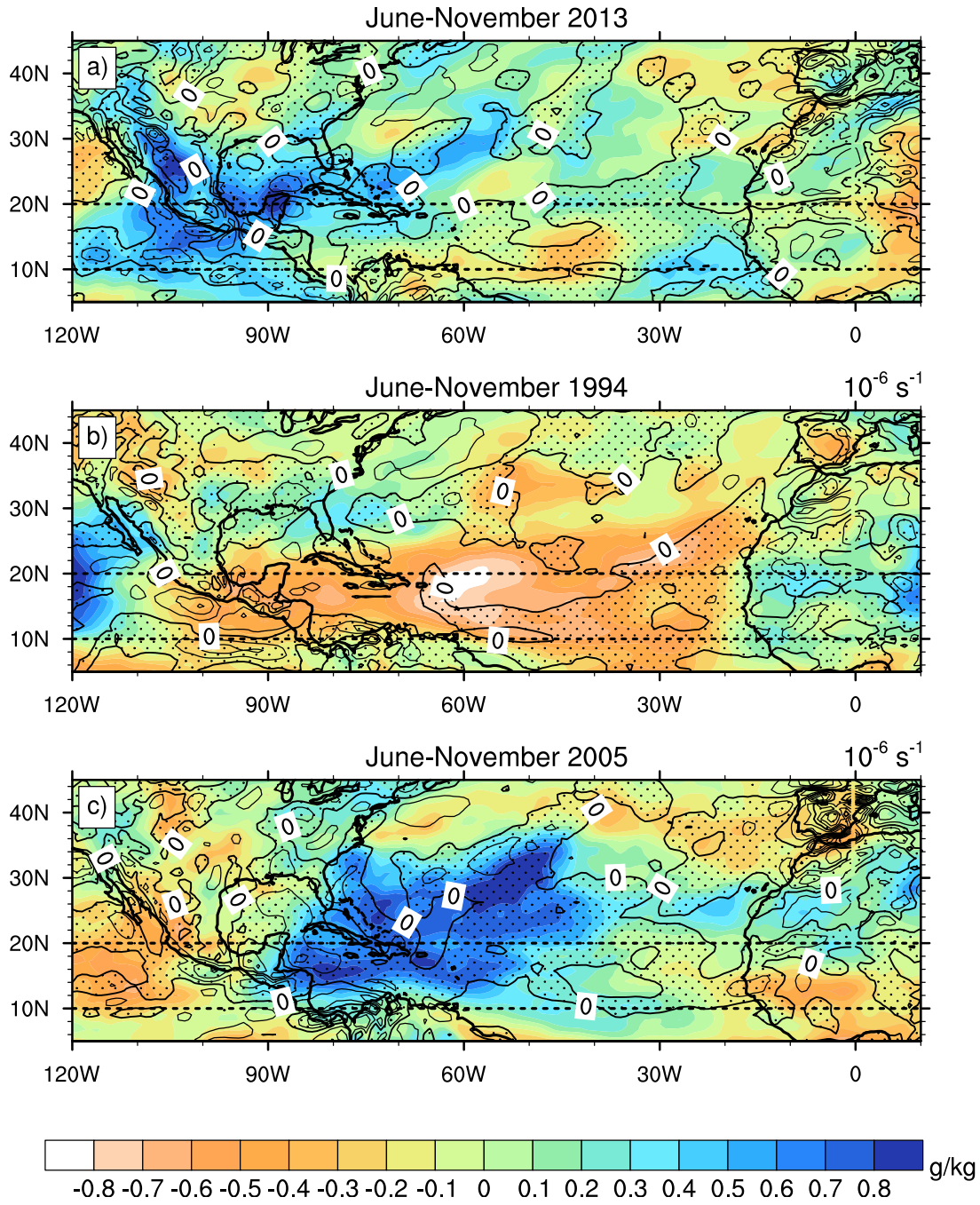

Figure 4.9: Specific humidity anomaly at 700 hPa in g kg^{-1}(shaded contour) and relative vorticity anomalies at 850 hPa in $10^{-6}s^{-1}$ (contour lines) from June to November. Dotted regions indicate a positive relative vorticity anomaly.

The moisture content being strongly correlated to the storm tracks can also be seen in the hurricane season 2005 (Figure 4.9(c), shaded contour). On average, the mid-levels have been about 0.8-1.0 g kg^{-1} moister west of 40°W than in the rest of the MDR. Especially in the eastern MDR near the West African coast, however, the mid-levels have been drier than average. The storm tracks of the season 2005 (Figure 4.4(b)) reflect this anomaly distribution just as well as the ones of season 2013. Most of the storms in 2005 developed west of 40°W and none near the West

African coast. In 1994, the entire MDR and also part of the subtropics were anomalously dry (Figure 4.9(b)). This could be one major reason why only seven named storms developed in the hurricane season 1994.

The relative vorticity anomalies were primarily positive (dotted regions) in the MDR in the hurricane season 2013 (Figure 4.9(a), contour lines), which acted enhancing on principle. However, as mentioned before, relative vorticity is strongly dependent on the pressure systems in the atmosphere and therefore more important for a single pressure system as it is for an averaged period of time. The relative vorticity anomalies basically represent the paths of tropical disturbances and tropical storms. The positive anomalies imply that the regions were crossed by more tropical disturbances and storms on average. This can especially be seen in Figure 4.9(c) for the hurricane season of 2005, where an extraordinary high number of tropical storms traveled into the subtropical region above the MDR. Positive relative vorticity anomalies were found especially in this subtropical region.

Main Hurricane Season from August to October

In the ASO period of 2013, the specific humidity anomalies were more distinct (Figure 4.10(a)). Especially in the central MDR and in the eastern subtropics and mid-latitudes, dry air anomalies existed with a significance of up to -0.75 σ. Slightly positive humidity anomalies were present in the eastern MDR, in the Gulf of Mexico and in the subtropics near 60°W. Dry air masses in the central MDR affected the development of TCs negatively as many TCs form in this region or have to cross this region on their path westward. Dry air masses can not only inhibit development of tropical disturbances, but also weaken an already ongoing deep convection, when dry air intrudes into the circulation and lead to downdrafts. However, also significant (+1 σ) positive specific humidity anomalies could be found just north of the MDR near 60°W.
In the main hurricane seasons of 1994 and 2005, the anomalies did not change much in comparison to their respective entire season (Figure 4.10(b) and (c)). The dry anomalies of the ASO period of 1994, however, show higher significance values (up to -1.25 σ) than the ASO period of 2013. This means that the season of 1994 was significantly drier than the season of 2013. Comparing the extent of the dry air anomalies of these seasons (Figure 4.10(a) and (b)), it is noticeable that it was a lot drier in 1994 in a broader region than it was in 2013.

Monthly Discussion of the Main Hurricane Season

In August 2013 (Figure A.13(a)), the negative humidity anomalies concentrated on a band in the subtropics. In the eastern and central MDR, as well as in the western MDR and in the Gulf of Mexico, positive anomalies were present. The most distinctive phase of dry air masses occurring in the central MDR was in September 2013 (Figure A.14(a)). No tropical storm could develop in this region. In the same time period, the positive humidity anomalies were most distinctive in the Gulf of Mexico, but also present in the eastern MDR near the east North American coast and in

the eastern MDR. All storms that occured in September 2013 developed in the moister regions. In October 2013 the humidity anomalies were weak in the entire MDR (Figure A.15(a)).

Looking at the single months in 1994 (Figure A.13(b), A.14(b) and A.15(b)), there was no big difference between the strong negative anomalies in the MDR and the subtropics. In 2005 the positive humidity anomalies concentrated in the western MDR and western subtropics in August and October (Figure A.13(c) and Figure A.15(c)), whereas in September (Figure A.14(c)) the anomalies were weaker. However, in September 2005, five tropical storms developed, all of them reaching hurricane status and two even became major hurricanes. All of these hurricanes developed in the area with positive humidity anomalies (not shown).

Dry air masses were present in the central MDR in the ASO period of 2013. This led to reduced hurricane activity, as tropical disturbances were either detained to develop, or were weakened while passing the large dry air anomaly traveling westward. However, the hurricane season 2013 was not as dry as the hurricane season 1994, when the MDR and large regions of the subtropical Atlantic were anomalously dry and inhibited the hurricane activity rigorously.

4.2.5 Potential Vorticity

A climatological examination of PV anomalies for a longer period of time does not show significant results. Just as relative vorticity, PV is especially important for extratropical cyclogenesis, but also for the subtropical troposphere. Rossby Wave Breaking (RWB), which can be detected by PV outbreaks that head either further south or further north, can lead to stratospheric air intrusions into the troposphere and lead to a change of trace in the air masses, as stratospheric air is very dry (Funatsu and Waugh, 2008).

In the following the PV anomalies of the single months of the main hurricane season 2013 are discussed. Also single PV outbreak cases are presented and later on, the case studies will be investigated with respect to possible PV outbreaks in Chapter 5 .
In August 2013, positive PV anomalies were present in the eastern subtropical region and part of the central MDR. Strong negative anomalies were located just west of the positive anomalies in the subtropics (Figure A.16, shaded contour). In September 2013, primarily positive PV anomalies existed in the entire examined region on average with maxima over the North African coast, in the central subtropical region and the strongest one near the east coast of North America (Figure 4.11). A large area of negative PV anomalies in the subtropics can be found in the October-2013-average, whereas in the eastern and central MDR weak positive PV anomalies were present (Figure A.17). Compared with the humidity anomalies in 700 hPA of the respective months (contour lines), it is conspicuous that the positive humidity anomalies by trend lie downstream of the positive PV anomalies.

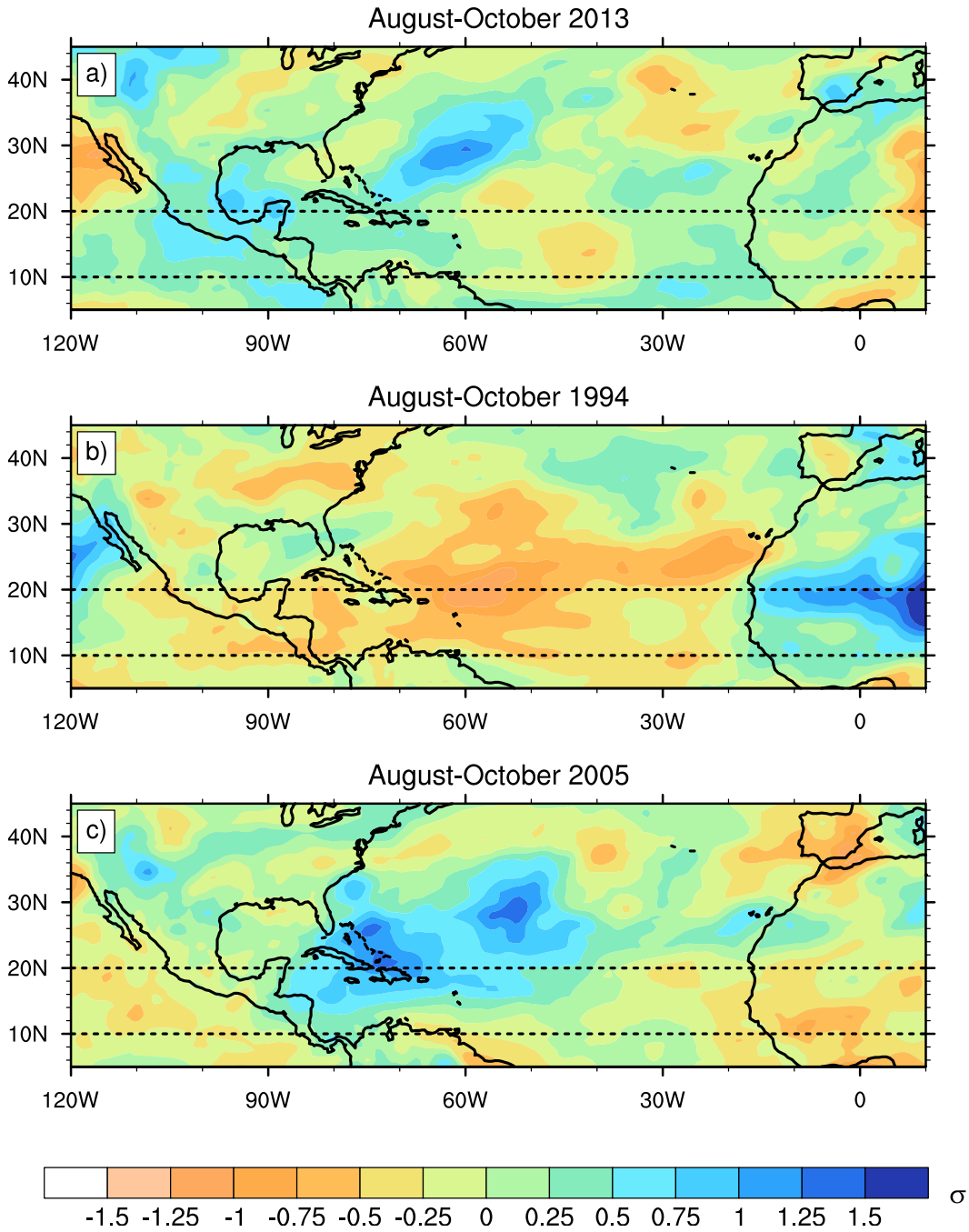

Figure 4.10: Standardized specific humidity anomaly at 700 hPa in σ (shaded contour) from August to October.

Funatsu and Waugh (2008) hypothesized that upper positive PV anomalies can initiate and maintain convection. The correlation found in this study for the humidity and PV anomalies can support this hypothesis. Negative humidity anomalies existed in the region of maximum positive PV anomaly on average. Dry stratospheric air could descend into the troposphere and led to negative humidity anomalies within the broken PV trough. This connection was also described by Allen et al. (2009). They suggested that RWB might lead to mid-level dryness of the subtropical regions. The dry air masses can then be advected into tropical regions by pressure systems. When

advected by a high pressure system, the sinking motion of the system leads to further subsidence of the stratospheric dry air masses into mid-levels.

As mentioned before, case specific PV outbreaks and RWB are more reasonable to examine. In the following, two cases of RWB are discussed regarding their type of wave breaking. Also their correlation with the mid-level humidity at 700 hPa is examined. The PV field was averaged between 100-400 hPa for the chosen dates.
The first case is from 14 August 2013, 00 UTC (Figure 4.12a). In the PV field the tropopause is visible as the black solid line. Three cases of RWB can be seen. Near the European coast a beginning RWB became apparent and in the central suptropics an advanced case of a breaking wave can be found, whereas over the Gulf of Mexico the remains of a former RWB still lingered. The two breaking rossby waves are the LC1 type. They broke anticyclonal and equatordward.
Comparing the averaged PV field with the specific humidity at 700 hPa, it is striking that the regions containing dry air match to a certain extent and dry stratospheric air sunk to the mid-levels (Figure 4.12b). Especially for the easternmost breaking rossby wave, the dry air mass lied directly underneath the PV maximum (34°N 23°W). The dry air masses reaching further into the subtropics and tropics descended from the weakening break in the central subtropics. They subsided further and mixed with the surroundings, following the air currents of the pressure systems. Conspicuos is also the sharp gradient between dry air masses and moister air just downstream of the PV maximum near the European coast. A similar gradient can be found over Canada, where another maximum of PV existed, whereas the remainings of the central breaking RWB did not show a sharp gradient anymore. In the following days the easternmost RWB intensified and finally a cut off took place. As for the dry air masses, they first increased before they mixed up with the environmental air (not shown).

Another case presented here is 11 October 2013, 00 UTC (4.13(a)). Over Florida a sharp PV trough and near 30°W beginning RWB can be seen. It is not clear whether the PV trough over Florida was RWB. Looking at the evolution of this trough a slight anticyclonical turn could be observed (not shown), indicating RWB of type LC1. A large region of dry air masses was found especially upstream of the PV trough (Figure 4.13(b)). This suggests that stratospheric dry air mass did subside into the troposphere and have been mixed up with the environmental air current. Slightly downstream of the PV maximum over Florida, moist air masses were present and also deep convection could be found on satellite pictures (not shown). The beginning RWB near 30°W is of the type LC1 and intesified during the next days (not shown). Both dry air masses could be found in the center and upstream of the PV trough maximum and moister air masses with linked convection existed in the southeast of the PV maximum.

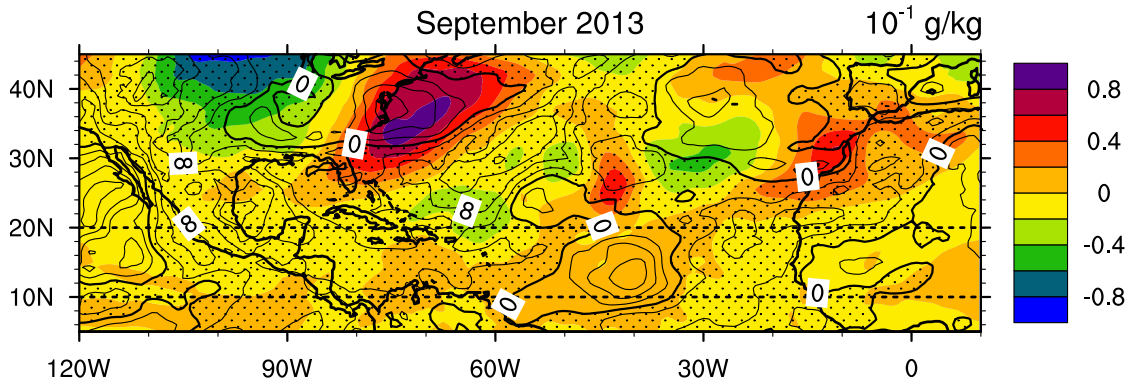

Figure 4.11: Potential Vorticity (averaged between 100-400 hPa) anomalies (contour shaded) and specific humidity anomalies in 700 hPa (contour lines) from September 2013 regarding the 31 year period from 1983-2013. Positive humidity anomalies are shaded with dots.

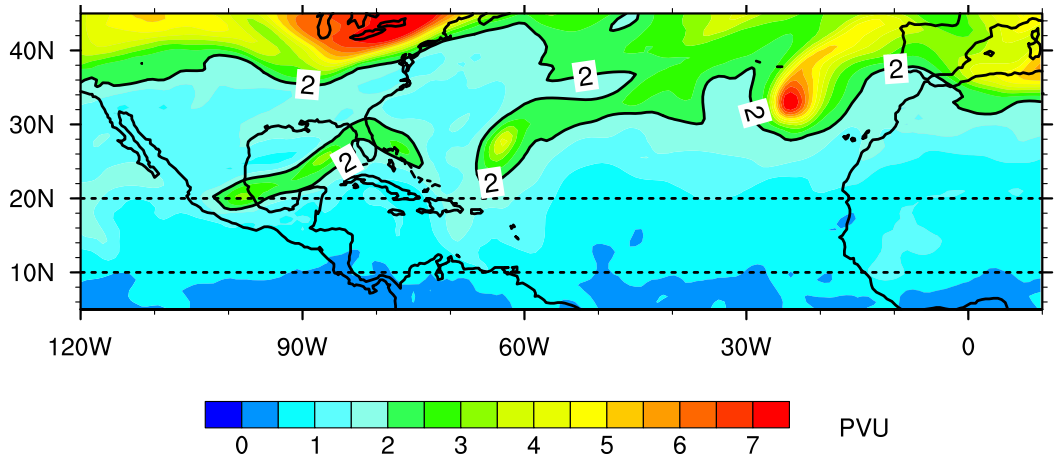

(a)

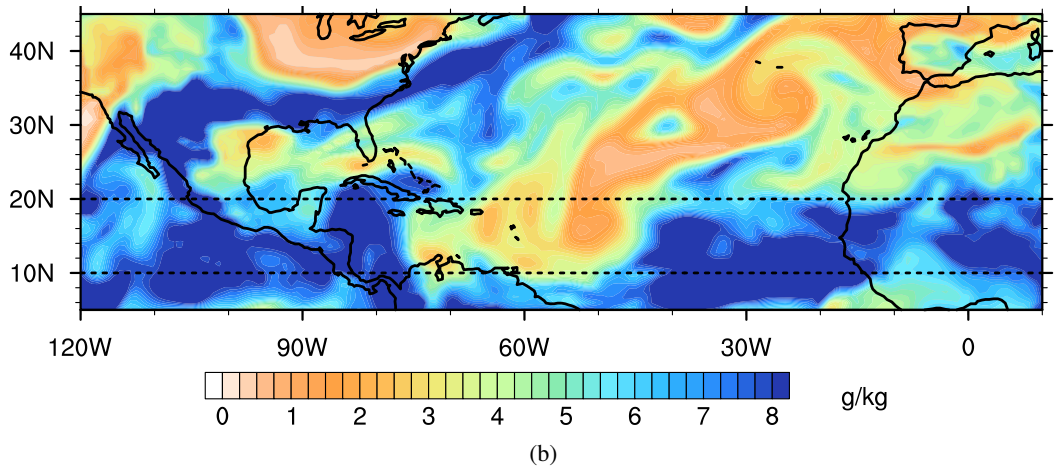

(b)

Figure 4.12: Rossby wave breaking on 14 August 2013, 00 UTC is examined with (a) Potential Vorticity, averaged between 100-400 hPa (contour shaded) and (b) specific humidity at 700 hPa. The thick solid line in (a) indicates the position of the tropopause near the 2 PVU surface.

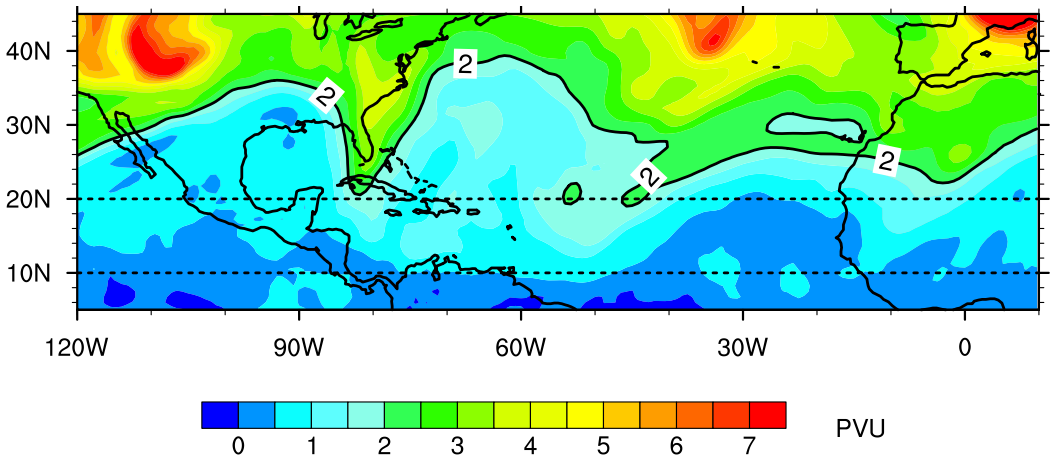

(a)

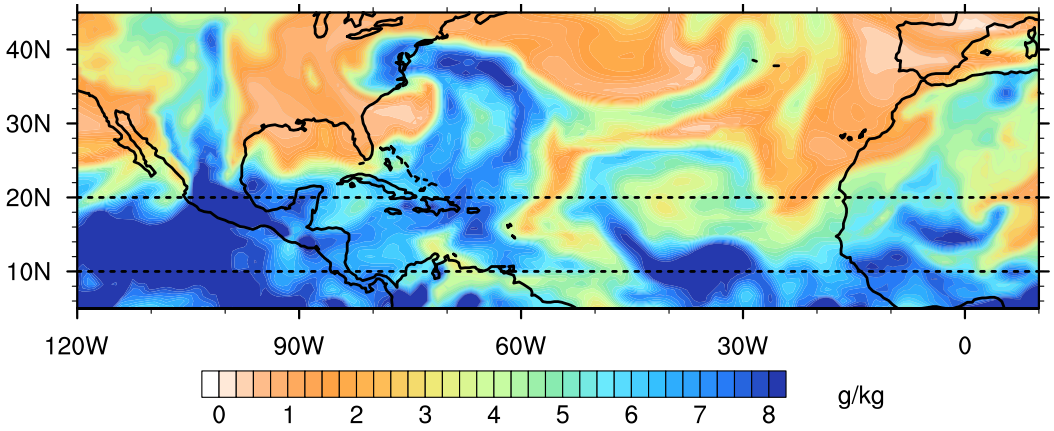

(b)

Figure 4.13: Rossby wave breaking on 11 October 2013, 00 UTC is examined with (a) Potential Vorticity, averaged between 100-400 hPa (contour shaded) and (b) specific humidity at 700 hPa. The thick solid line in (a) indicates the position of the tropopause near the 2 PVU surface.

5. Case Studies of African Easterly Waves

To further investigate the role and origin of dry air masses in tropical cyclogenesis in the eastern MDR, AEWs as typical precursors of Cape Verde hurricanes, were analyzed. During the Atlantic hurricane season 2013 several AEWs left the west African coast propagating westward onto the Atlantic. To choose an AEW for further analysis SSTs, vertical shear of the horizontal wind components, integrated precipitable water between 850 hPa and 600 hPa and relative vorticity at 700 hPa were averaged over bands of 5° latitude each and illustrated in Figure 5.2,5.6,5.10 and 5.15, focusing primarily on the AEWs that were embedded into dry air masses. The black dots indicate AEWs, whereas the green dots indicate a tropical storm. SSTs and vertical wind shear are the dominant environmental conditions that can enhance or inhibit tropical cyclogenesis. Furthermore, an initial mesocyclonical convective system needs enough moisture in lower- to mid-levels to maintain its energy cycle and enough absolute vorticity to initiate and maintain rotation. Given that absolute vorticity is the sum of planetary and relative vorticity, higher values of relative vorticity enhance tropical cyclogenesis, as planetary vorticity is latitude dependent. High values of moisture are essential for tropical cyclogenesis, hence advected dry air masses are an important factor that inhibit the latter. The Atlantic hurricane season 2013 was anomalously dry in the central MDR, but the eastern MDR was slightly moister than average. One question to be answered in this chapter is whether the dry air mass outbreaks of the single cases had their origin in the SAL or in the subtropics.

In the following, the analysis of four different AEWs, that occurred between July and October 2013, are presented. Three non-developing AEWs, accompanied with dry air masses, were chosen and as a comparative study, the AEW that later developed into hurricane Humberto was further analyzed. To investigate the air mass origin that was present when the AEW first was identified by the AEW tracking program (cf. Chapter 3.5), five day backward trajectories were calculated with Lagranto (cf. Chapter 3.6) for five pressure levels between 850 hPa and 500 hPa, as well as for a gridbox of $8° \times 8°$ containing 121 trajectories around the identification point for three pressure levels.

5.1 16 July 2013, 06 UTC

In June, the environmental conditions were too hostile for a TC to form. During July, the conditions improved and the first chosen AEW was detected at 12°N 23°W just west of the African coast. The SSTs just reached 26°C (299 K) in the eastern MDR with tendency to rise westwards (Figure 5.2(a)). The vertical shear of the horizontal wind component was well below 8 m s^{-1} during the appearance of the AEW (Figure 5.2(b)) and relative vorticity values of up to 3 $10^{-5}s^{-1}$ were present (Figure 5.2(c)). Although the AEW met favorable conditions, it did not develop. A possible reason was the region containing dry air masses it propagated into, while still being embedded into moister air masses (Figure 5.2(d)).

The backward trajectories show the origin of the air masses present at the detection date. The air masses at various levels came from different regions. Looking at the trajectory that ended at 500 hPa (red dots), for example, the air mass originated from regions deep into the African continent (Figure 5.3(a)) and did not alter its pressure course much over the time period of five days (Figure 5.3(b)). The air mass at 600 hPa (yellow dots) came from the Sahara (Figure 5.3(a)) and changed its altitude strongly (Figure 5.3(b)). Five days earlier, the air mass was located near 800 hPa, rose until 650 hPa in roughly 30 hours, sunk to almost 900 hPa 40 hours before the detection and rose again to the 600 hPa level. During this course, the specific humidity of the air mass did only vary between 6.5-8 g kg^{-1} (Figure 5.3(c)), leaving it three times moister than the air mass at 500 hPa. Both air masses from the lowest two levels (black and blue dots) came from the African continent, making a slight turn after going north, whereas the air mass from the 700 hPa level (green dots) came straight from the subtropics (Figure 5.3(a)). It is important to note that all these air masses subsided from higher levels to levels below 800 hPa during the first three days before rising again in the last 48 hours (Figure 5.3(b)). The strongest subsidence could be found for the 700 hPa level. The air mass started near the 500 hPa level five days prior, being even drier than the initial 500 hPa air mass (red dots), it subsided almost 350 hPa and moistened around 4 g kg^{-1} during the advection in low levels, before it rose again 24 hours before the detection, indicating convective processes.

To verify the origins of the air masses, 121 backward trajectories from the observed gridbox (8°N-16°N 19°W-27°W) were calculated, as single trajectories can not show the origin of a broader air mass. In fact, trajectories starting from the same level in the gridbox did not always have the same origin. The trajectories at 600 hPa, however, did not show strong variance with respect to their origin. All 121 trajectories originated near the Sahara and were very dry (Figure A.18(a) and (b)). Coming from two different regions, the trajectories at 700 hPa merged near the west African coast. The south-eastern part of the air masses came from the subtropics, whereas the north-western part came from the Saharan region. The trajectories are colored depending on their current pressure (Figure 5.4(a) and (c)) and moisture content (Figure 5.4(b) and (d)). The air masses coming from the subtropics started at levels around 600 hPa containing very little moisture, subsided over the African continent moistening during that process and rose again over the Atlantic. The other part

of the trajectories remained mostly at levels around 700 hPa and were a lot moister than the air masses that came from the subtropics (Figure 5.4(a) and (b)). The split of trajectories was also found at the 850 hPa level, although not as distinct as with the trajectories starting at 700 hPa. Part of the trajectories starting at 850 hPa had their origin over central Africa and subsided while moving westward towards the coast. Trajectories traveling more southward contained up to two times more moisture as the ones that started farther north. The other part subsided either from the subtropics containing very little moisture, or stayed at almost the same level meandering around the west African coast (Figure 5.4(c) and (d)).

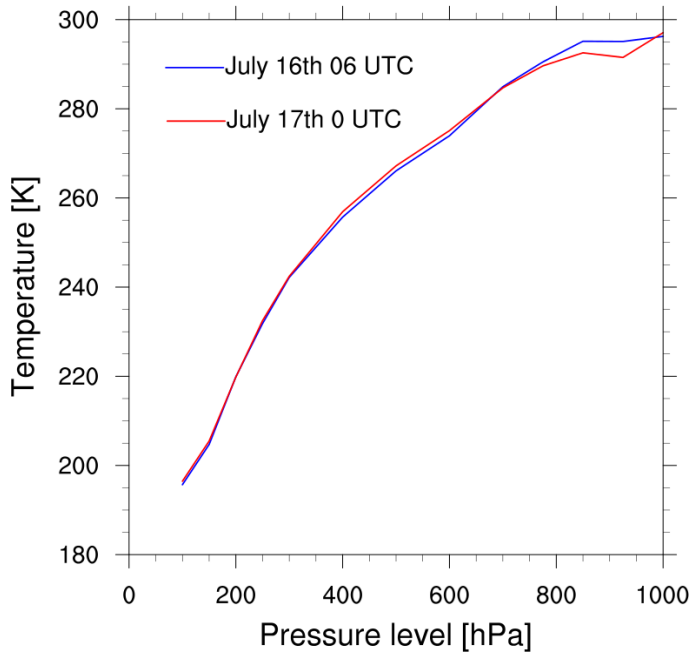

Figure 5.1: Temperature course on 16 July 06 UTC (blue) and 17 July 0 UTC (red) at 12°N 23°W.

Satellite images showed no remarkable deep convective activity induced by the AEW during its course over the ocean (not shown). The images from the Mid-IR/Water Vapour channel of the geostationary satellite Meteosat-SEVIRI at July 11th, 06 UTC, reveal the existence of dry air masses near the Northwest African coast, where the traced air masses had their origin (Figure 5.5(a)). Five days later, at 16 July, 06 UTC, the air masses near the coast moistened up, however the air masses over the ocean still contained very little moisture (Figure 5.5(b)). Another satellite image is shown in Figure 5.5(c), where the ongoing advection of dry air masses from the subtropics can be seen. Smaller convective systems formed during the passing of the AEW, but could not develop further, as the dry air in the middle and lower troposphere acted as a lid. Evaporation of cloud droplets led to a cooling effect and formed a stable layer with a distinct inversion near 850 hPa that strengthened over time (Figure 5.1). As air masses from the SAL were involved as well, the inversion could also come from the absorption of solar radiation by dust particles. However, the air coming from the Sahara contained a lot more moisture, whereas the air that was present

near the detection point of the AEW and downstream of its path came from subtropical regions and was exceptionally dry with values about 3-4 g kg^{-1}. This leads to the assumption that this AEW did not develop due to the major presence of dry air masses from the subtropics.

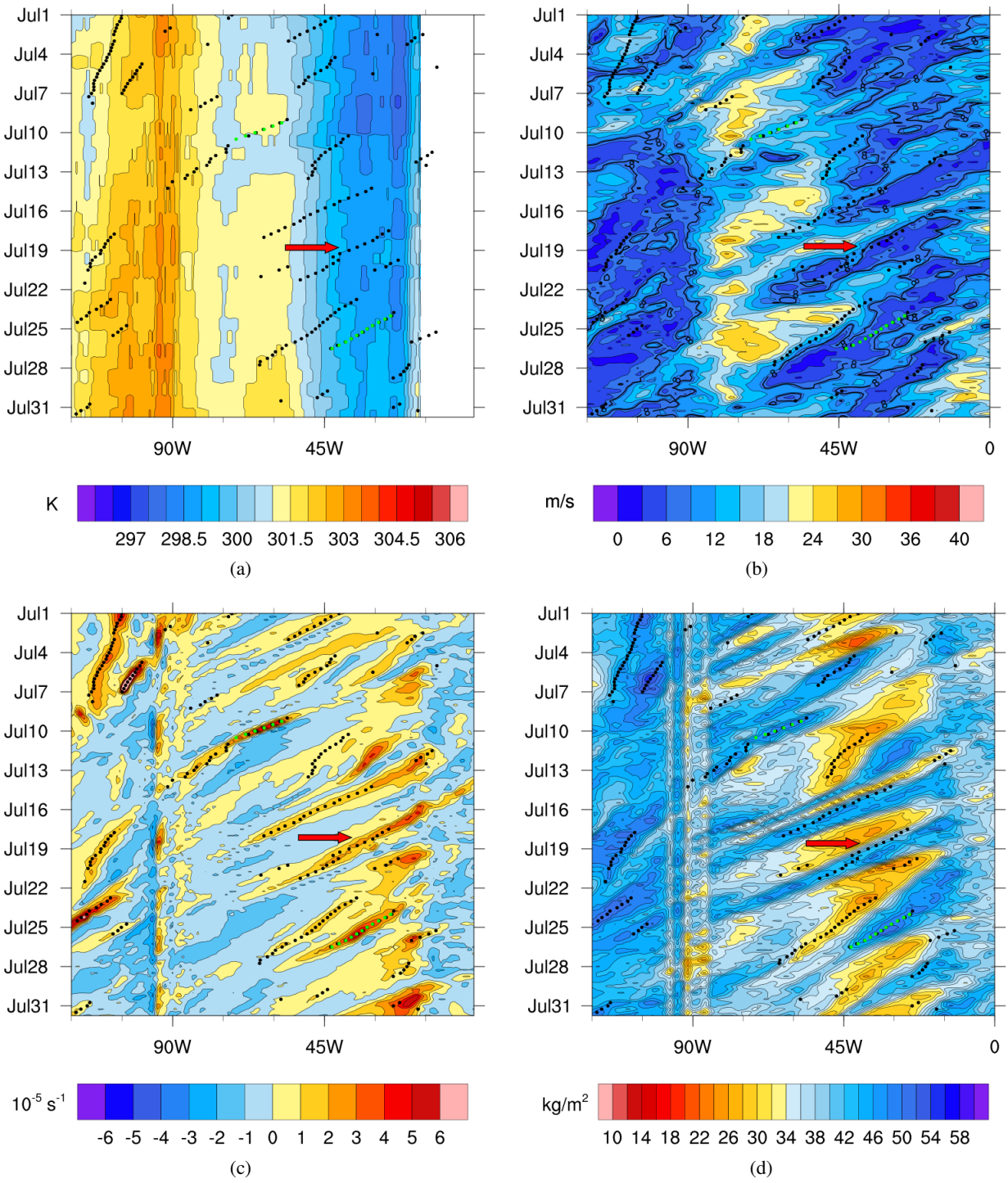

Figure 5.2: Hovmöller diagrams from July 2013 averaged between 12.5°N and 17.5°N, black dots indicate a detected AEW, green dots indicate a detected named storm. (a) Sea surface temperatures in K, (b) Vertical shear of the horizontal wind components between 200 hPa and 850 hPa in m s^{-1}, (c) Relative vorticity averaged between 700 hPa and 1000 hPa in $10^{-5}s^{-1}$, (d) Integrated precipitable water content between 850 hPa and 600 hPa in kg m^{-2}.

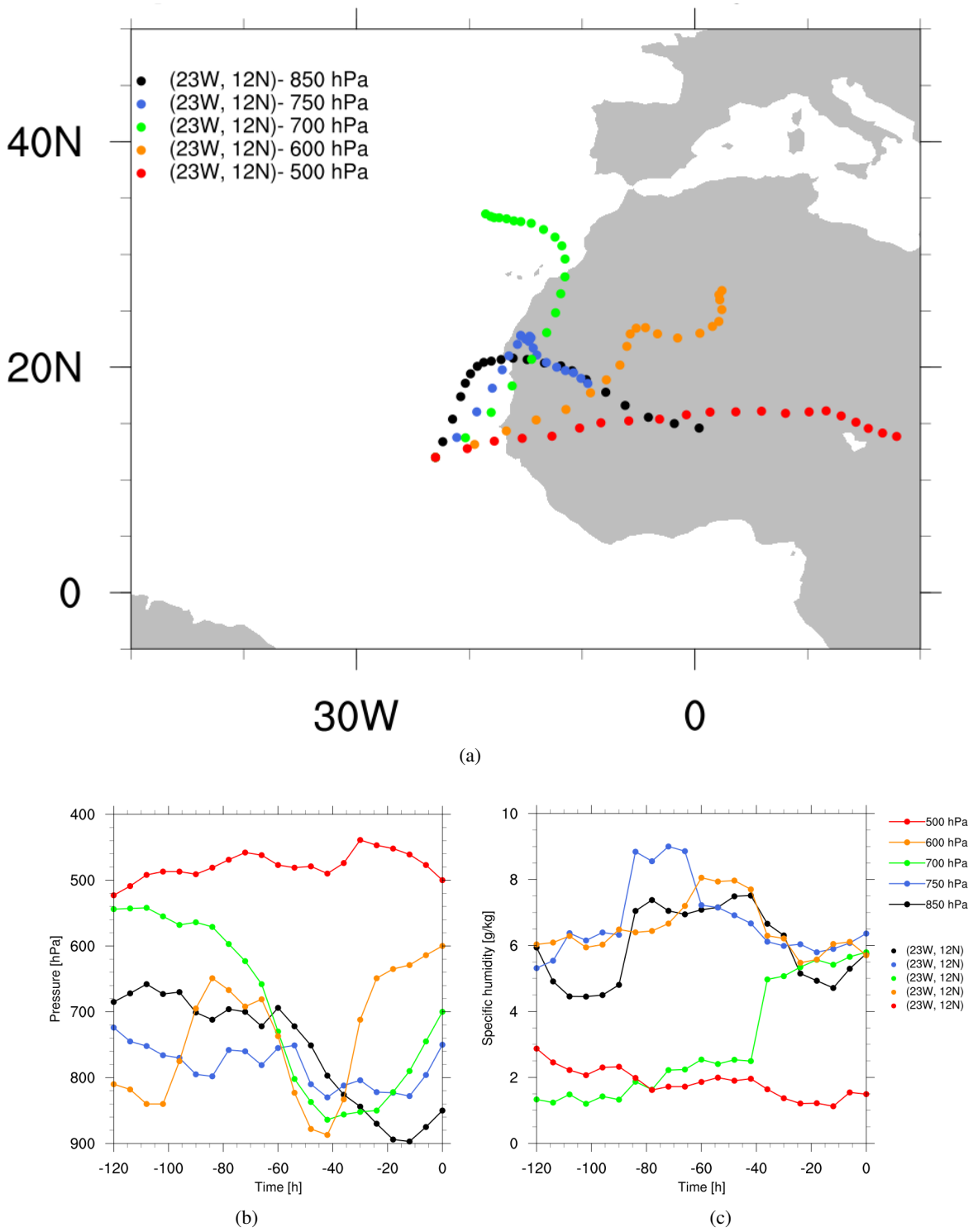

Figure 5.3: Backward trajectories starting at 16 July 2013, 06 UTC, and at the starting point (12° N 23° W). Calculated with Lagranto for five days in 500 hPa (red), 600 hPa (yellow), 700 hPa (green), 750 hPa (blue), 850 hPa (black). The time period between two dots is 6 hours. (a) Map, (b) pressure course, (c) moisture content course.

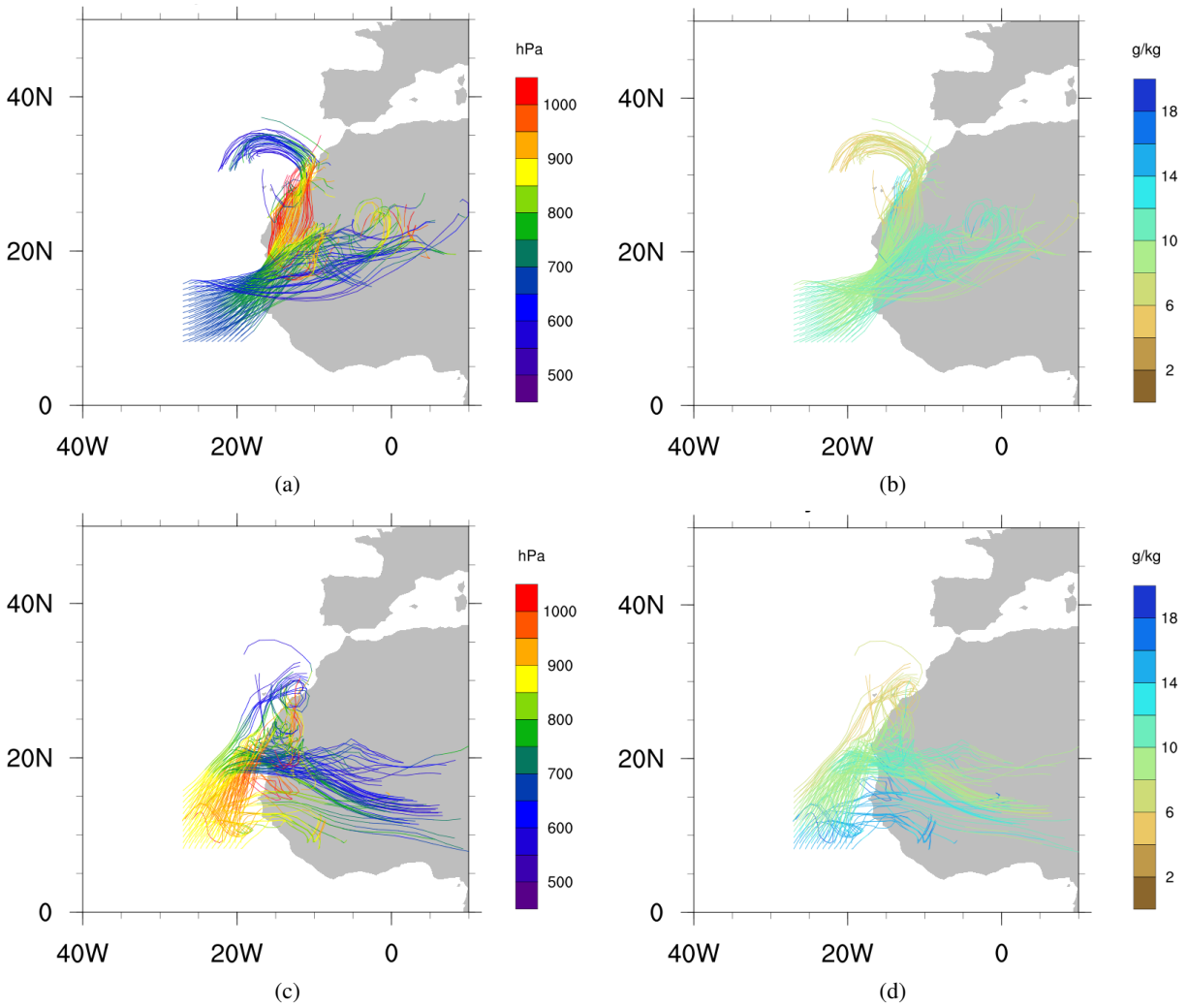

Figure 5.4: 121 Backward trajectories equidistantly distributed in a gridbox (8-16°N 19-27°W) starting at 16 July 2013, 06 UTC. Calculated with Lagranto for five days at 700 hPa ((a) and (b)) and 850 hPa ((c) and (d)). (a) Pressure course at 700 hPa, (b) moisture content course at 700 hPa, (c) Pressure course at 850 hPa, (d) moisture content course at 850 hPa.

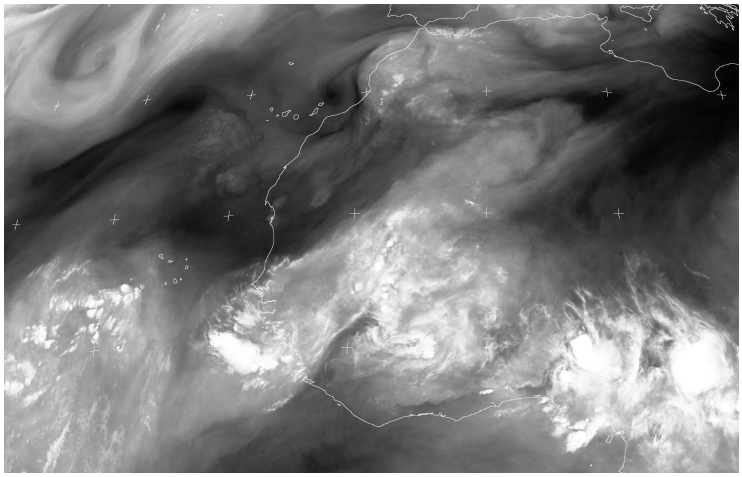

(a)

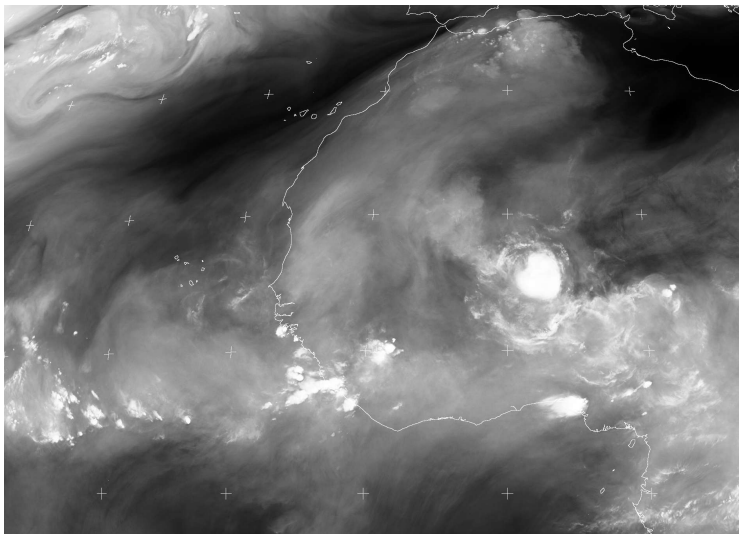

(b)

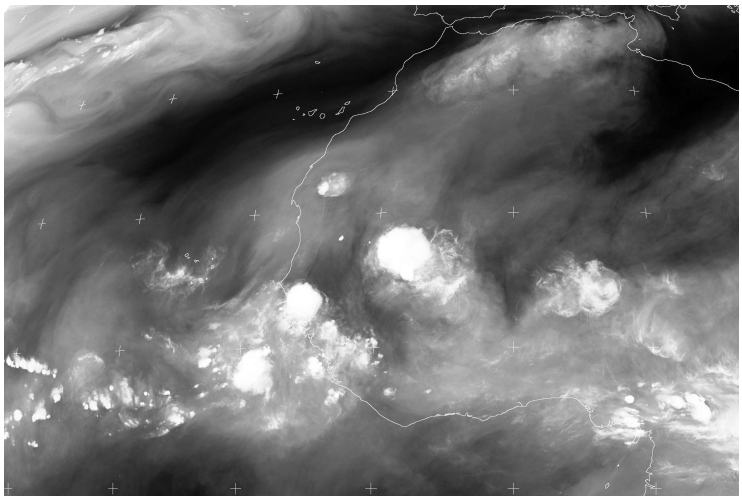

(c)

Figure 5.5: Geostationary satellite imagery from Meteosat SEVIRI 000.0E. The channel 5.35-7.15 μm Mid-IR / Water Vapour was taken to observe the water vapour and deep convection (white). Dark areas indicate dry air. (a) 11 July 2013, 06 UTC, (b) 16 July 2013, 06 UTC, (c) 17 July 2013, 00 UTC. (Credit NEODAAS/University of Dundee).

5.2 9 August 2013, 06 UTC

The AEW fulfilled the identification criteria farther west of the African coast and met different environmental conditions than the AEW in July (Chapter 5.1). The SST was about 2 K warmer, but the vertical wind shear was assimilably low. The relative vorticity values were slightly lower and the environment was significantly drier before and after the AEW appeared, compared to the environment in the previous case (Figure 5.6).

The backward trajectories, calculated from the starting point (15.5°N 37.5°W) of different levels, show that the air masses followed a narrow path from the west African coast to the starting point. Only exception was the trajectory in 500 hPa, beginning its path very close to the starting point and moving a lot slower than the rest of the air masses. The 750 hPa-trajectory came directly from regions above the Sahara, whereas the 700 hPa-trajectory stayed over the ocean (Figure 5.7(a)). All air masses below 500 hPa had the tendency to rise during the first two days and only subsided around 20 hPa during the next three days (Figure 5.7(b)). The three middle layers (750 hPa, 700 hPa, 600 hPa) became drier during their course, the air mass of the 850 hPa level became drier at first, but moistened again in the last 30 hours (Figure 5.7(c)).

The trajectory band from the 8×8° gridbox around the starting point showed similar origins and moisture contents and the pathway was overall more dense compared to the trajectories in the July-case (Figure 5.4). In 600 hPa, the trajectories were traced backwards to the West African coast where they split up. Most of the trajectories originated from the African continent being very dry, but some of them, coming from the subtropical Atlantic, contained even less moisture. The trajectories originating from the continent rose quickly at the beginning from levels around 900 hPa to around 600 hPa, whereas the other trajectories stayed around 600 hPa for the course of five days (Figure A.18(c) and (d)). Similar distributions could be found in lower levels, though the pathway stayed not as concentrated as in the 600 hPa level while going higher in pressure level. The trajectory band in 700 hPa split up close to the African coast as well, but showed three main directions instead of two. One part came from the subtropical Atlantic, staying at nearly the same height and containing very little moisture values. The second part originated from the Saharan regions remained mostly at the same level, only few of the air masses rose from levels around 900 hPa and were significantly moister, as humidity reached values around 10 g kg^{-1}. In comparison the rest of these air masses containing moisture around 4 g kg^{-1} (Figure 5.8(a) and (b)). The third part meandered close to the coast, rising from levels around 800 hPa and was the moistest from all air masses meeting at this level on 9 August, 06 UTC (Figure 5.9(a) and (b)). In the 850 hPa level most of the air masses came from the African continent, rising nearly from the ground five days prior. Being very dry at first, the air masses moistened up during their descent above the ocean. The other air masses came from the subtropics, where they followed the coastline southward until rising near 20°N. These air masses contained much more moisture but met a few dry air masses from the continent and dried up because of mixing processes (Figure 5.8(c) and (d)).

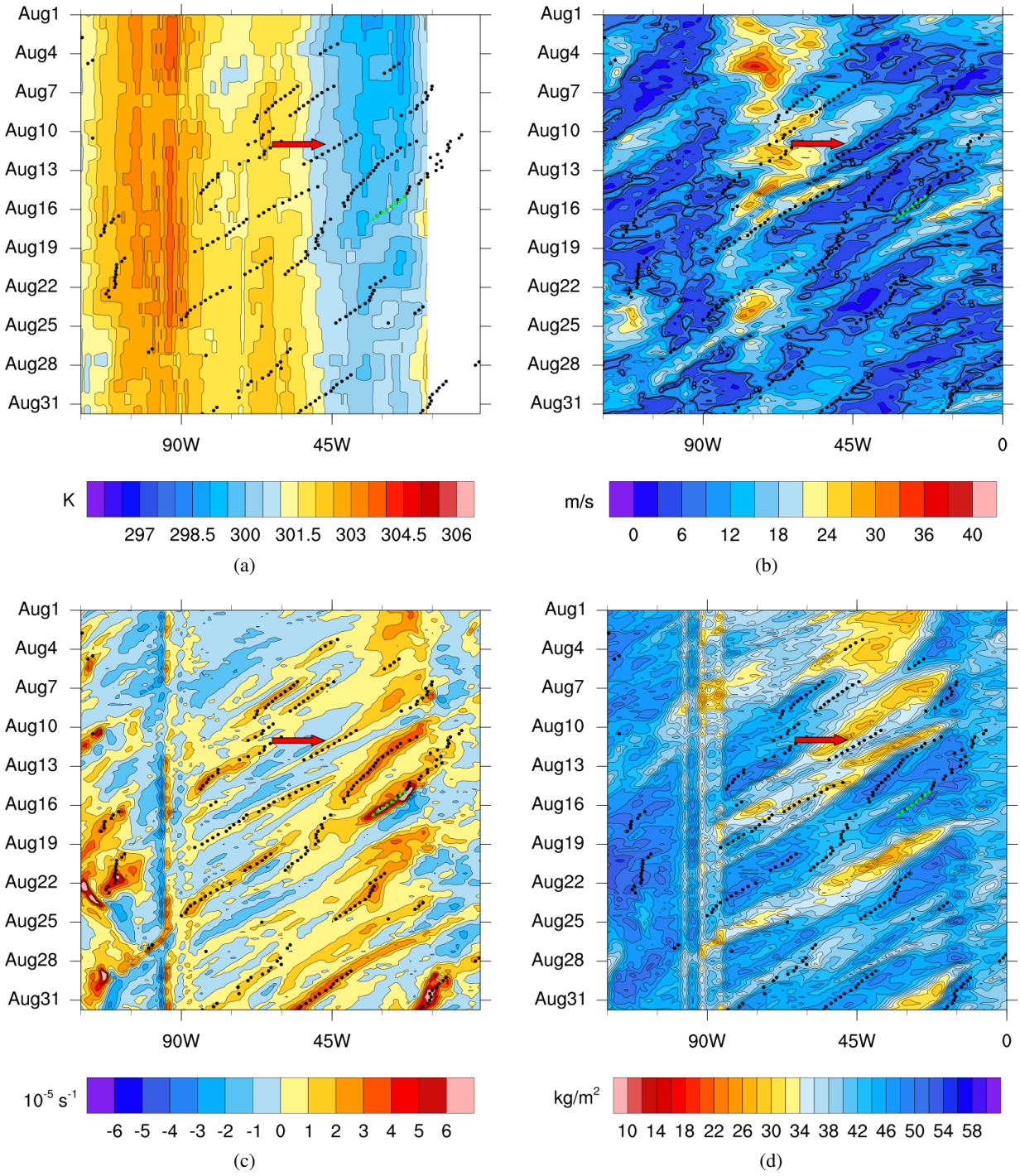

Figure 5.6: Hovmöller diagrams from August 2013 averaged between 12.5°N and 17.5°N, black dots indicate a detected AEW, green dots indicate a detected named storm. (a) Sea surface temperatures in K, (b) Vertical shear of the horizontal wind components between 200 hPa and 850 hPa in m s^{-1}, (c) Relative vorticity averaged between 700 hPa and 1000 hPa in $10^{-5}s^{-1}$, (d) Integrated precipitable water content between 850 hPa and 600 hPa in kg m^{-2}.

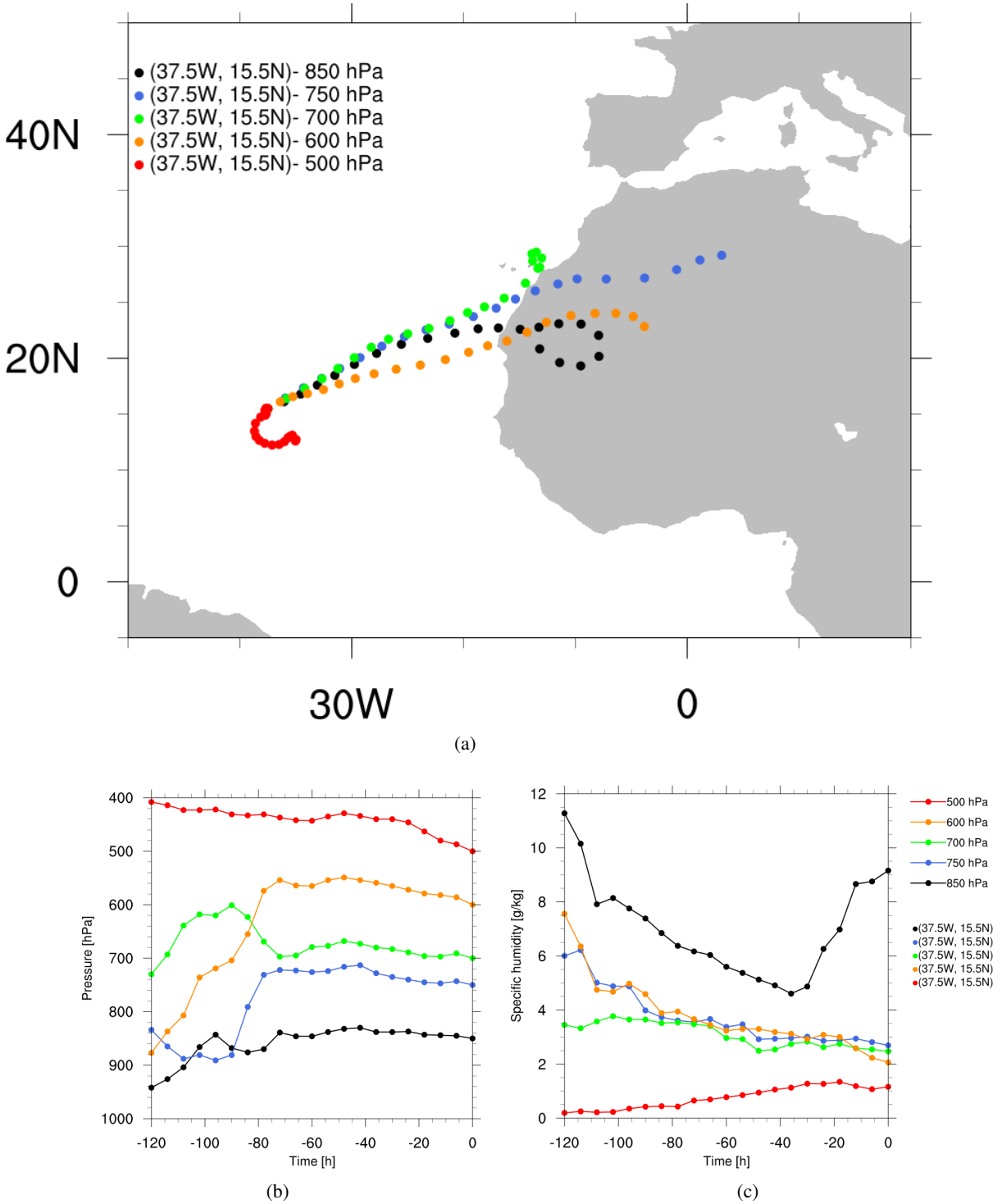

Figure 5.7: Backward trajectories starting at 9 August 2013, 06 UTC, and at the starting point (15.5°N 37.5°W). Calculated with Lagranto for five days in 500 hPa (red), 600 hPa (yellow), 700 hPa (green), 750 hPa (blue), 850 hPa (black). The time period between two dots is 6 hours. (a) map, (b) pressure course, (c) moisture content course.

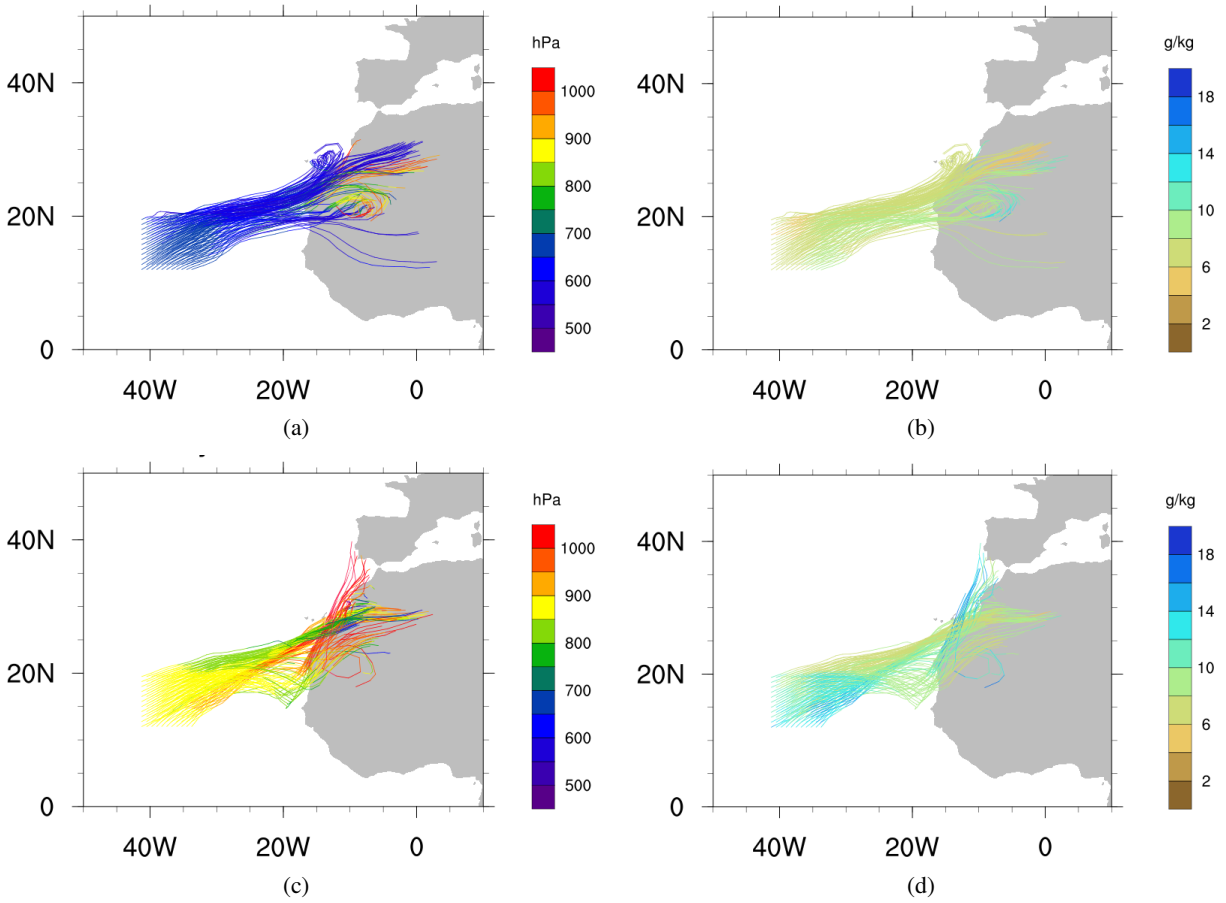

Figure 5.8: 121 Backward trajectories equidistantly distributed in a gridbox (11.5-19.5°N 33.5-41.5°W) starting at 9 August 2013, 06 UTC. Calculated with Lagranto for five days at 700 hPa ((a) and (b)) and 850 hPa ((c) and (d)). (a) Pressure course at 700 hPa, (b) moisture content course at 700 hPa, (c) Pressure course at 850 hPa, (d) moisture content course at 850 hPa.

Looking at the Meteosat-SEVIRI Mid-IR/Water Vapour channel image of the starting date and five days prior (Figure 5.9(a)), it can be seen that dry air is located of the Sahara where most of the air masses had their origin at 4 August, 06 UTC. Five days later at September 9th, 06 UTC, the dry air masses propagated onto the Atlantic, suppressing most of the convective action (Figure 5.9(b)).

Altogether, this AEW was not strongly enhanced by the environment. Dry air masses from the SAL supposably inhibited the development of greater convective systems. Looking at the averaged PV fields, RWB could be found prior to the AEW starting date (Figure A.19). The investigation of the specific humidity content for a sequence of single timesteps showed that the dry air masses seen in Figure 5.9(b) were a combination of dry stratospheric air and air from the SAL. A strong dry signal ahead of an AEW is a factor that often led to non-development (cf. Chapter 2.2.1).

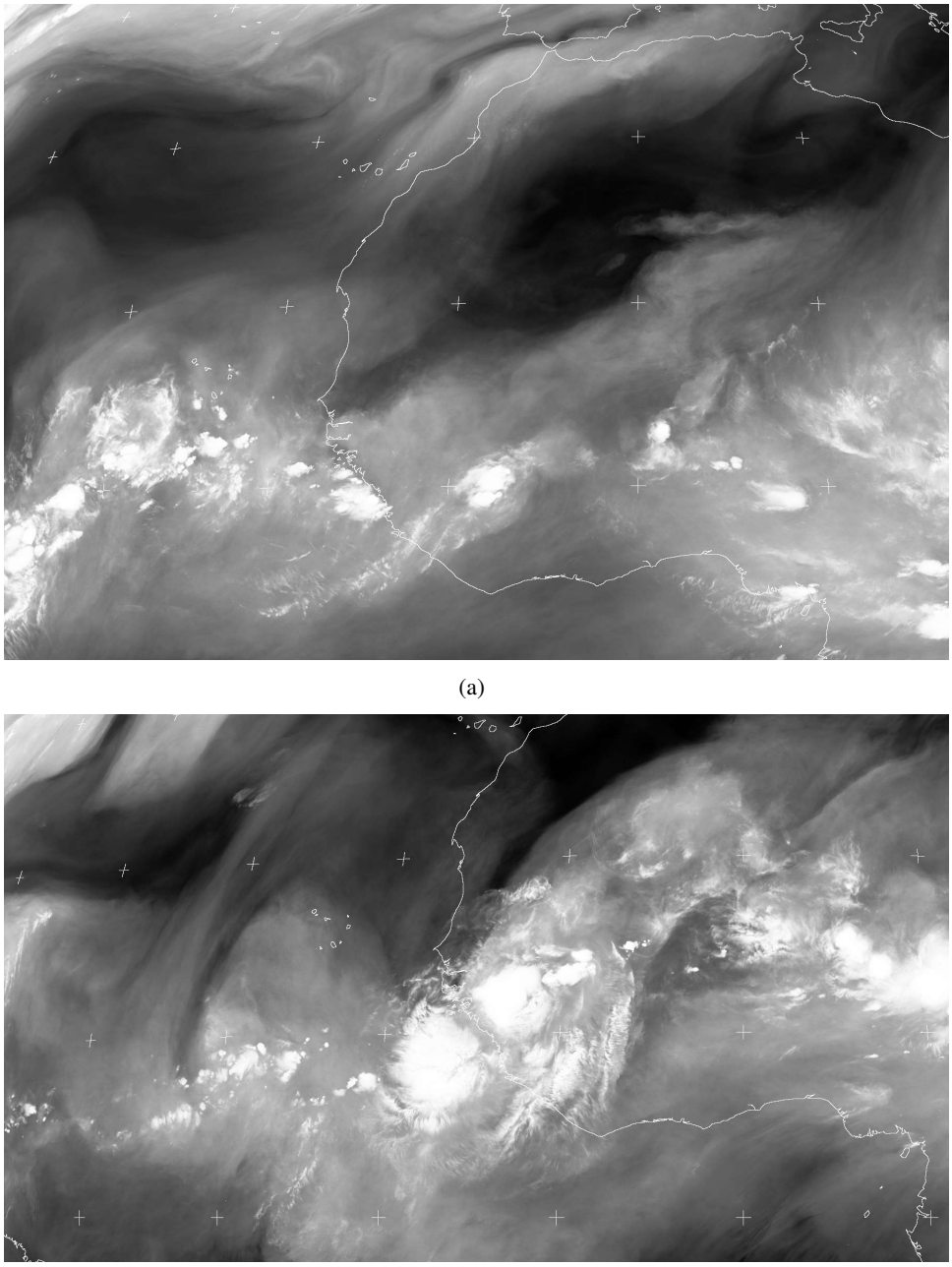

(a)

(b)

Figure 5.9: Geostationary satellite imagery from Meteosat SEVIRI 000.0E. The channel 5.35-7.15 μm Mid-IR / Water Vapour was taken to observe the water vapour and deep convection (white). Dark areas indicate dry air. (a) 4 August 2013, 06 UTC, (b) 9 August 2013, 06 UTC.
(Credit NEODAAS/University of Dundee)

5.3 3 September 2013, 18 UTC and 7 September 2013, 06 UTC (Hurricane Humberto)

For comparison with the non-developers, the analysis of the AEW that strengthened to hurricane Humberto at 11 September 2013 is presented. To understand the role of different air masses better, two dates were investigated. One starting point was placed over the African continent at 3 September and one point was placed just west of the African coast four days later. Over the continent the vertical wind shear was about 50 % higher than for the previously analyzed cases (Chapter 5.1,5.2), but the air masses were moister and higher values of relative vorticity were found (not shown).
Four days later, the AEW propagated onto the Atlantic and encountered vertical wind shear below 8 m s^{-1}. The conditions for strengthening were further enhanced by high SSTs, even moister air masses and ongoing high values of relative vorticity (Figure 5.10(a-d)).

The trajectory analysis (Figure 5.11(a)) showed that especially the air masses for the first date came from very different directions. Whereas the air masses in 500 hPa and 750 hPa came from central Africa, the air masses in 700 hPa and 850 hPa came from southwest and south respectively. The air mass in 600 hPa meandered just southeast of the starting point for the five day calculation. Descending or rising motion was, however, not significantly distinct in the lower levels (Figure 5.11(c)). The air masses in 500 hPa and 600 hPa lost moisture during their rise, whereas the air masses in lower levels became moister during the five day course (Figure 5.11(e)).

Looking at the trajectories four days later (Figure 5.11(b)) the direction, where the air masses originated, became more concentrated. At this time, the air masses from all calculated levels came from central Africa. Their pressure course (Figure 5.11(d)) showed even less changes than the course of the air masses four days prior and their moisture content remained nearly constant, except for the air mass in 750 hPa, which lost about 30 % of its moisture during the observed period and the air mass in 700 hPa, which gained moisture (Figure 5.11(f)).

Altogether, the air masses in this case showed less pressure changes in five days and were two to three times moister than the cases in July and August (Chapter 5.1 and 5.2). The investigation of the air masses from gridboxes around the starting points showed a different result. In 700 hPa, the origin pattern of 121 starting points (Figure 5.12(a)) resembles the appearance of the pattern of only one starting point (Figure 5.11(a)). To note is that the 121 trajectories were calculated from only one starting level (700 hPa), whereas the trajectories from Figure 5.11(a) were calculated for five different levels.

Two main directions can be found in the trajectory pattern from the gridbox (Figure 5.12(a)). Most of the air masses traveled north and stayed at nearly the same height, but had unexpectedly

dry values (6 g kg^{-1}). The other main origin region was given by air masses from central Africa that did not change much in height and were significantly moister (14 g kg^{-1}) than the air masses from the south. Some couple trajectories can be found rising from westsouthwest directions and containing even more moisture (Figure 5.12(c)). Comparing the first starting date with the starting date four days later, it can be seen that in 700 hPa, there were air masses originating from central Africa, staying at a pressure level around 700 hPa and air masses rising northeastward from the tropical Atlantic (Figure 5.12(b)). All tracked air masses had a specific humidity of more than 8 g kg^{-1}, which is significantly more than the air masses of the July and August trajectory bands (Figure 5.4(b) and 5.8(b)). The lower level in 850 hPa is even more significant. Most of the air masses rose from the south or southwest, containing a lot of moisture in the five day period prior to the first starting date at 3 September (Figure 5.13(a) and (c)). Looking at the trajectories four days later at 7 September, a split of directions can be found. Part of the trajectories came from central Africa and descended near the west African coast. The other part came mainly from southwest directions and rose during the five day period (Figure 5.13(b)). The moisture content of the air masses was slightly lower compared to the air masses of the earlier starting point but nevertheless provided the AEW with enough moisture to enhance the development of the disturbance (Figure 5.13(d)). In all levels, the air masses rose as a result of the ongoing convection. At 8 September, the disturbance was categorized as tropical storm and strengthened to a hurricane category 1 at 11 September. After two days, Humberto weakened to a tropical storm and decayed completely about a week later.

The Mid-IR/Water Vapour channel of the satellite Meteosat-SEVIRI (Figure 5.14) shows the drier air in the south of the west African coast and moister air over central Africa and the west coast with embedded convective systems (Figure 5.14(a)) for 3 September, 06 UTC. Four days later, the AEW propagated westward, reaching the West African coast. In the satellite image moist air and especially the enhanced convective activity is visible (Figure 5.14(b)). Additionally, a satellite image of the Near-IR to Shortwave-IR channel (Figure 5.14(c)) is given to show the size of hurricane Humberto at September 12th compared to the initial developing system in Figure 5.14(b).

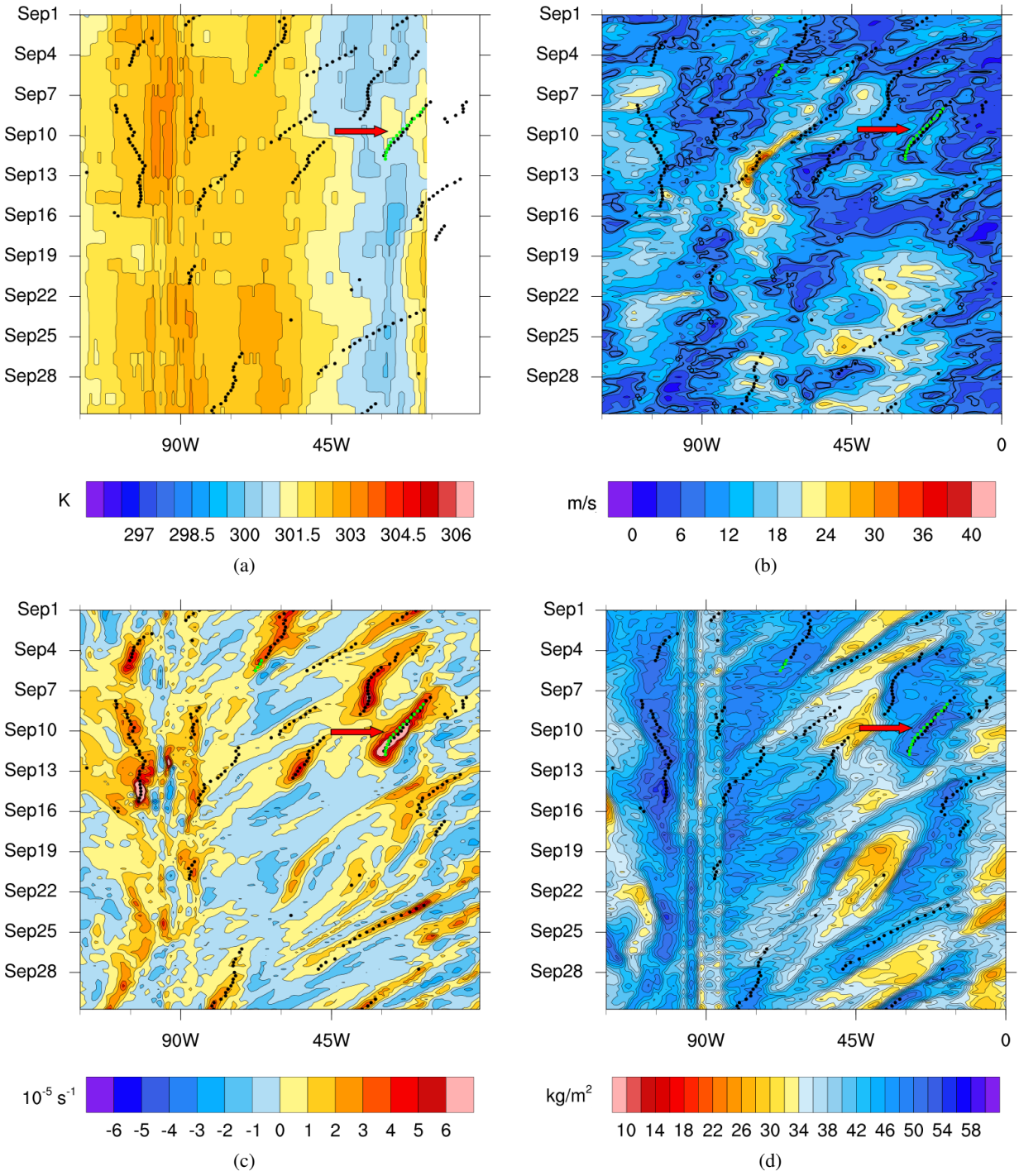

Figure 5.10: Hovmöller diagrams from September 2013 averaged between 12.5°N and 17.5°N, black dots indicate a detected AEW, green dots indicate a detected named storm. (a) Sea surface temperatures in K, (b) Vertical shear of the horizontal wind components between 200 hPa and 850 hPa in m s^{-1}, (c) Relative vorticity averaged between 700 hPa and 1000 hPa in $10^{-5}s^{-1}$, (d) Integrated precipitable water content between 850 hPa and 600 hPa in kg m^{-2}.

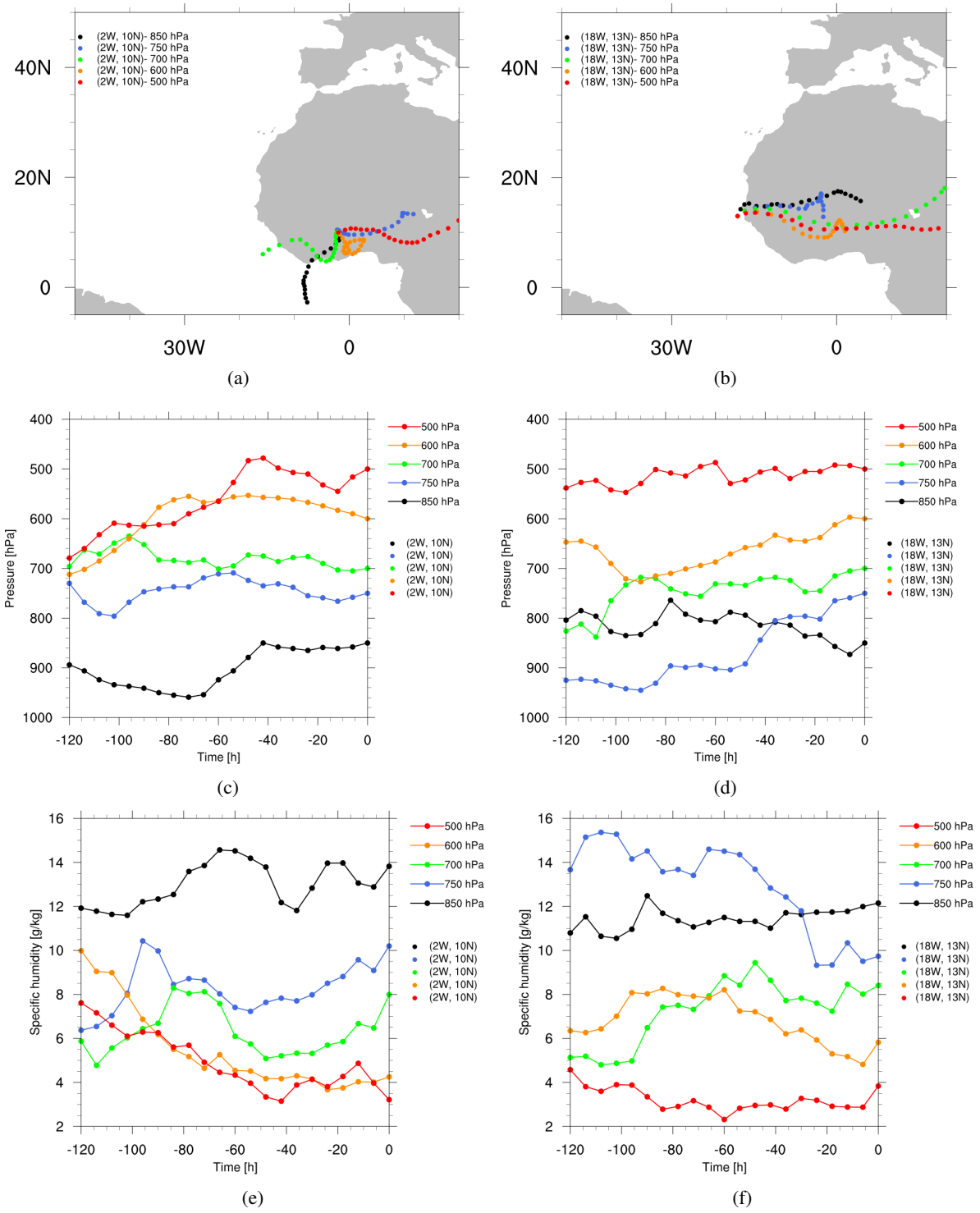

Figure 5.11: Backward trajectories starting at 3 September 2013, 18 UTC, at the starting point (10°N 2°W) (left panel) and 7 September 2013, 06 UTC, at the starting point (13°N 18°W)(right panel). Calculated with Lagranto for five days in 500 hPa (red), 600 hPa (yellow), 700 hPa (green), 750 hPa (blue), 850 hPa (black). The time period between two dots is 6 hours. (a) map, (b) pressure course, (c) moisture content course.

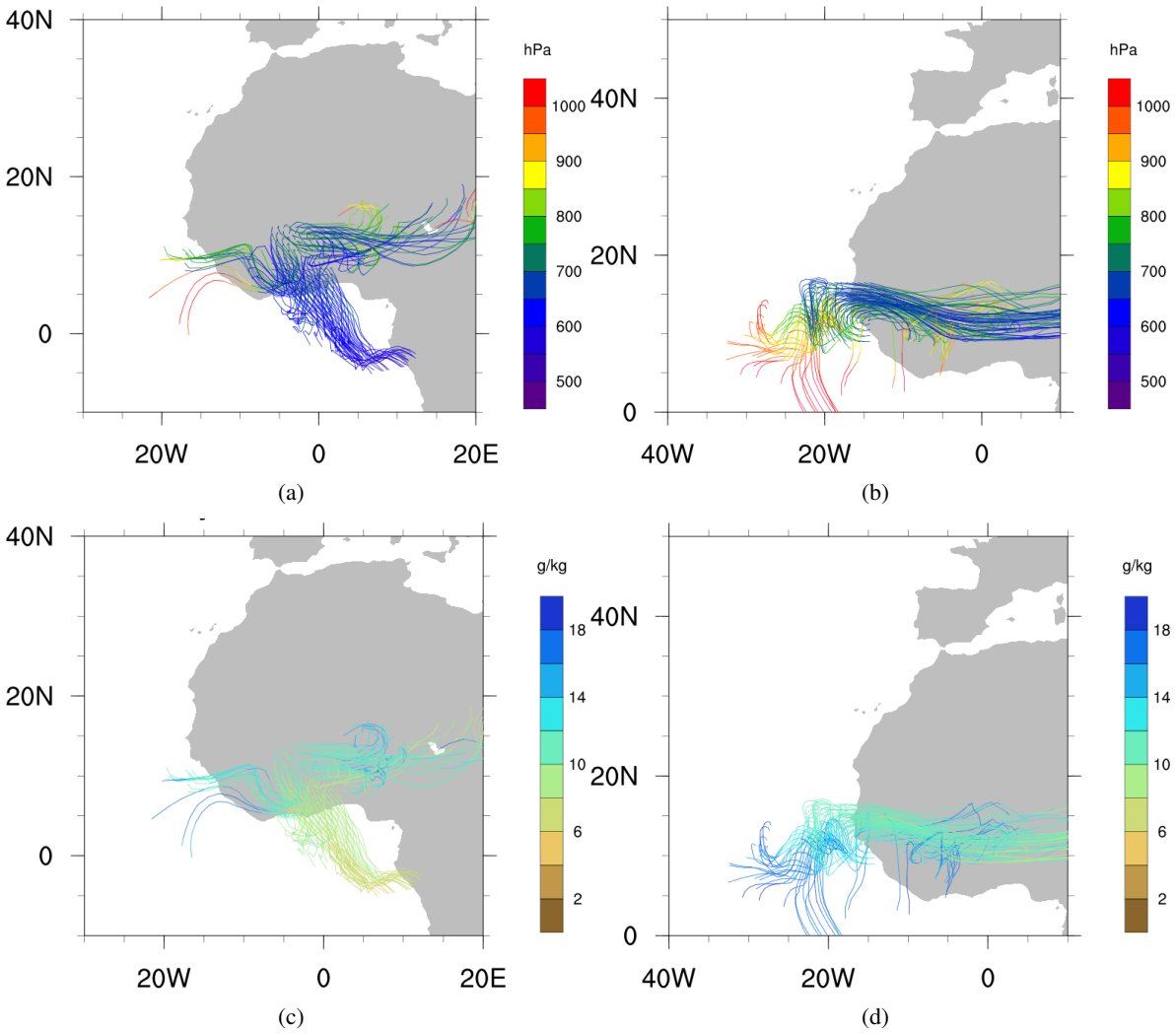

Figure 5.12: 121 Backward trajectories equidistantly distributed in a gridbox (6-14°N 2°E-6°W) starting at 3 September 2013, 18 UTC, (left panel) and in a gridbox (9-17°N 14-22°W) starting at 7 September 2013, 06 UTC, (right panel). Calculated with Lagranto for five days at 700 hPa. (a) and (b) pressure course, (c) and (d) moisture content course.

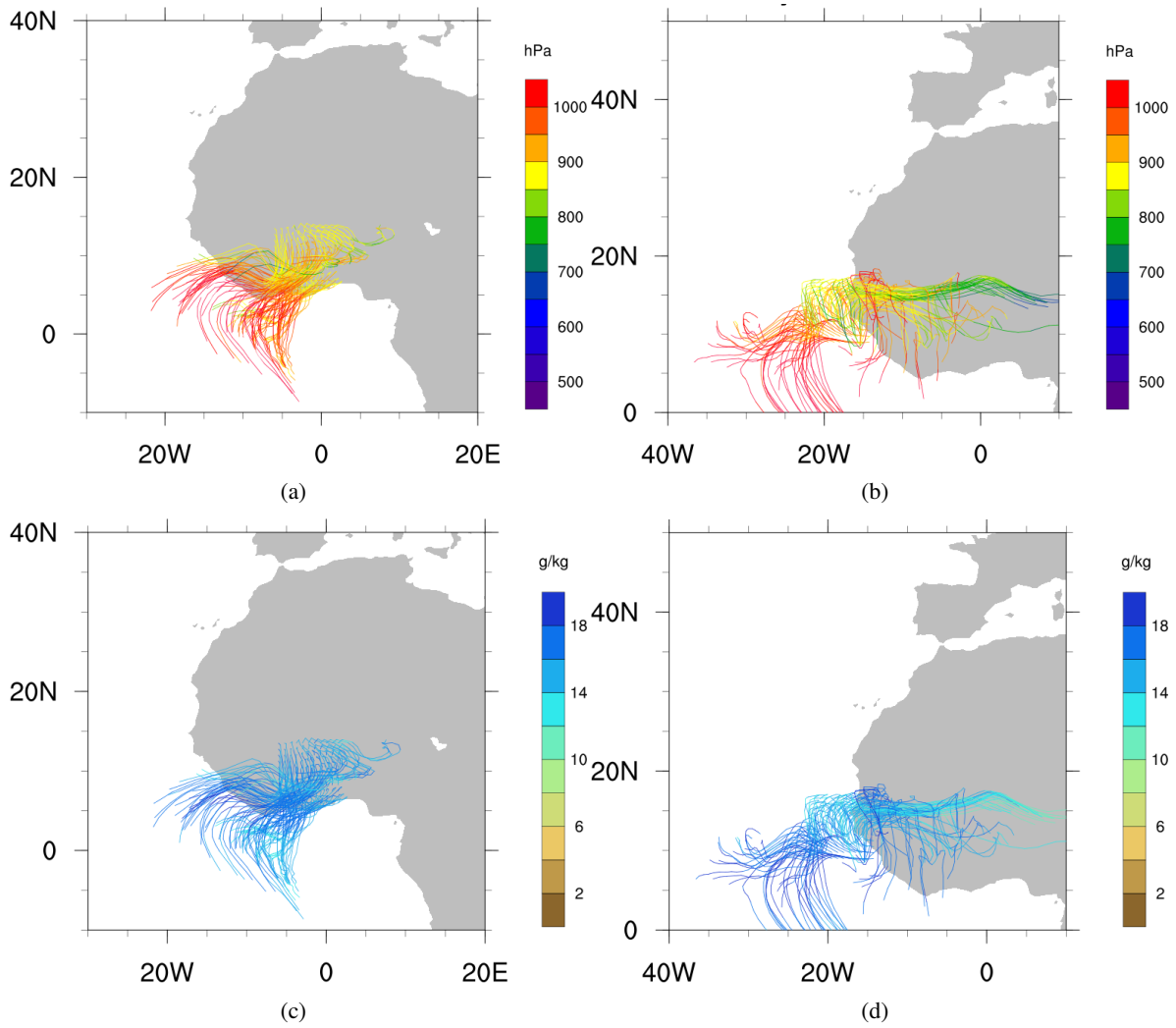

Figure 5.13: 121 Backward trajectories equidistantly distributed in a gridbox (6-14°N 2°E-6°W) starting at 3 September 2013, 18 UTC, (left panel) and in a gridbox (9-17°N 14-22°W) starting at 7 September 2013, 06 UTC, (right panel). Calculated with Lagranto for five days at 850 hPa. (a) and (b) pressure course, (c) and (d) moisture content course.

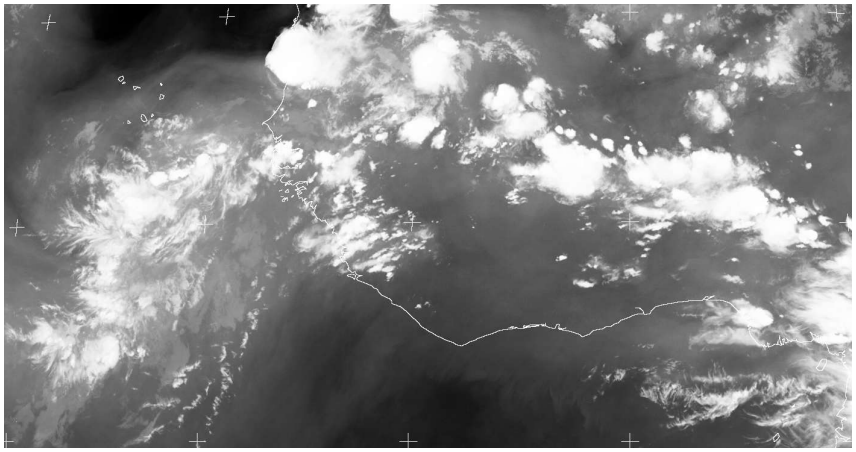

(a)

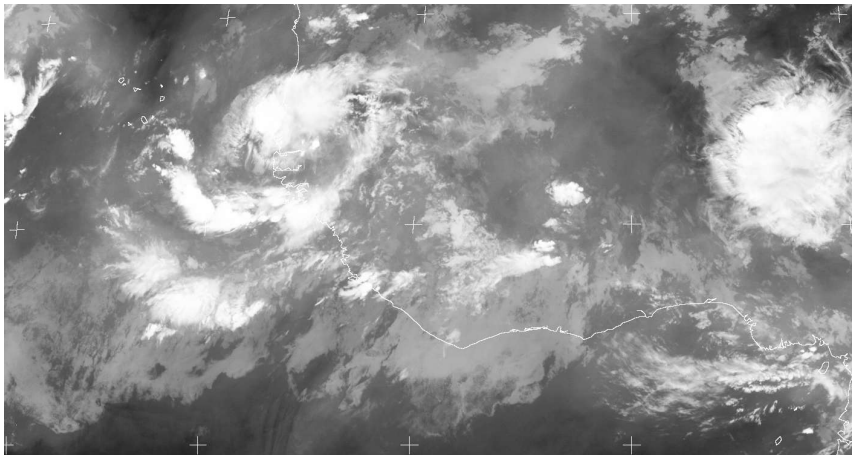

(b)

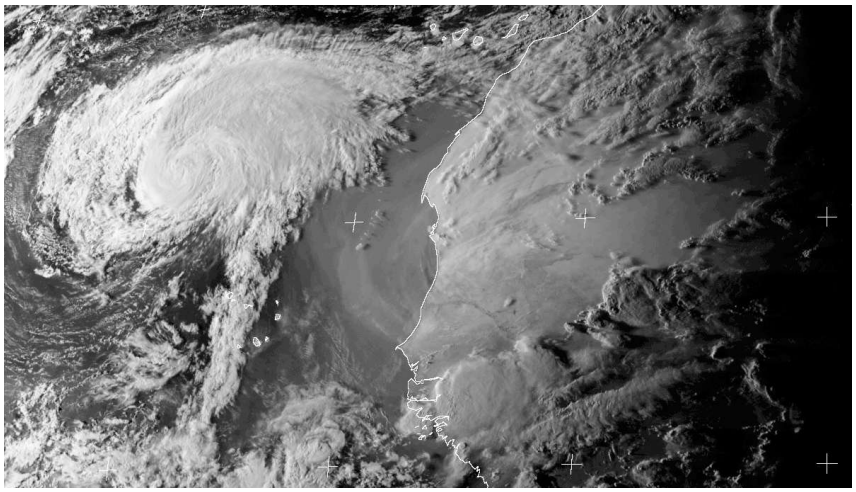

(c)

Figure 5.14: Geostationary satellite imagery from Meteosat SEVIRI 000.0E. The channel 6.85-7.85 μm Mid-IR / Water Vapour was taken to observe the water vapour and deep convection (a) and (b) and the channel 1.50 - 1.78 μm Near-IR to Shortwave-IR was taken for the display of hurricane Humberto. (a) 3 September 2013, 18 UTC, (b) 7 September 2013, 06 UTC, (c) 12 September 2013, 18 UTC.
(Credit NEODAAS/University of Dundee)

5.4 5 October 2013, 12UTC

The AEW of the last case was again embedded in dry air masses (Figure 5.15(d)) and apart from this, did not meet another important criteria for favorable TC genesis. The vertical wind shear (Figure 5.15(b)) exceeded the threshold that is considered to be harmless for development, over three times. Although the values of relative vorticity and SSTs were high enough (Figure 5.15(a) and (c)), strong vertical wind shear was a strongly inhibiting factor for development. Consequently, the non-development of this AEW can not only be reasoned with present dry air masses.

Looking at the Hovmöller diagrams (Figure 5.15), the question why the AEW that appeared a week later near 45°W was not chosen. Overall the environmental conditions were better and upstream dry air masses existed as well. This AEW did, however, develop into tropical storm Lorenzo on October 21st.
Looking at the trajectory analysis from 5 October, it can be seen that the air masses propagated into a ridge and made an anticyclonal turn after coming from either the west African coast (750 hPa, 700 hPa), from west (600 hPa) or from the subtropical Atlantic in the northwest (500 hPa) (Figure 5.16(a)). The influence of the ridge can be seen at the course of the pressure level, as the air masses in all levels started subsiding roughly 60 hours before the starting date (Figure 5.16(b)). The moisture content sunk drastically in the 850 hPa level, whereas the content in the remaining levels stayed constantly low (Figure 5.16(c)).

These observations were confirmed by the analysis of the trajectory band of 121 trajectories with the starting points located equidistantly around the starting point of the AEW. In 700 hPa the air masses were very dry and slightly subsided over the time period of five days (Figure 5.17(a) and (b). The trajectory of the 850 hPa level had the strongest subsidence, which can also be seen in the band of trajectories starting at this level. Most of the trajectories subsided and became drier, as some of the air masses that started in the tropical Atlantic right south of the starting point were two times moister (Figure 5.17(c) and (d)). Around the 5 October 2013 RWB (type LC1) could be found in the subtropical Atlantic (Figure A.19(b)) advecting dry air masses from the subtropics into the tropical region. The strong anticyclone could also be found looking at a sequence of specific humidity during that period.

The Mid-IR/Water Vapour channel of the satellite Meteosat-SEVIRI confirms the conditions found by investigating the trajectories. In Figure 5.18(a), the beginning of the trajectories at 30 September, 12 UTC, can be seen. Drier air is located near the west African coast where the air masses of the midlevels were coming from. Five days later, at the starting date of the AEW, no significant convective activity can be found near the location of the AEW at 32.5°W 15.5°N in the Mid-Infrared channel, but dry air that subsided from the subtropical ridge can be seen in Figure 5.18(b).

Given the investigation of the origin of the air masses present at the detection date of the four

AEWs, the assumption that both, subtropical dry air intrusions in a greater extent, and dry air masses advected by the SAL led to reduced TC activity in the eastern and central MDR.

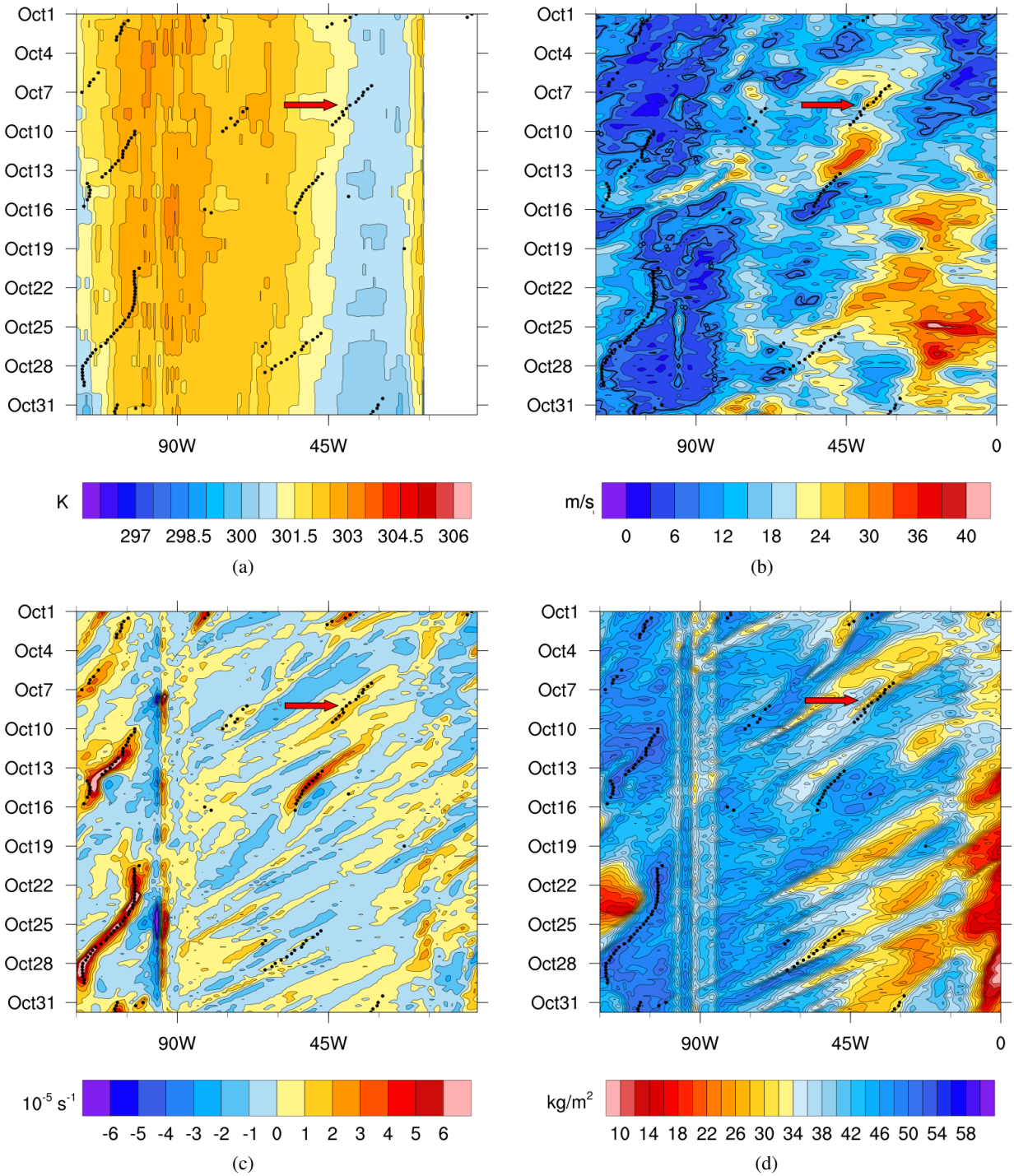

Figure 5.15: Hovmöller diagrams from October 2013 averaged between 12.5°N and 17.5°N, black dots indicate a detected AEW, green dots indicate a detected named storm. (a) Sea surface temperatures in K, (b) Vertical shear of the horizontal wind components between 200 hPa and 850 hPa in m s^{-1}, (c) Relative vorticity averaged between 700 hPa and 1000 hPa in $10^{-5}s^{-1}$, (d) Integrated precipitable water content between 850 hPa and 600 hPa in kg m^{-2}.

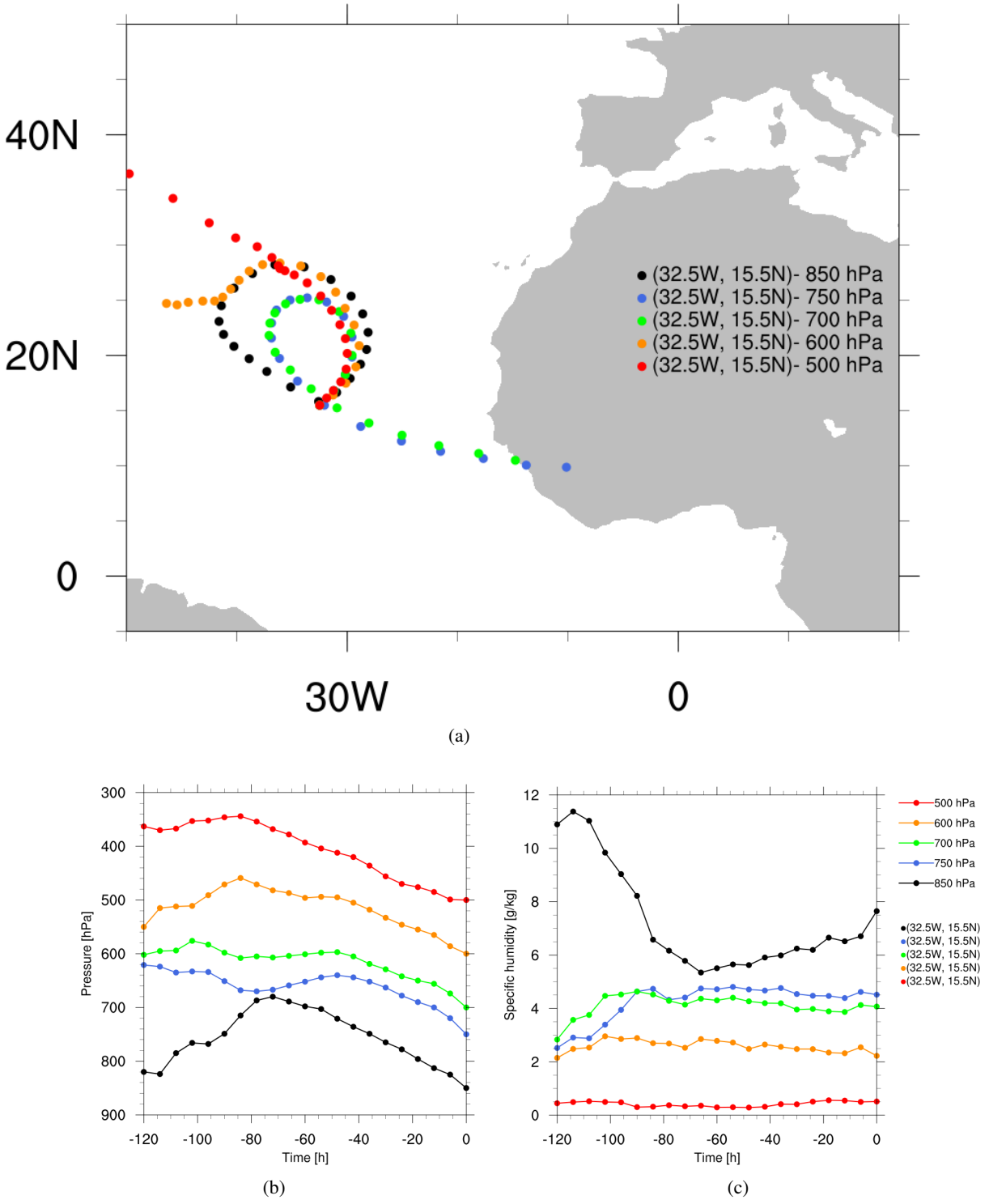

Figure 5.16: Backward trajectories starting at 5 October 2013, 12 UTC, and at the starting point (15.5°N 32.5°W). Calculated with Lagranto for five days in 500 hPa (red), 600 hPa (yellow), 700 hPa (green), 750 hPa (blue), 850 hPa (black). The time period between two dots is 6 hours. (a) map, (b) pressure course, (c) moisture content course.

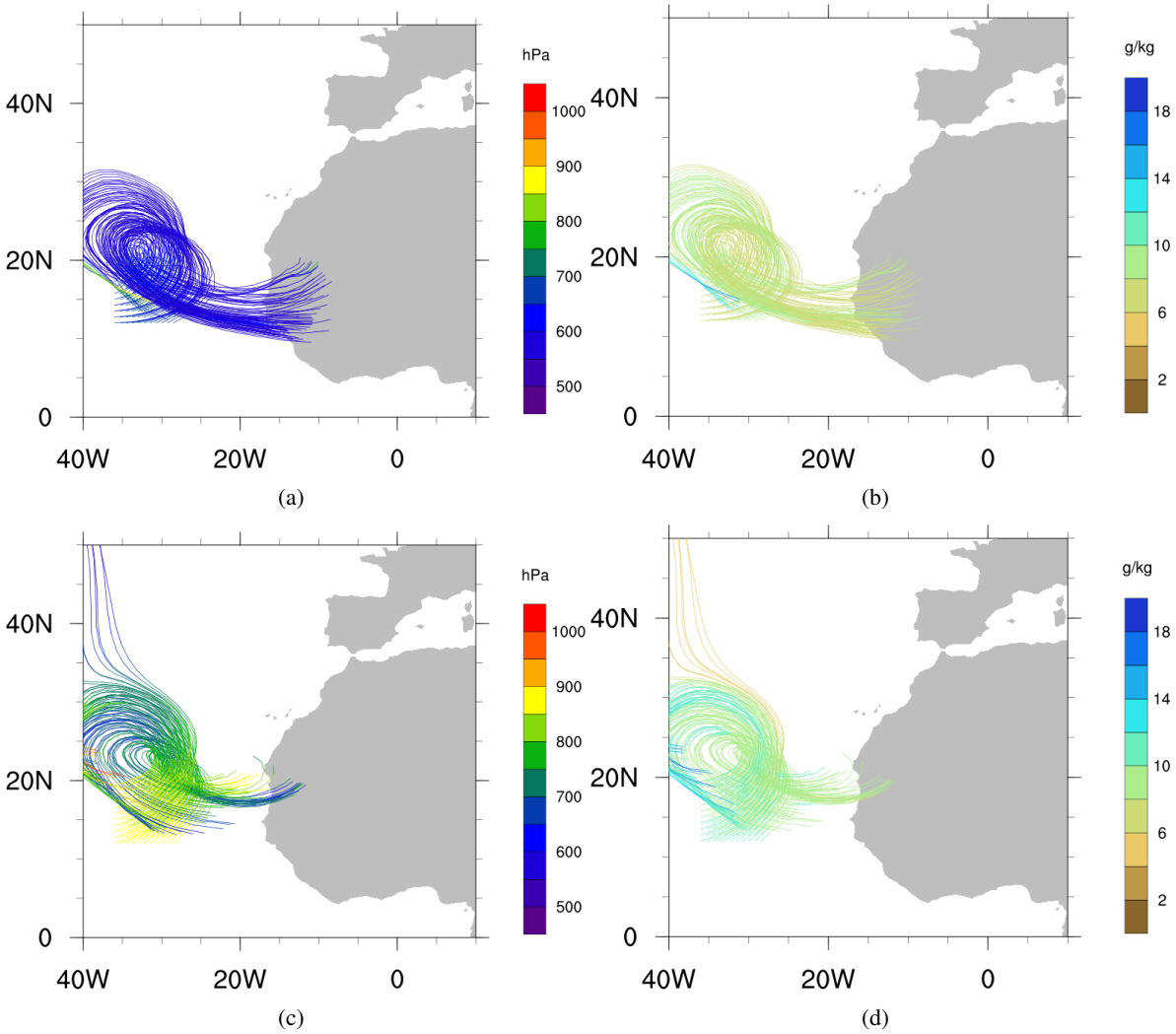

Figure 5.17: 121 Backward trajectories equidistantly distributed in a gridbox (11.5-19.5°N 28.5-36.5°W) starting at 5 October 2013, 12 UTC. Calculated with Lagranto for five days at 700 hPa ((a) and (b)) and 850 hPa ((c) and (d)). (a) Pressure course at 700 hPa, (b) moisture content course at 700 hPa, (c) Pressure course at 850 hPa, (d) moisture content course at 850 hPa.

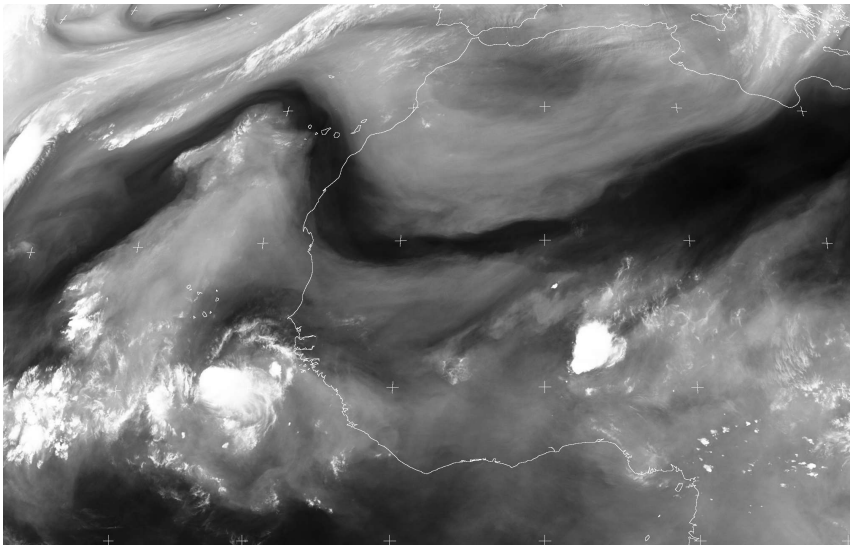

(a)

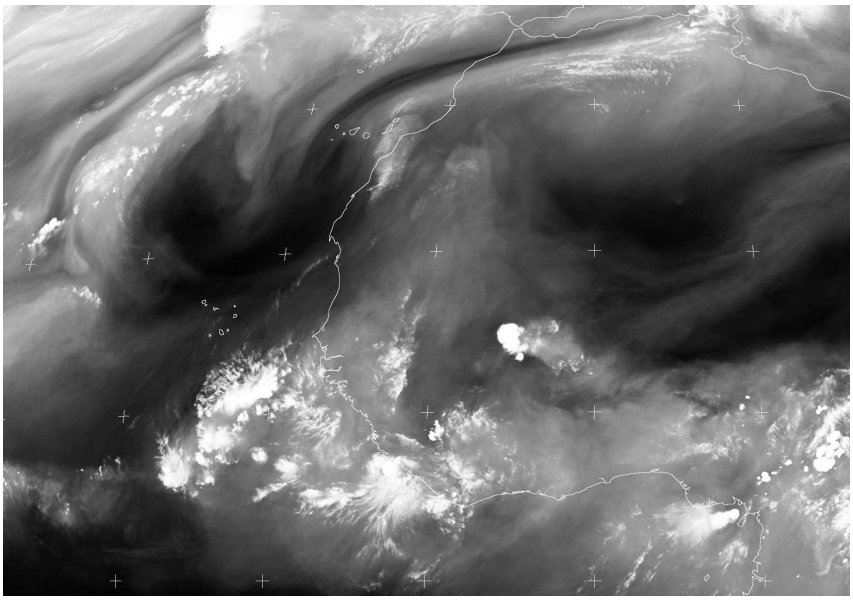

(b)

Figure 5.18: Geostationary satellite imagery from Meteosat SEVIRI 000.0E. The channel 5.35-7.15 μm Mid-IR / Water Vapour was taken to observe the water vapour and deep convection. (a) 30 September 2013, 12 UTC, (b) 5 October 2013, 12 UTC.
(Credit NEODAAS/University of Dundee)

6. Summary, Discussion and Outlook

The purpose of this study was to find explanations for the Atlantic hurricane season of 2013 being unexpectedly quiet, with a special focus on the origins of dry air intrusions into the MDR influencing TC genesis negatively.

As a first step, for the entire season as well as for the core season lasting from August to October, a climatological analysis was carried out on the classical hurricane parameters that can enhance or inhibit the generation of hurricanes and have been used for examination of seasonal hurricane activity by Klotzbach and Gray (2013a). These include SST, vertical wind shear, the sea level pressure and the mid-level moisture content. Additionally, to analyze the upper level pressure structure, the geopotential in 300 hPa was investigated by looking at the troughpoints. Also the low level relative vorticity, as it is essential for tropical cyclogenesis, and the upper level potential vorticity, as indication for RWB, were examined. To analyze potential vorticity and the troughpoints, C3Workflows have been applied to ERA-Interim data from the ECMWF, whereas for the remaining parameters, the ERA-Interim dataset was used directly. For comparison, the same analysis was performed for two other seasons occurring in the climatological time span considered. As the season of 2013 was the quietest one since 1994, the latter was investigated as well. Also a climatological analysis for the parameters of the Atlantic hurricane season 2005 containing the highest hurricane activity on record has been added.

The climatological analysis showed that most of the tropical storms developing during the Atlantic hurricane season 2013 had their origin in the eastern MDR or in the Gulf of Mexico. Despite primarily above-average SSTs in the entire MDR and a low vertical wind shear in the eastern MDR, few tropical storms developed. Inhibiting factors for tropical cyclogenesis have been mid-level dryness in the central MDR in first place and high vertical wind shear in the Caribbean Sea as a result of existing TUTTs. This increased vertical wind shear is hence not a result of the ENSO phenomenon. On average, high pressure existed just north of the central and eastern MDR, advecting dry air masses from the subtropics into the tropical regions. Upper level convergence found in negative troughpoint anomalies over the eastern subtropical Atlantic favored increasing subsidence of very dry stratospheric air. A distinct upper-level wave pattern has been found, that has occurred to this extent only in the even quieter season of 1994. Investigating the averaged PV field in the upper troposphere suggests that RWB is a guiding factor leading to dry air intrusions in both, subtropical and tropical regions alike.

In a next step, four exemplary cases were considered for determining the origin of the uncommonly dry air masses present in the MDR, being either located in subtropical regions or over the Sahara. Making use of Lagranto, five-day-backward trajectories of three non-developing AEWs and one developing AEW, that strengthened to hurricane Humberto, were analyzed regarding their vertical displacement and moisture content. Two non-developing AEWs were identified being embedded in dry air masses that originated from both, the subtropics and from the Saharan region. In the case of 16 July 2013, the air masses coming from the SAL were moister than the subtropical air masses. Here, the subtropical dry air intrusions were identified as being the main inhibiting factor. The case of 5 October 2013 was characterized by extremely dry air from the SAL at 700 hPa, whereas also subtropical dry air intrusions could be found at 850 hPa. The air masses of the other examined non-developing AEW (9 August 2013) had their origin only in the Sahara, although the air masses the AEW propagated into were also very dry as a result of subtropical intrusion. In contrast, for the surrounding air masses embedding the AEW that would develop into hurricane Humberto, remarkably moist air was advected from starting points over the Gulf of Guinea and the tropics over Africa.

Finally, combining the results from both, the case studies and the climatological analysis, the hypothesis regarding the leading role of RWB accompanied by upper level convergence being a major reason for enhanced subtropical dry air intrusions, could be strengthened.
Subsiding dry air from the subtropics inhibited deep convection initiated by AEWs or essentially weakened ongoing deep convection. Negative influences from the SAL have been only an additional inhibiting factor for selected cases. In the western MDR, mainly increased vertical wind shear, enhanced by TUTTs, affected the genesis of TCs negatively.

Gray et al. (2014) and Blunden and Arndt (2014) hypothesized that the unfavorable conditions were likely a result of a sudden change in the Atlantic ocean Thermohaline oscillation (THC). A weakening, as it occurred between the winter and spring months of 2013, led to increased cold water advection southward in the eastern Atlantic. This strengthened the subtropical anticyclone, leading to increased subsidence and mid-level dryness.

For future work, it is desirable to analyze a greater amount of non-developing AEWs with respect to the question, whether mainly subtropical dry air intrusions or rather dry air masses advected with the SAL lead to the inhibiting and weakening of tropical deep convection.
Also a quantitative analysis of RWB should be considered, as it is crucial to estimate the extent stratospheric dry air subsides into the troposphere. Furthermore, other exceptionally dry seasons need to be included into both, the climatological- and into the trajectory analysis. Especially the hurricane season of 1994, where higher values of negative humidity anomalies were present is to be compared with the season of 2013 in greater detail to understand the relevance of subtropical dry air intrusions.

Sudden changes in the AMO and THC should be investigated regarding more hurricane seasons. There might be a correlation between a sudden increase or decrease in strength during the winter and spring time and tropical cyclone activity in the North Atlantic. Therefore, also the other hurricane related parameters should be investigated in respect to the AMO and THC. By finding correlations the seasonal forecasts can be improved.

Bibliography

Allen, G., Vaughan, G., Brunner, D., May, P., Heyes, W., Minnis, P., and Ayers, J. (2009). Modulation of tropical convection by breaking rossby waves. *QJR Meteorol. Soc*, 135:125137.

Arnault, J. and Roux, F. (2011). Characteristics of African easterly waves associated with tropical cyclogenesis in the Cape Verde Islands region in JulyAugustSeptember of 20042008. *Atmospheric Research*, 100(1):6182.

Baldwin, M. P. and Holton, J. R. (1988). Climatology of the stratospheric polar vortex and planetary wave breaking. *Journal of the atmospheric sciences*, 45(7):11231142.

Bell, G., Blake, E., Landsea, C., Mo, K., Pasch, R., Chelliah, M., and Goldenberg, S. (2000). The 1999 north atlantic hurricane season: A climate perspective. *Climate Assessment for 1999. Bull. Amer. Meteor. Soc*, 81:S19S23.

Blake, E. S. (2014). 2013 Atlantic Annual Summary - National Hurricane Center. www.nhc.noaa.gov/data/tcr/summary_atlc_2013.pdf.

Blunden and Arndt (2014). State of the Climate in 2013. *Bulletin of the American Meteorological Society*, 95(7):S1S279. doi: 10.1175/2014BAMSStateoftheClimate.1.

Braun, S. A. (2010). Reevaluating the role of the saharan air layer in atlantic tropical cyclogenesis and evolution. *Monthly Weather Review*, 138(6):20072037.

Briegel, L. M. and Frank, W. M. (1997). Large-scale influences on tropical cyclogenesis in the western north pacific. *Monthly weather review*, 125(7):13971413.

Chen, T.-C., Wang, S.-Y., and Clark, A. J. (2008). North atlantic hurricanes contributed by african easterly waves north and south of the african easterly jet. *Journal of Climate*, 21(24):67676776.

Dee, D., Uppala, S., Simmons, A., Berrisford, P., Poli, P., Kobayashi, S., Andrae, U., Balmaseda, M., Balsamo, G., Bauer, P., et al. (2011). The era-interim reanalysis: Configuration and performance of the data assimilation system. *Quarterly Journal of the Royal Meteorological Society*, 137(656):553597.

Dunion, J. P. and Velden, C. S. (2004). The impact of the saharan air layer on atlantic tropical cyclone activity. *Bulletin of the American Meteorological Society*, 85(3):353365.

Frank, N. L. and Clark, G. (1980). Atlantic tropical systems of 1979. *Monthly Weather Review*, 108(7):966972.

Frank, W. M. (1987). Tropical cyclone formation. *A global view of tropical cyclones*, page 5390.

Fröhlich, L. and Knippertz, P. (2008). Identification and global climatology of upper-level troughs at low latitudes. *Meteorologische Zeitschrift*, 17(5):565573.

Funatsu, B. M. and Waugh, D. W. (2008). Connections between potential vorticity intrusions and convection in the eastern tropical pacific. *Journal of the Atmospheric Sciences*, 65(3):9871002.

Gabriel, A. and Peters, D. (2008). A diagnostic study of different types of Rossby wave breaking events in the northern extratropics. *Journal of the Meteorological Society of Japan*, 86(5):613631.

Goldenberg, S. B., Landsea, C. W., Mestas-Nuñez, A. M., and Gray, W. M. (2001). The recent increase in atlantic hurricane activity: Causes and implications. *Science*, 293(5529):474479.

Gray, W. M. (1984). Atlantic seasonal hurricane frequency. part i: El nino and 30 mb quasi-biennial oscillation influences. *Monthly Weather Review*, 112(9):16491668.

Gray, W. M., Klotzbach, P., et al. (2014). Why the atlantic was surprisingly quiet in 2013.

Gray, W. M., Landsea, C. W., Mielke, Paul .., J., and Berry, K. J. (1994). Predicting Atlantic Basin Seasonal Tropical Cyclone Activity by 1 June. *Weather and Forecasting*, 9:103115.

Haynes, P. H., Mcintyre, M. E., Douglass, A. R., Rood, R. B., and Pfister, L. (1995). Stratosphere-troposphere exchange. *Rev. Geophys*, 33(4):403439.

Hodges, K. et al. (1994). A general-method for tracking analysis and its application to meteorological data. *Monthly Weather Review*, 122(11):25732586.

Hopsch, S. B., Thorncroft, C. D., and Tyle, K. R. (2010). Analysis of african easterly wave structures and their role in influencing tropical cyclogenesis. *Monthly Weather Review*, 138(4):13991419.

HRD, C. N. (2013). Noaa atlantic hurricane season outlook -2013, noaa atlantic hurricane season outlook -2013 update. *National Weather Service - Climate Prediction Center*.

Klotzbach, P. and Gray, W. (2013a). Summary of 2013 atlantic tropical cyclone activity and verification of authors'seasonal and two-week forecasts.

Klotzbach, P. and Gray, W. M. (2013b). Extended range forecast of atlantic seasonal hurricane activity and landfall strike probability for 2013.

Klotzbach, P. and Gray, W. M. (2013c). Forecast of Atlantic Seasonal Hurricane Activity and Landfall Strike Probability for 2013.

Klotzbach, P., Gray, W. M., et al. (2013). Extended range forecast of atlantic seasonal hurricane activity and landfall strike probability for 2013.

Knippertz, P. (2004). A simple identification scheme for upper-level troughs and its application to winter precipitation variability in northwest africa. *Journal of climate*, 17(6):14111418.

Landsea, C. (2011). What is a tropical disturbance, a tropical depression or a tropical storm. *FAQ. Hurricane Research Division: Atlantic Oceanographic & Meteorological Laboratory. Web Accessed April*, 26:2014.

Madden, R. A. and Julian, P. (1994). Observations of the 40-50 day tropical oscillation - a review. *Monthly Weather Review*, 122:814837.

McIntyre, M. E. and Palmer, T. (1983). Breaking planetary waves in the stratosphere. *Nature*, 305(5935):593600.

NOAA (2013). Noaa atlantic hurricane season outlook - 2013. *National Weather Service - Climate Prediction Center*.

NOAA (2015). Background information: The north atlantic hurricane season. *National Weather Service - Climate Prediction Center*.

Postel, G. A. and Hitchman, M. H. (1999). A climatology of rossby wave breaking along the subtropical tropopause. *Journal of the atmospheric sciences*, 56(3):359373.

Ritchie, E. A. and Holland, G. J. (1999). Large-scale patterns associated with tropical cyclogenesis in the western pacific. *Monthly weather review*, 127(9):20272043.

Ross, R. S. and Krishnamurti, T. (2007). Low-level african easterly wave activity and its relation to atlantic tropical cyclogenesis in 2001. *Monthly Weather Review*, 135(12):39503964.

Sadler, J. C. (1967). The tropical upper tropospheric trough as a secondary source of typhoons and a primary source of tradewind disturbances. Technical report, DTIC Document.

Saffir, H. S. (1973). Hurricane wind and storm surge, and the hurricane impact scale. *The Military Engineer. Alexandria, Virginia*, (423).

Schwendike, J. and Jones, S. C. (2010). Convection in an african easterly wave over west africa and the eastern atlantic: A model case study of helene. *QJR Meteorol. Soc*, 136(s1):364396.

Simpson, R. H. and Saffir, H. (1974). The hurricane disaster potential scale. *Weatherwise*, 27(8):169.

Sprenger, M. and Wernli, H. (2015). The lagranto lagrangian analysis tool â version 2.0. *Geoscientific Model Development*, 8(8):25692586.

Thorncroft, C. and Hodges, K. (2001). African easterly wave variability and its relationship to atlantic tropical cyclone activity. *Journal of Climate*, 14(6):11661179.

Zipser, E. J., Twohy, C., Tsay, S.-C., Thornhill, K. L., Tanelli, S., Ross, R., Krishnamurti, T., Ji, Q., Jenkins, G., Ismail, S., et al. (2009). The saharan air layer and the fate of african easterly wavesnasa's amma field study of tropical cyclogenesis.

A. Appendix

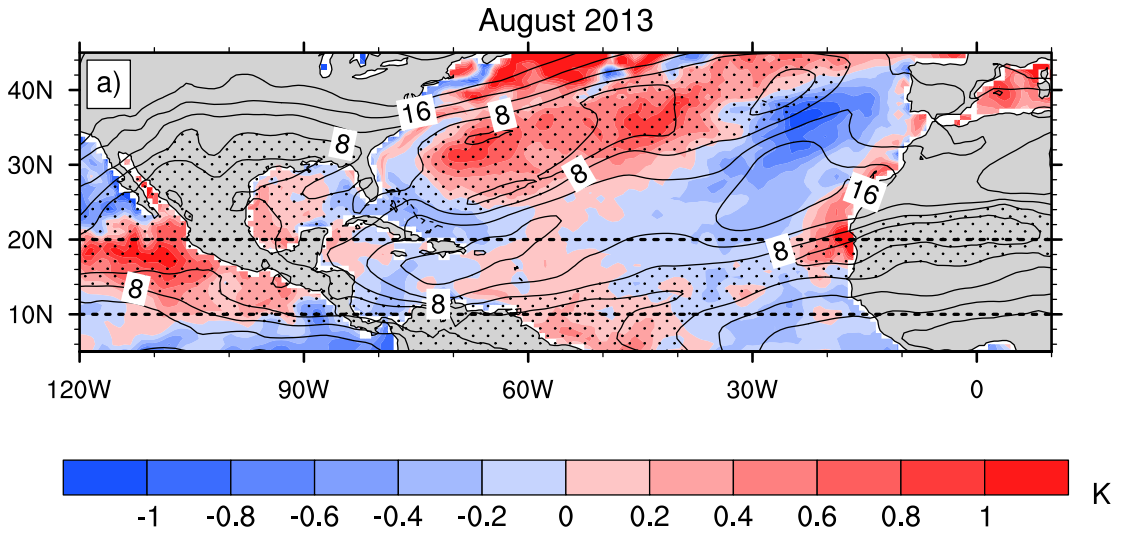

Figure A.1: SST anomaly in K (shaded contour) and average vertical wind shear in m s^{-1} (contour lines) for August 2013. Dotted regions indicate averaged wind shear below 8 m s^{-1}.

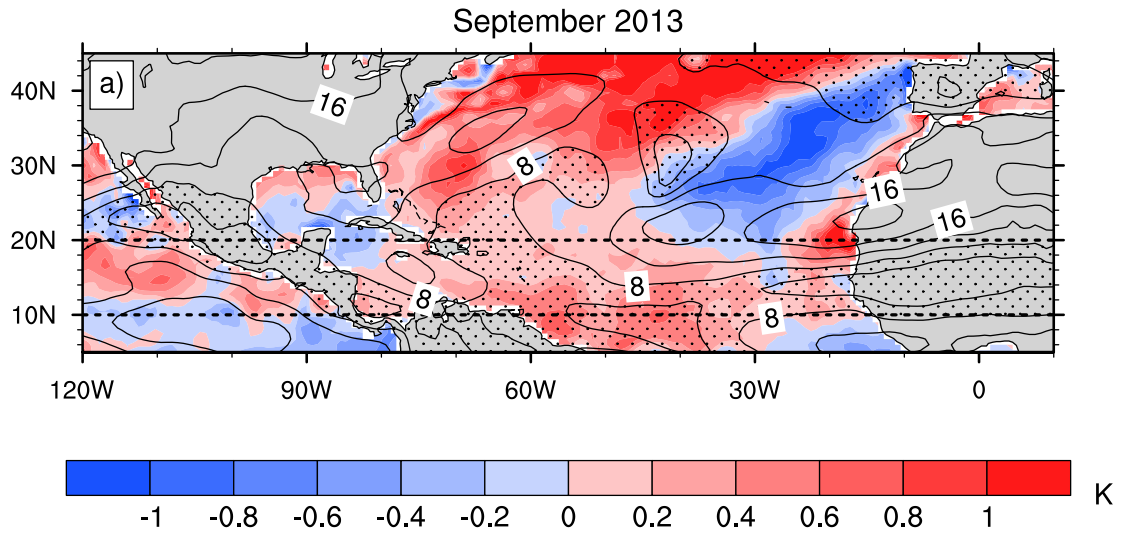

Figure A.2: SST anomaly in K (shaded contour) and average vertical wind shear in m s^{-1} (contour lines) for September 2013. Dotted regions indicate averaged wind shear below 8 m s^{-1}.

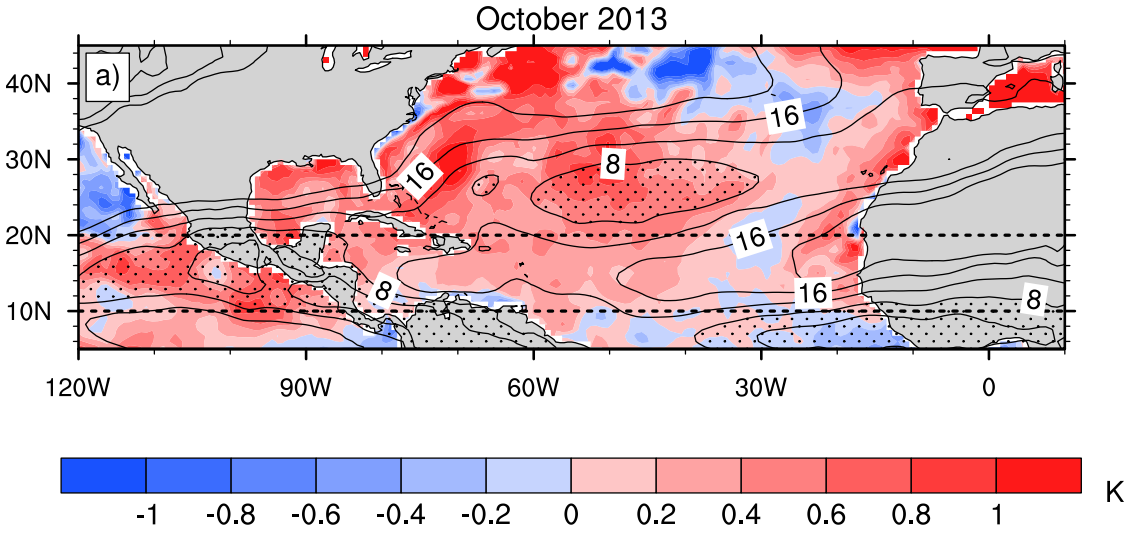

Figure A.3: SST anomaly in K (shaded contour) and average vertical wind shear in m s^{-1} (contour lines) for October 2013. Dotted regions indicate averaged wind shear below 8 m s^{-1}.

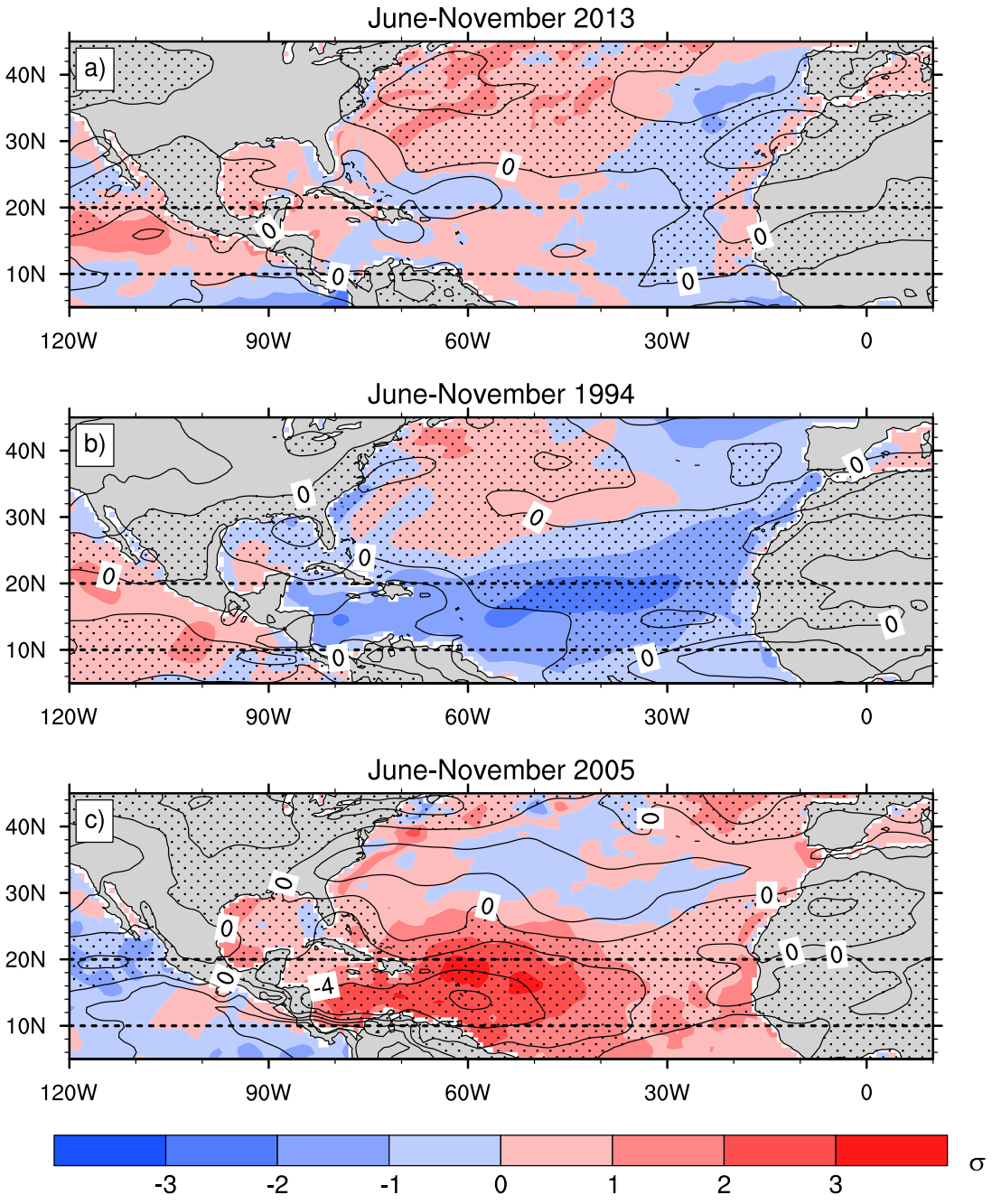

Figure A.4: Normalized SST anomaly in σ (shaded contour) and vertical wind shear anomaly in m s^{-1} (contour lines) from June to November. Dotted regions indicate positive shear anomaly

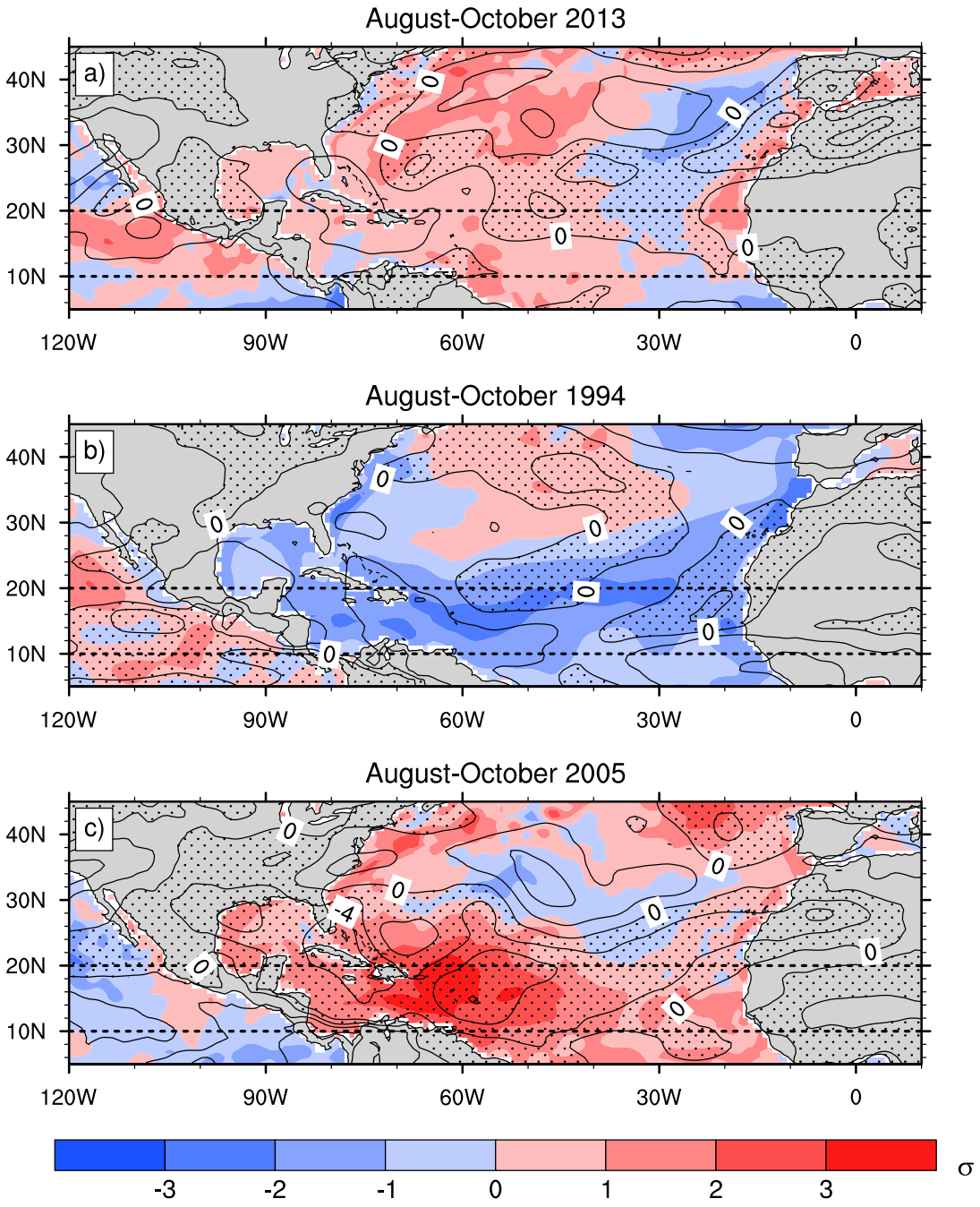

Figure A.5: Normalized SST anomaly in σ (shaded contour) and vertical wind shear anomaly in m s^{-1} (contour lines) from August to October. Dotted regions indicate positive shear anomaly

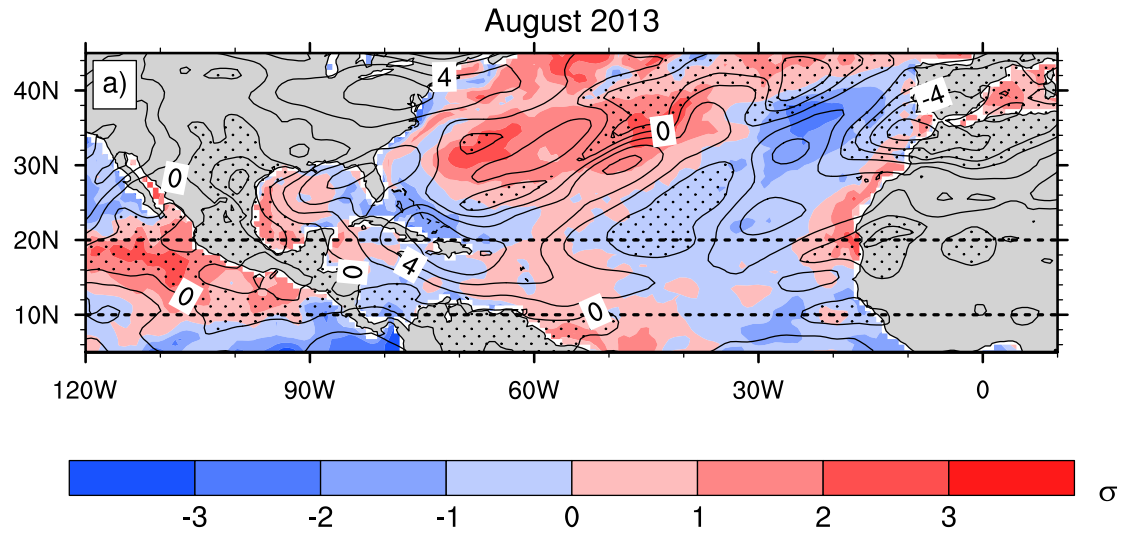

Figure A.6: Normalized SST anomaly in σ (shaded contour) and vertical wind shear anomaly in m s^{-1} (contour lines) for August 2013. Dotted regions indicate positive shear anomaly

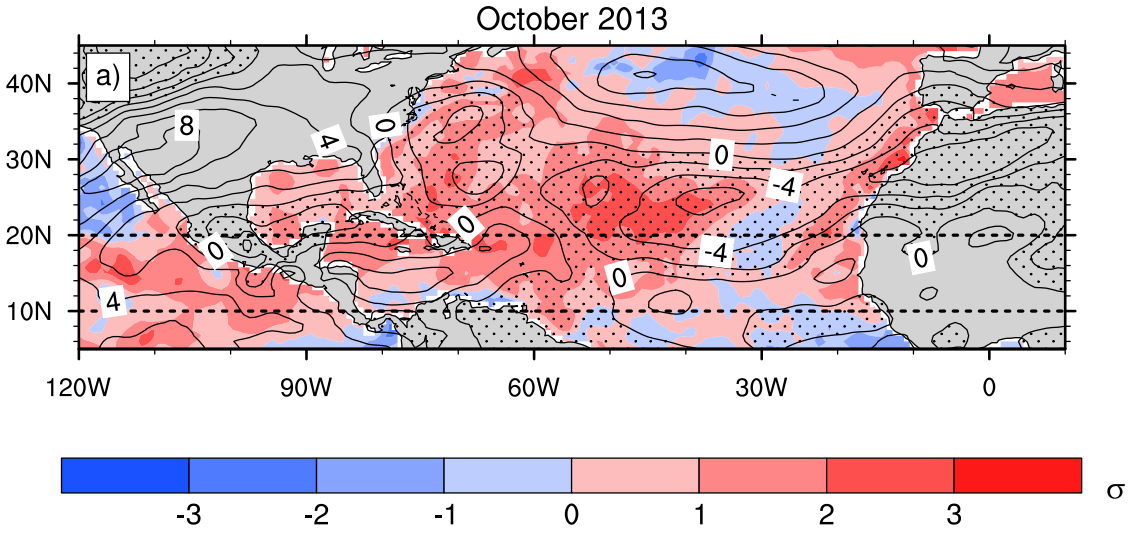

Figure A.7: Normalized SST anomaly in σ (shaded contour) and vertical wind shear anomaly in m s^{-1} (contour lines) for October 2013. Dotted regions indicate positive shear anomaly

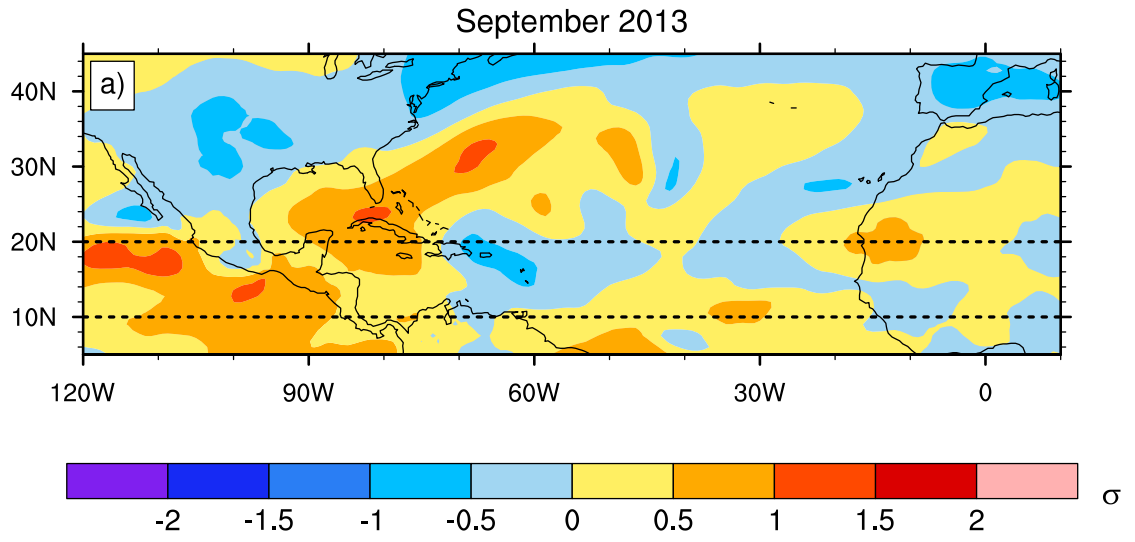

Figure A.8: Normalized vertical wind shear anomaly in σ for September 2013.

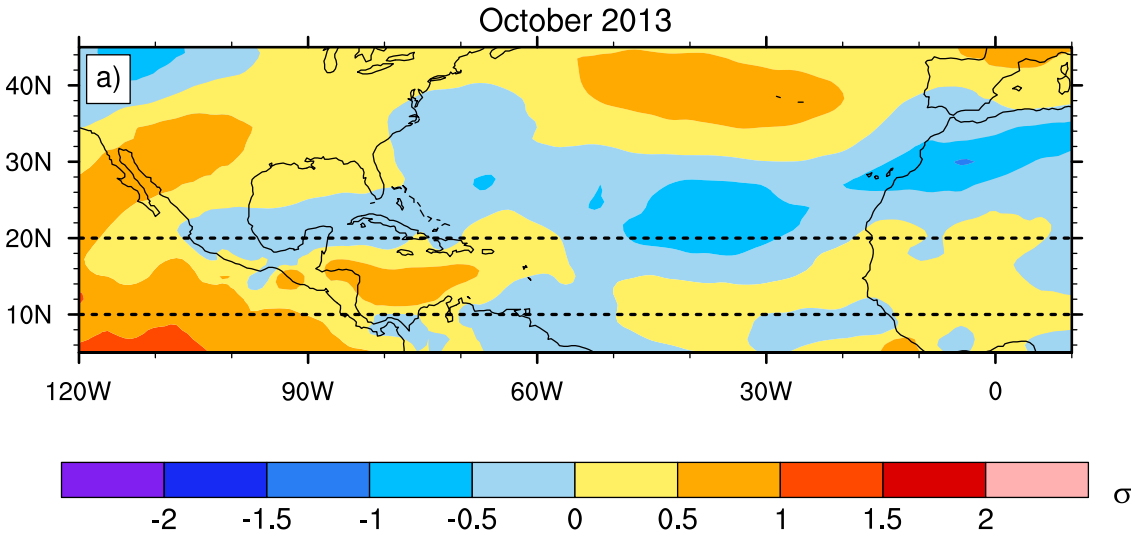

Figure A.9: Normalized vertical wind shear anomaly in σ for October 2013.

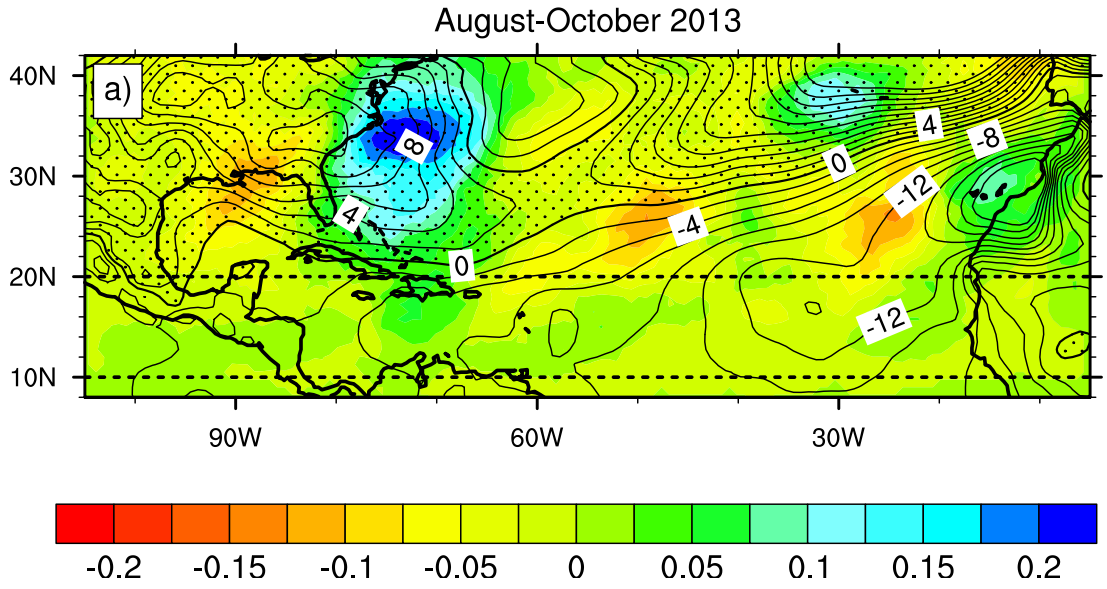

Figure A.10: Troughpoint anomaly at 300 hPa (shaded contour) and surface pressure anomaly in 10^{-1} hPa (contour lines) from August to October 2013. Dotted regions indicate a positive sea level pressure anomaly.

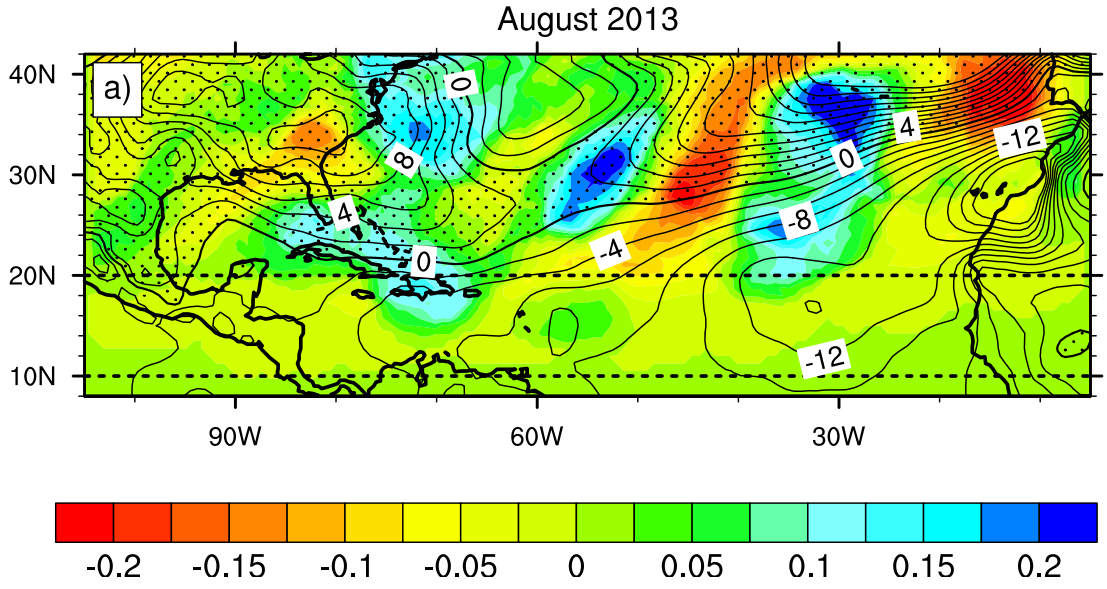

Figure A.11: Troughpoint anomaly at 300 hPa (shaded contour) and surface pressure anomaly in 10^{-1} hPa (contour lines) from August 2013. Dotted regions indicate a positive sea level pressure anomaly.

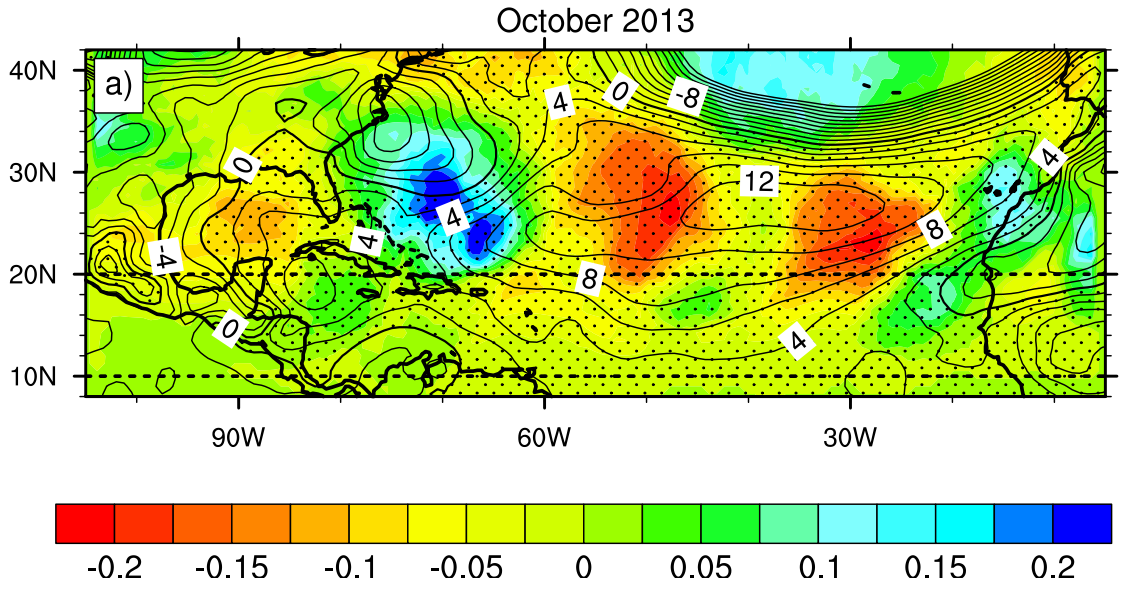

Figure A.12: Troughpoint anomaly at 300 hPa (shaded contour) and surface pressure anomaly in 10^{-1} hPa (contour lines) from October 2013. Dotted regions indicate a positive sea level pressure anomaly.

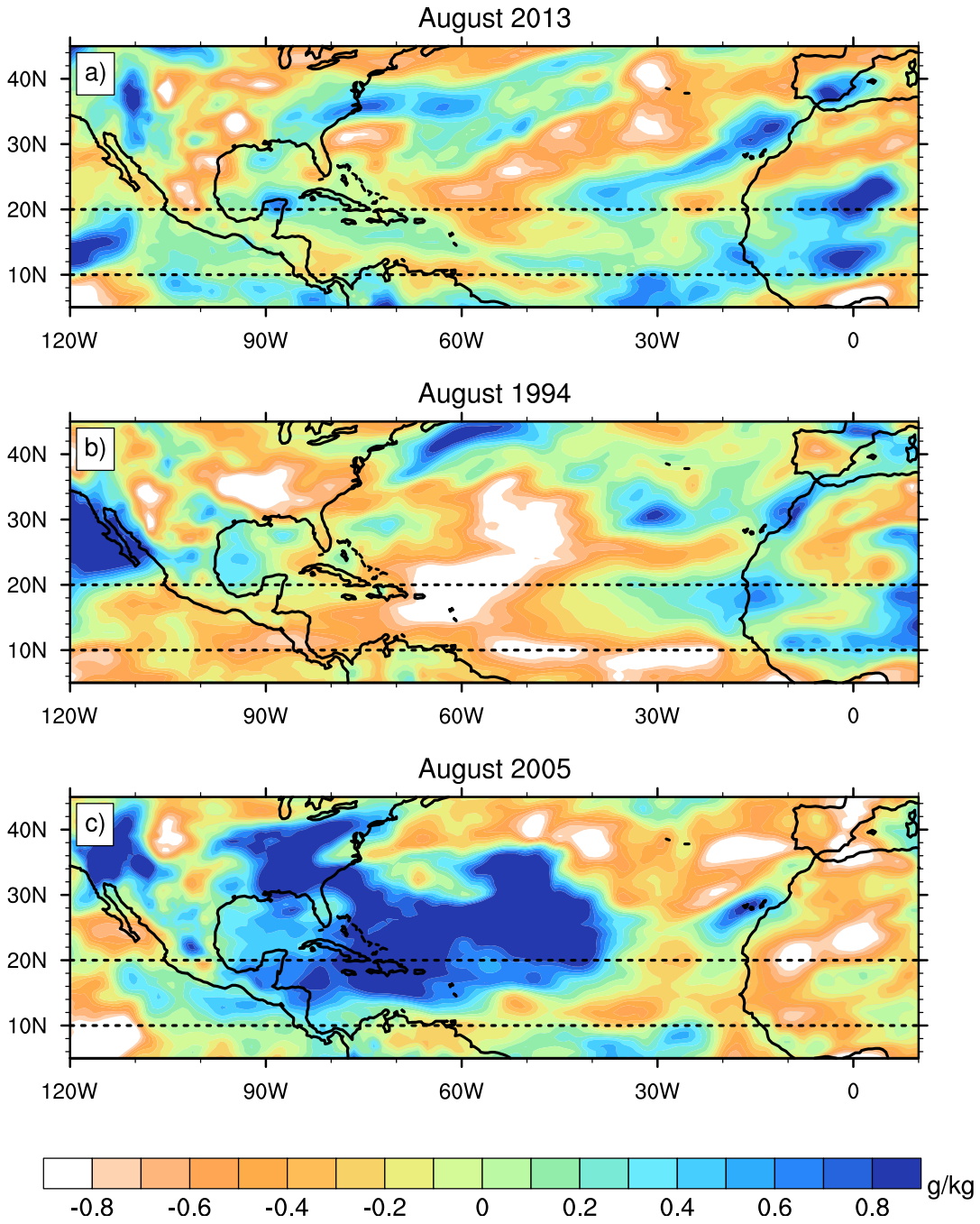

Figure A.13: Specific humidity anomaly at 700 hPa in g kg^{-1}(shaded contour).

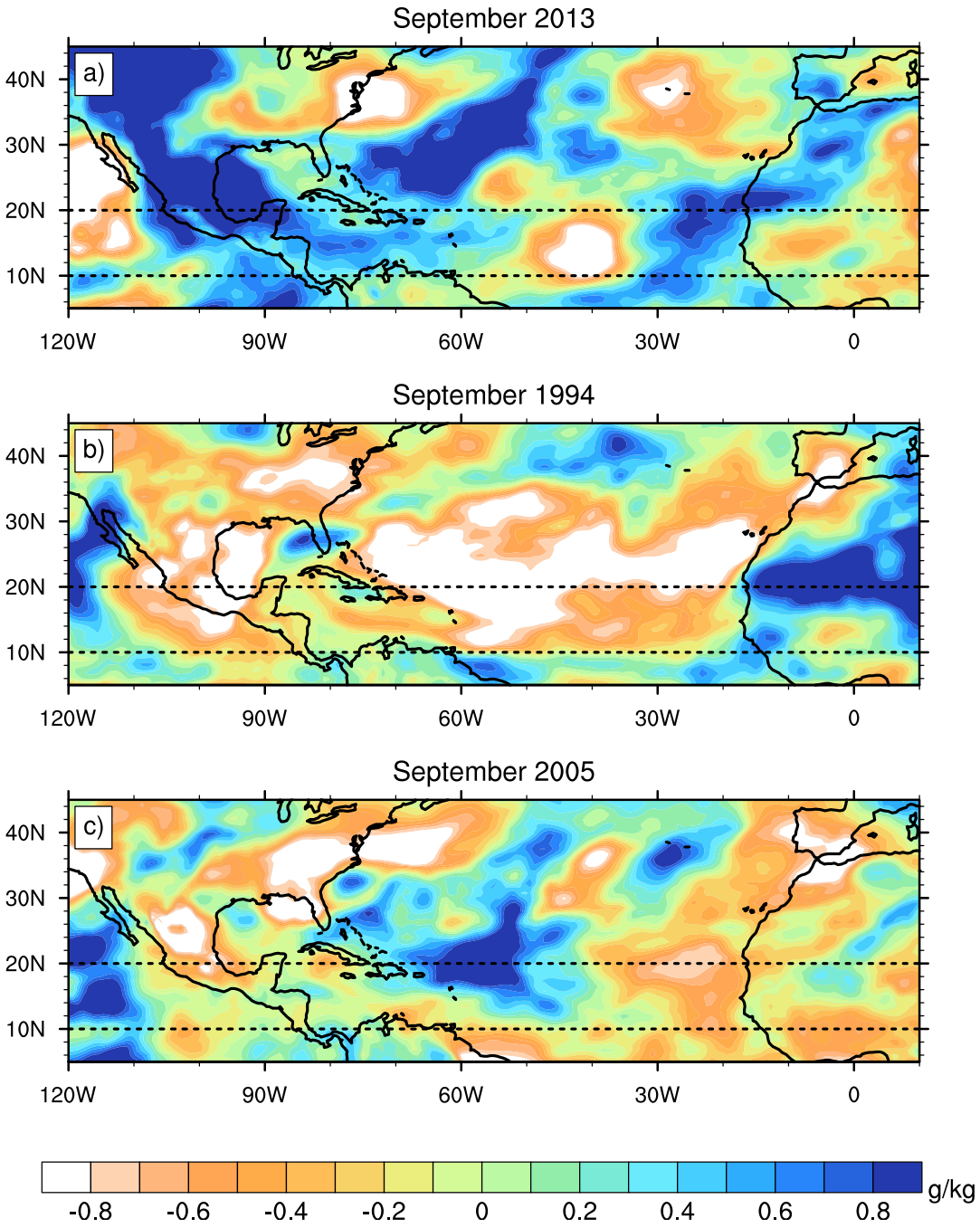

Figure A.14: Specific humidity anomaly at 700 hPa in g kg^{-1}(shaded contour).

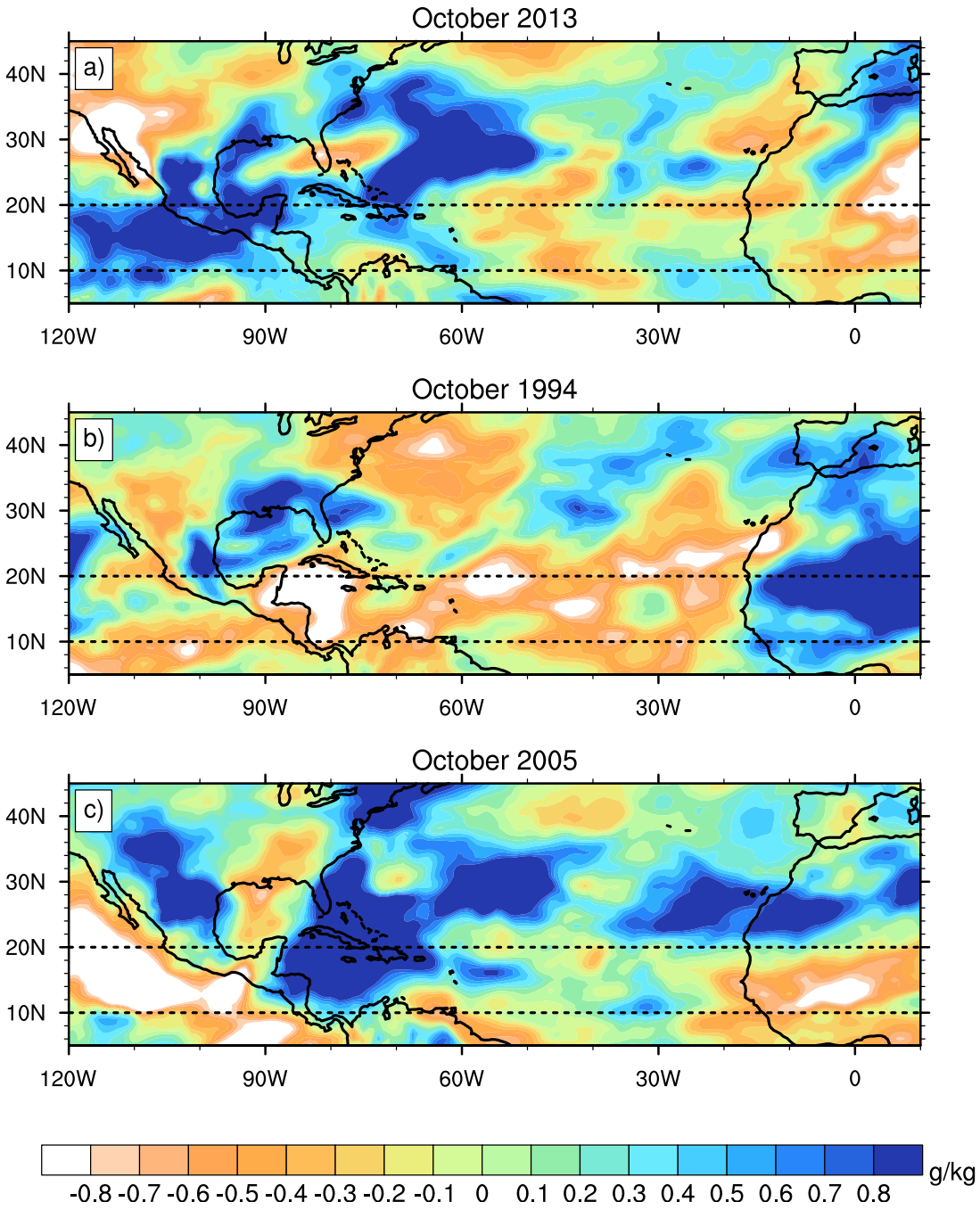

Figure A.15: Specific humidity anomaly at 700 hPa in g kg^{-1}(shaded contour).

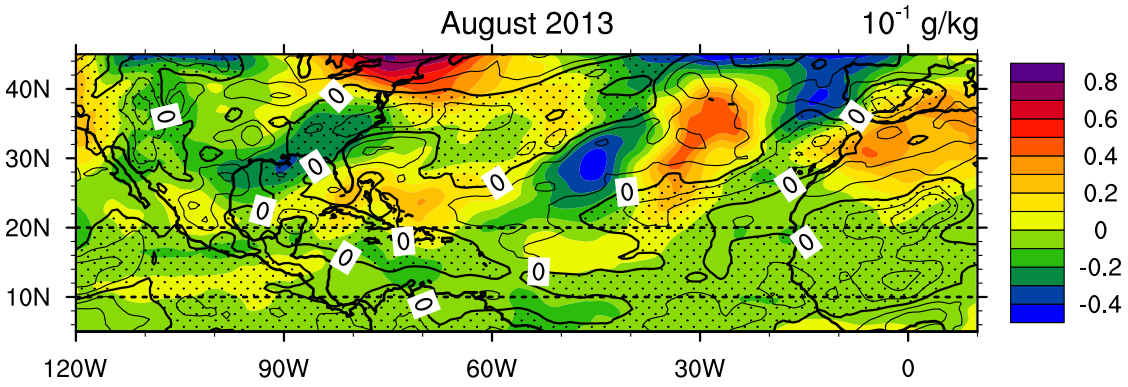

Figure A.16: Potential Vorticity (averaged between 100-400 hPa) anomalies (contour shaded) and specific humidity anomalies in 700 hPa (contour lines) from August 2013 regarding the 31 year period from 1983-2013. Positive humidity anomalies are shaded with dots.

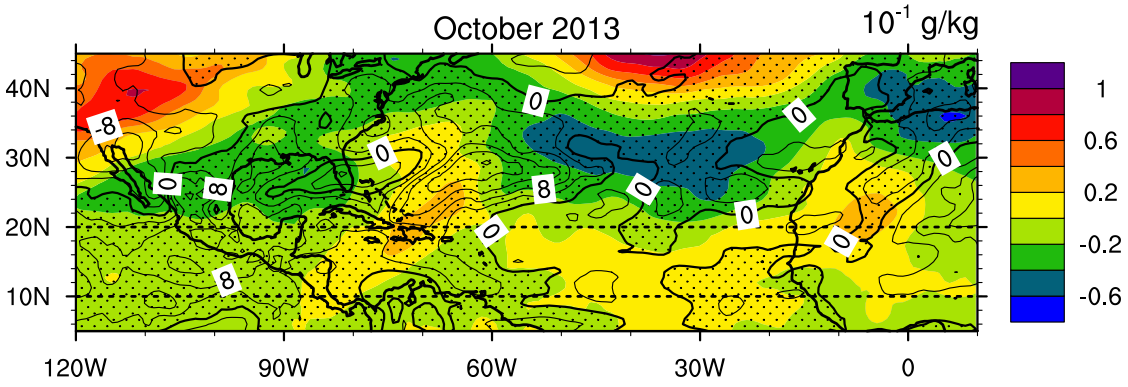

Figure A.17: Potential Vorticity (averaged between 100-400 hPa) anomalies (contour shaded) and specific humidity anomalies in 700 hPa (contour lines) from October 2013 regarding the 31 year period from 1983-2013. Positive humidity anomalies are shaded with dots.

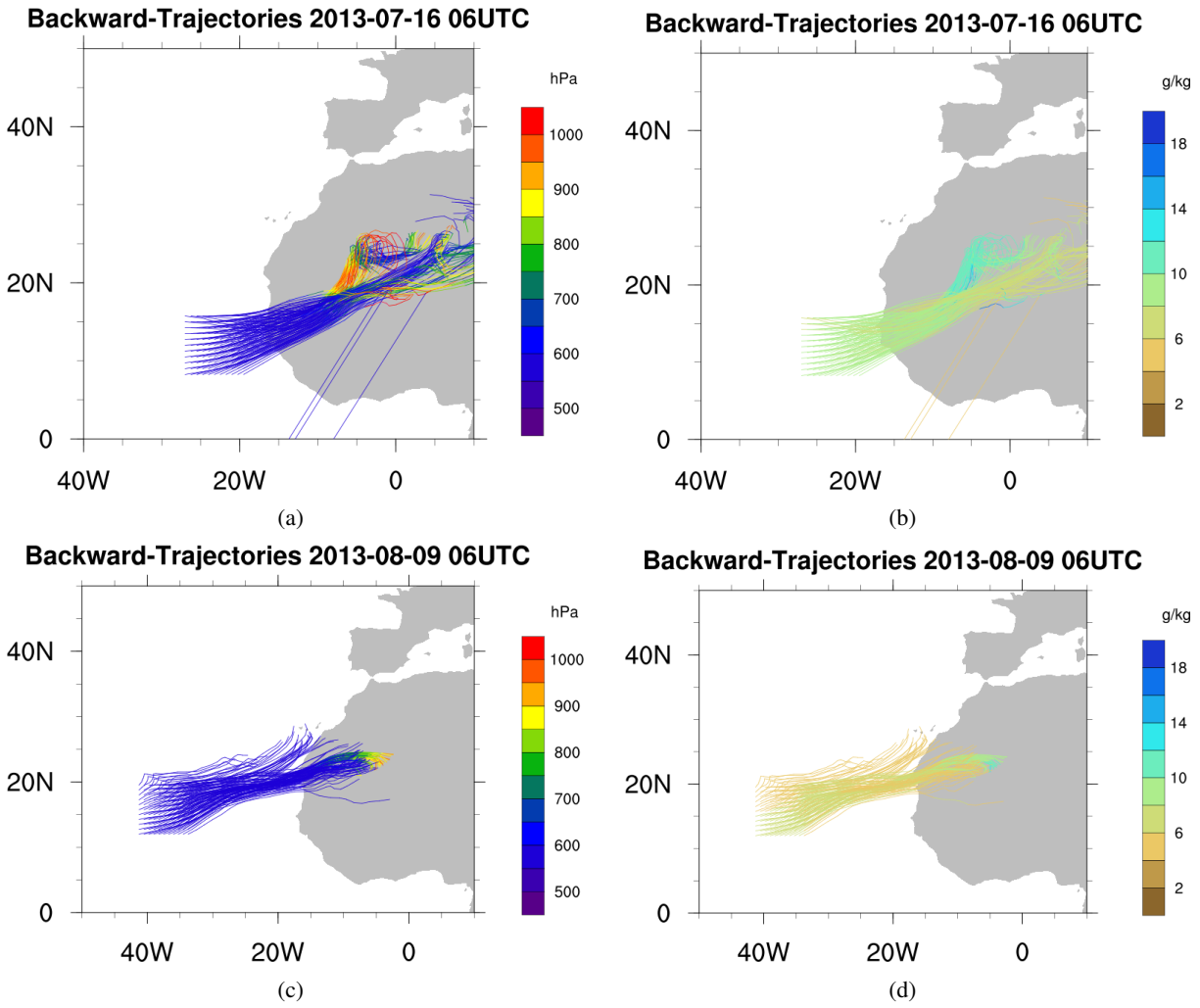

Figure A.18: 121 Backward trajectories equidistantly distributed in a gridbox (19-27°W, 8-16°N) starting at 16 July 2013, 06 UTC, (top panel) and in a gridbox (33.5-41.5°W, 11.5-19.5°N) starting at 9 August 2013, 06 UTC. Calculated with Lagranto for five days at 600 hPa. (a) and (c) pressure course, (b) and (d) moisture content course.

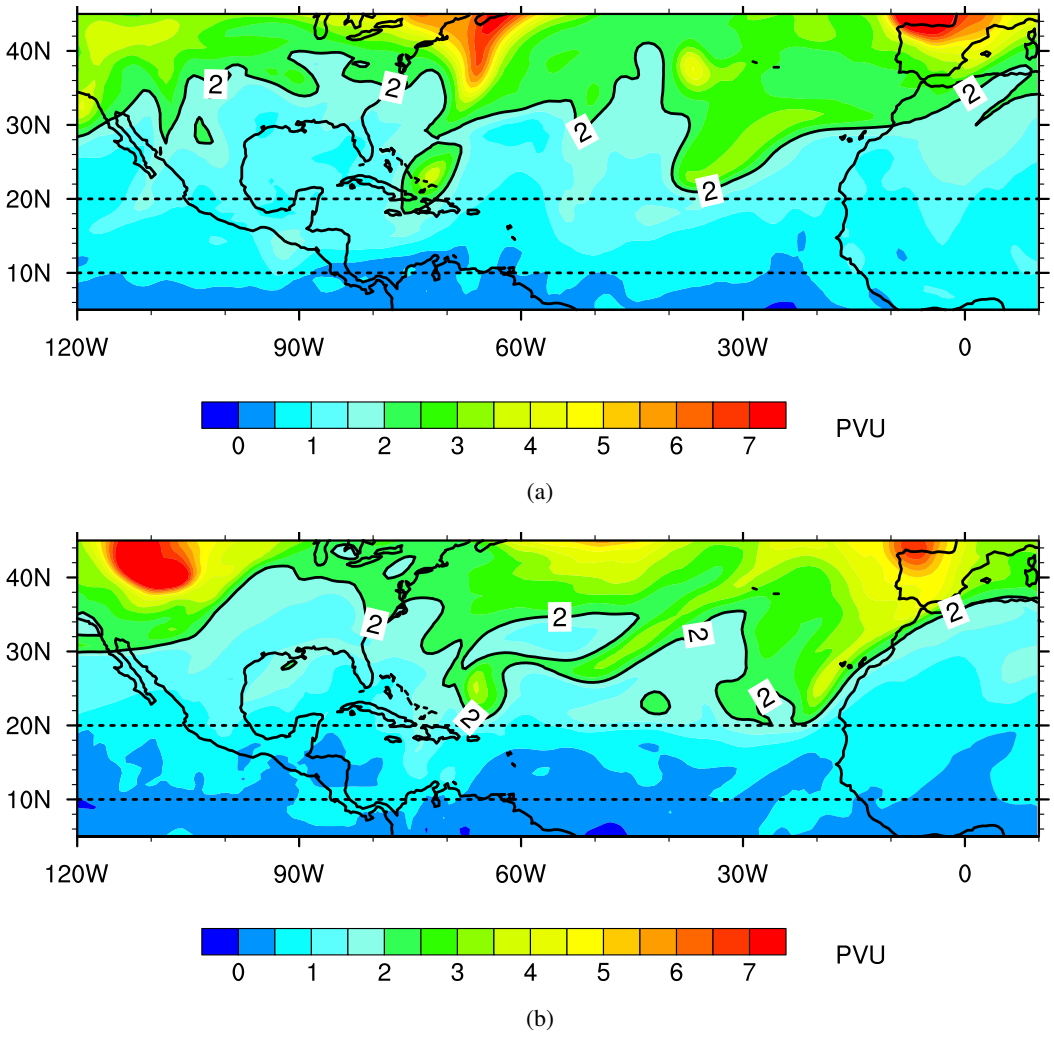

Figure A.19: Rossby wave breaking of the type LC1 examined with PV, averaged between 100-400 hPa (contour shaded). The thick solid line indicates the position of the tropopause near the 2 PVU surface. (a) 7 August 2013, 12 UTC, (b) 4 October 2013, 12 UTC

List of Acronyms

Accumulated Cyclone Enegery	ACE
African Easterly Jet	AEJ
African Easterly Waves	AEW
Atlantic Multidecadal Oscillation	AMO
August September October	ASO
Climate Data Operators	CDO
Climate Prediction Center	CPC
Colorado State University	CSU
Consortium of Small-scale Modelling	COSMO
El Niño Southern Oscillation	ENSO
European Centre for Medium-Range Weather Forecasts	ECMWF
European Seasonal to Inter-annual Prediction Ensemble	EUROSIP
Hurricane	H
Hurricane Days	HD
Hurricane Research Division	HRD
Lagrangian Analysis Tool	Lagranto
Main Developing Region	MDR
Major Hurricane	MH
Major Hurricane Days	MHD
Mesoscale Convective System	MCS
Named Storm	NS
Named Storm Days	NSD
NASA-African Monsoon Multidisciplinary Analysis	NAMMA
National Hurricane Center	NHC
National Oceanic and Atmospheric Administration	NOAA
Net Tropical Cyclone Activity	NTC
Potential Voriticity	PV
Potential Vorticity Unit	PVU
Rossby Wave Breaking	RWB
Saharan Air Layer	SAL
Schwendike and Jones	SJ
Sea Surface Temperatures	SST
Subtropical Storm	SS
Tropical Cyclone	TC
Tropical Depression	TD
Tropical Storm	TS
Tropical Storm Risk	TSR
Tropical Upper Tropospheric Trough	TUTT
Troughaxis	TA
Troughaxispoint	TAP
Troughpoint	TP

Table A.1: Tropical storm classification and the Saffir-Simpson hurricane wind scale.

Tropical Storm Classification	
TD	$\leq$ 62 km h^{-1}
TS	63-118 km h^{-1}

Saffir-Simpson Hurricane Wind Scale	
Category	**Sustained Winds**
1 (H)	119-153 km h^{-1}
2 (H)	154-177 km h^{-1}
3 (MH)	178-208 km h^{-1}
4 (MH)	209-251 km h^{-1}
5 (MH)	252 km h^{-1} or higher

Acknowledgments

At this point I want to express my deep gratitude to all the people that helped me completing this thesis and my studies. I am very grateful to Prof. Dr. Andreas Fink for supervising this thesis. Thank you for giving me the opportunity to write about tropical cyclones, for supporting me and for all the motivating discussions we had. Furthermore, I want to thank Prof. Dr. Peter Knippertz for being my second adviser and for having time when I had questions.

I want to thank my working group for the nice atmosphere and the support they gave me during my thesis. Especially, I am very grateful to Gregor Gläser for downloading the ERA-Interim dataset and for helping me with all the programs I had to use during my master's thesis. Also I want to thank Thomas Engel for helping me with the AEW-tracking program. Thank you, Florian Pantillon, for discussing tropical processes with me whenever I stood in front of your desk and for the helpful tips you gave me for writing my thesis.

I am also very grateful to Gerhard Brückel for fixing all hard- and software related problems. Lisa-Ann Quandt, thank you for helping me gaining insight to Rossby wave related processes and for all the conversations we had about tropical cyclones.

Furthermore, I am very grateful to the ECMWF in Reading for providing the ERA-Interim dataset I used for this thesis. Also I want to thank NEODAAS/University of Dundee for providing the Meteosat-SEVIRI satellite images.

I am now looking back at five years of studying meteorology and want to thank all of my friends and fellow students for all the memories we created. Annika, thank you for being there for me in every aspect of my life and for reminding me to also take some breaks, also for never letting me fall. Adrian, we share the fascination for tropical cyclones and extreme weather events. Thank you for all the conversations we had and for discussing the satellite pictures. Verena, I thank you for being there for me since school times and all the memories we created. Nils and Maren, the last five years were a roller coaster ride with loopings, thank you for sharing this fun times with me. Lisa and Lukas, thank you for creating such a friendly atmosphere in our room, for all the funny conversations and also for helping me whenever I had a problem. I always looked forward to coming to university when I knew you were there. I also want to thank the four guys of the extraordinary Ξ group of 2010 for the unforgettable memories.

Ich möchte noch ganz herzlich meiner Familie danken. Vielen Dank, dass Ihr mich immer unterstützt habt und immer für mich da wart. Oma, ich danke Dir sehr für deine regelmäßigen Anrufe, es war schön mit dir über Gott und die Welt zu reden. Opa, danke dass du mich stets daran erinnert hast, wie wichtig das Studium ist. Mama, danke für alles was du in den letzten 25 Jahren mit mir durchgestanden hast und dass du auf alle aufgepasst hast. Helen, danke dass du da bist und für deine Fahrdienste :P. Und wie schon Loriot gesagt hat, ein Leben ohne Mops ist möglich, aber sinnlos.

Simon, thank you that you have been there, always. Here's to the next chapter.

Erklärung

Hiermit erkläre ich, dass ich die vorliegende Arbeit selbst verfasst und nur die angegebenen Hilfsmittel verwendet habe.

Ich bin damit einverstanden, dass diese Arbeit in Bibliotheken eingestellt wird und vervielfältigt werden darf.

Karlsruhe, den 5. November 2015

Name